EMERSON ELECTRIC CO.
ELECTRONICS AND SPACE DIVISION

8100 florissant avenue, st. louis , mo., 63136 colfax 1-1800

Report Number 2074 Volume I

RADIOACTIVE-TYPE DUAL ABLATION MEASURING SYSTEM

Final Report

Prepared for:

National Aeronautics and Space Administration
Langley Research Center
Langley Field, Virginia

Under NASA Contract NAS 1-5342

EMERSON ELECTRIC OF ST. LOUIS

ELECTRONICS AND SPACE DIVISION

8100 florissant avenue, st. louis , mo., 63136 colfax 1-1800

Report Number 2074 Volume I

RADIOACTIVE-TYPE DUAL ABLATION MEASURING SYSTEM

Final Report

Prepared for:

National Aeronautics and Space Administration
Langley Research Center
Langley Field, Virginia

Under NASA Contract NAS 1-5342

15 January, 1968

Prepared by:

John D. Bartley, Jr.

FOREWORD

This Final Report documents the work performed by Emerson Electric Company for the National Aeronautics and Space Administration, Langley Research Center, under Contract NAS 1-5342. The period of performance was thirty months. In conjunction with the appendix and the supporting outsize drawing package, the report presents all the information necessary to fabricate, check, calibrate, and operate a Radioactive-Type Dual Ablation Measuring System.

Approved:

John D. Bartley, Jr.

John D. Bartley, Jr.
Program Manager
Thermal Systems Department

SUMMARY

Emerson Electric Company has investigated the feasibility of using a nucleonic technique for continuous and simultaneous measurement of ablative heat shield total and virgin material recession at the same flight vehicle location. The concept makes use of the chemical and nuclear properties of two radioactive compounds and of the fact that the radioactive intensity of these two compounds incorporated into an Ablation Sensor Plug, composed of the parent heat shield material, is related to the two thicknesses to be measured.

During the performance of this contract two radioactive chemical compounds were found minute amounts of which could be incorporated into phenolic nylon and phenolic graphite without altering the ablative properties of these heat shield materials. Methods were developed and demonstrated to homogeneously incorporate these compounds into Ablation Sensor Plugs. Ablation tests demonstrated that at the end of the test the intensity of radiation remaining of one compound, $ZrNb^{95}$, was proportional to the total heat shield thickness while that of the other compound, In^{114m}, was proportional to the virgin material thickness remaining. Subsequently, isotope accuracy ablation tests were performed. The average thickness at the end of the test obtained from isotope data agreed with the physically measured thickness within plus or minus .02 inches.

In a parallel effort, a scintillation crystal photomultiplier radiation detector was designed and fabricated that would withstand 150g shock and the other specified environmental criteria. Circuits of a flight, dual channel, radiation energy analyzer were designed. breadboarded, and tested. The dual channel analyzer provided two D.C. output channels, compatible with recording and telementry systems typical of advanced research vehicles and ground based equipment. System output was a D.C. voltage proportional to the input count rate of the two discrete nuclear energy levels corresponding to the virgin material radio-

indicator and the total length radio-indicator. Two miniaturized, prototype flight systems were fabricated of the printed circuit board, soldered component, potted module variety.

The Ablation Sensor Plugs, Radiation Detector, and prototype systems were integrated. System operational ablation tests were performed with serial number one system. System test results showed that the average sensor output at the end of the test agreed with physical measurements of test specimen thickness remaining. However, the instantaneous sensor indication fluctuated widely during the test. These fluctuations, due primarily to statistical uncertainties in the low count rate resulting from limited amounts of activity in test specimens, prevented the precise determination of measurement accuracy. Additional tests at higher levels of activity and ablation rates are recommended.

The two prototype systems were delivered to the NASA for use with phenolic nylon and phenolic graphite heat shield materials. Subsequent thermal environment testing, performed by the NASA, indicated that the systems were not properly thermally compensated. However, the specified shock, vibration, acceleration, and vacuum environments posed no problems to the Radiation Detector. (The electronics system was not exposed to these environments.)

A failure occurred in one system while being tested at the NASA. Both systems and Radiation Detectors were returned to Emerson for re-work. During checkout at Emerson a failure occurred in the other electronics system, and one Radiation Detector could not be made to operate. Emerson repaired one system by replacing the pulse amplifier with an integrated circuit operational amplifier; and a breadboard system was made operational to conform. One packaged miniaturized and one breadboard system, both complete with Radiation Detectors, were returned to the NASA.

The feasibility of heat shield thickness measurement, both total thickness and virgin material remaining, by this radioactive technique has been established. The significant advantage of this technique is that with a minimum amount of foreign material incorporated into a sensor plug of parent heat shield material a continuous and simultaneous measurement of total and virgin

material thickness can be made, at the same vehicle location. The system works with a variety of heat shield materials including one that is an electric conductor in its virgin state.

Discussion of source preparation, system fabrication and calibration, flight mission requirements, system tests performed, and recommendations for future system proof tests are presented herein. Volume II of this report contains supporting test data, fabrication, checkout, and operating procedures.

TABLE OF CONTENTS

1.0 INTRODUCTION

1.1 General

Of the present known techniques of dissipating the energy and providing thermal protection to planetary entry vehicle payloads, the provision of an ablative heat shield is the most frequently used technique. Ablative heat shields absorb and block entry heating by surface re-radiation, material decomposition, transpiration of material decomposition products, and insulation of vehicle payloads. The most promising class of these ablatives, from the standpoint of vehicle protection from severe thermal environments, decomposes in two or more steps and provides a char surface capable of re-radiating significant amounts of entry heating to the atmosphere. The locations of this char-virgin material interface as well as the char surface at any time during vehicle entry (when combined with thermal environmental conditions) thus become important parameters in the characterization of a heat shield material for payload protection.

Emerson Electric Company, under the NASA, Langley Research Center, Contract NAS 1-5342, has investigated the feasibility of utilizing a nucleonic technique to provide simultaneous inflight measurements of these locations. Figure 1 shows one of the prototype Radioactive-Type Dual Ablation Measuring Systems fabricated to perform these measurements. (The scale in this picture indicates inches.)

1.2 Background

Past methods applicable to charring ablators provided step or event type measurement of either the char-virgin material interface (the make wire-sensor which is not applicable to materials that are electric conductors in their virgin state) or the ablator surface (light-pipe and spring-wire type sensors). These methods are discussed in NASA TN D-3686, by Peter J. LeBel and James M. Russell, III.

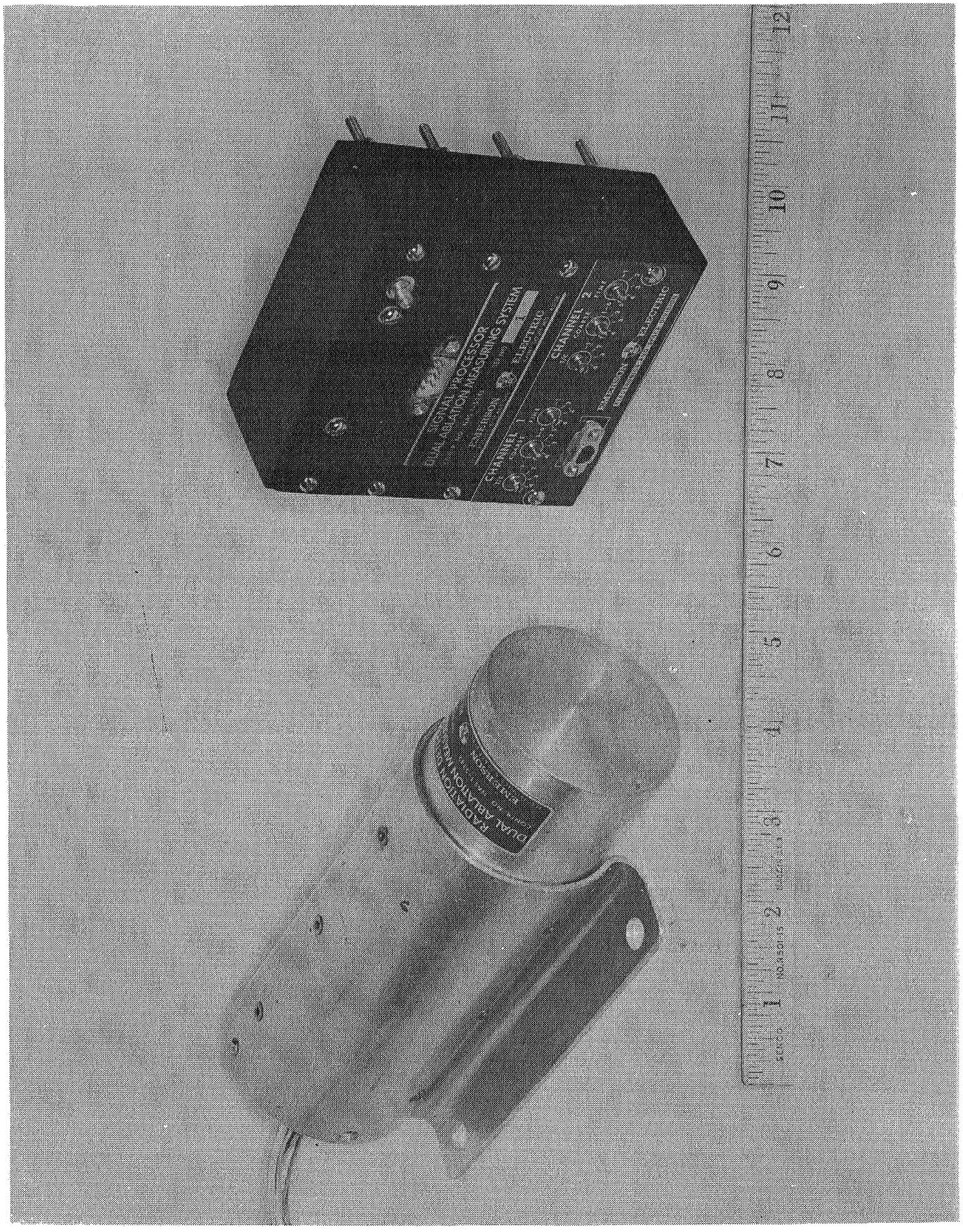

Figure 1. Radioactive-Type Dual Ablation Measuring System.

Two nucleonic techniques, capable of making continuous measurements of either surface (NASA TN D-3329, George W. Brandon) or virgin material-char interface recession (NASA TN D-3264, Wm. B. Davis), have been developed and are of note. These methods incorporate a radioactive compound into a suitable binder that is in turn enclosed in either an aluminum oxide or teflon tube. This tube is implanted in the parent heat shield. The recession of the tube is governed by the recession of the parent heat shield. Tube recession is monitored by detection of the decrease of radioactivity as the radioactive material within the tube decomposes and is exhausted overboard.

Other methods of monitoring heat shild recession have made use of thermocouples implanted in the parent heat shield material at known locations.

All of these methods implant a substantial foreign body or implement into the parent heat shield material at the precise location of the measurement being made. The question arises as to how much this foreign body affects the measurement being made.

Emerson Electric Company, under the NASA Contract NAS 9-2610, successfully developed techniques for homogeneously incorporating a radioactive compound into the parent Apollo heat shield material, AVCO 5026-39. The amount of radioactive material incorporated was less than .001 percent of the heat shield weight thus eliminating any perceptible changes in ablation characteristics of the parent heat shield material. Subsequent performance and environmental tests indicated that the location of the virgin material-char interface could be continuously measured with nucleonic techniques to within five per cent of its actual location, based on original thickness, over thermal environmental conditions simulating entry of the Apollo vehicle.

1.3 Contract Objectives

The overall objectives of this contract were investigation of the feasibility of a radioactive-type dual ablation measuring technique and the development of a prototype system. The system was to simultaneously measure surface and char interface recession, during ablation, of phenolic nylon and phenolic graphite heat shield materials. In order to meet these objectives, the following interim objectives had to be accomplished:

1.) Two radioactive chemical compounds compatible with the virgin and char phases of the two heat shield materials and gamma emitters at significantly different energy levels had to be selected.

2.) One of these compounds had to be selected such that its depletion rate, during ablation, corresponded to the recession rate of the heat shield material's char interfaces.

3.) The other compound had to be selected such that its depletion rate, during ablation, corresponded to the recession rate of the heat shield material's surfaces.

4.) Methods of homogeneously incorporating these compounds into the heat shield materials had to be determined.

5.) A radiation detector, compatible with specified environmental constraints, capable of discriminating between nuclear energy levels had to be developed.

6.) An electronic system had to be designed, tested, and fabricated that would detect, separate, and integrate pulses of the two different energy levels from the radiation detector and supply outputs in a form compatible with either recording or telemetry systems.

7.) Sufficient test data to prove correct system operation had to be obtained.

1.4 Scope of Report

System theory of operation, development, testing, and calibration are described herein. In addition flight mission requirements are presented for a given mission. Recommendations are made for future proof testing. The appendix volume to this report contains detailed supporting test data, checkout and fabrication procedures, and operating procedures. Circuit schematics and assembly drawings are included in a separate package.

2.0 ABLATION SENSING TECHNIQUE

2.1 General

The Radioactive-Type Dual Ablation Measuring System consists of three main components:

1. Ablation Sensor Plug
2. Radiation Detector
3. Signal Processor

as indicated on system block diagram of Figure 2. The system makes use of the chemical and nuclear properties of two radioactive chemical compounds, uniformly incorporated into the Ablation Sensor Plug, chosen as ablation indicators. The compounds emit gamma photons of different nuclear energy levels. The Radiation Detector detects the gamma emission from the chemical compounds and converts each detected disintegration into an electronic pulse. The pulse magnitude is proportional to the detected energy level of the emitted photon. The Signal Processor discriminates between the incoming pulse energy levels and creates output D.C. voltages proportional to the incoming frequency of pulses of the two levels.

2.2 Ablation Sensor Plug

A cylindrical Ablation Sensor Plug .25 inch diameter by 1.00 inch long was chosen as standard configuration for the performance of this contract because of ease of manufacture. It should be recognized that any rectangular or cylindrical shape may be chosen; the size depends on the range of thickness measurements to be made. The Ablation Sensor Plug is fabricated of the parent heat shield material. During fabrication, radioactive chemical compounds are homogeneously incorporated into the sensor plug. For porous heat shield materials, such as phenolic nylon, the radioactive materials may be impregnated into a completed sensor plug. For dense heat shield materials, such as phenolic graphite, better results are obtained if the radioactive

compounds are mixed into the uncured material before fabrication. Completed sensor plugs suitable for use on flight missions contain less than .01 percent by weight of radioactive indicators. The radioactive Ablation Sensor Plug is then installed in a vehicle heat shield in the location where the ablation measurements are to be made.

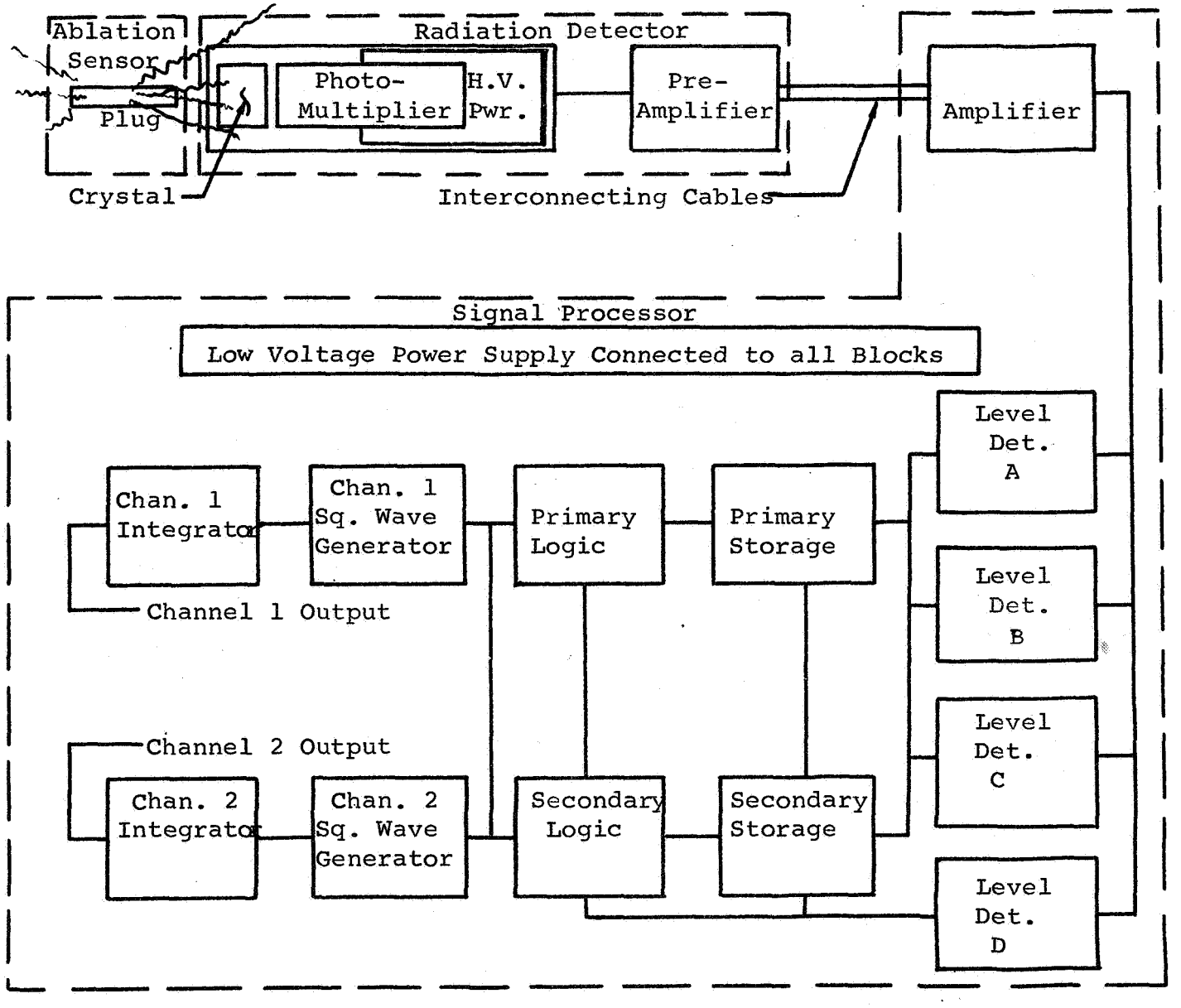

Figure 2. Dual Ablation Measuring System Simplified Block Diagram

The radioactive compounds are chosen as ablation indicators in the following manner. One compound, total recession indicator, is chosen to have a decomposition temperature equal to or above the highest char surface temperature expected for the ablation material. Thus it will remain in the char layer until oxidized or physically eroded from the char surface. The total amount of this compound present is a measure then of the total heat shield thickness. The second compound, virgin material recession indicator, is chosen so that its decomposition temperature is the same as the decomposition temperature of the heat shield virgin material. The decomposition products of this compound percolate through the char layer and are exhausted into the free stream. Thus the amount of this compound present provides a measure of heat shield virgin material thickness.

Both of these compounds are radioactive gamma emitters. Gamma rays will penetrate vehicle substructures of reasonable thickness with little attenuation, thus no access to the sensor plug need be provided from the vehicle interior. The indicator compounds must be chosen so that their gamma emission spectra may be readily discriminated from one another. An additional consideration is that the isotopes' half lives should be long enough to be still useable after unforeseen delays and the checkout time normally encountered during vehicle launch operations.

After correction for gamma spectrum overlap and Compton scatter, the frequency of gamma emissions at one energy level will be proportional to the amount of total heat shield thickness indicator present (thus total heat shield thickness), while the frequency of gamma emissions at a second energy level will be proportional to the amount of virgin heat shield material thickness indicator present (thus virgin heat shield material thickness).

2.3 Radiation Detector

The purpose of the Radiation Detector is to detect the gamma photons, of two different energy levels, given off by the Ablation Sensor Plug and supply an electronic pulse to the Signal Processor for each detected photon proportional in amplitude to the energy level of the detected photon. The Radiation Detector consists of a Cesium Iodide scintillation crystal coupled to a ruggedized (Venetian Blind type dynode) photomultiplier tube. The package contains a high voltage power supply wrapped around the photomultiplier tube.

Each gamma photon absorbed, wholely or partially, by the scintillation crystal causes the emission of a visible light photon. The intensity of this light photon is directly proportional to the energy lost by the incident gamma photon during its passage, or absorption, through the scintillation crystal. The photomultiplier tube senses the light burst and emits a current pulse proportional to the intensity of the light scintillation which is passed to accompanying circuitry.

Thus the Radiation Detector will supply pulses to the Signal Processor proportional in magnitude and equal in frequency to the gamma disintegrations occurring at the two primary energy levels of the radioisotopes incorporated into the Ablation Sensor Plug.

2.4 Signal Processor

Layout of the Signal Processor may be understood by reference to the Simplified Block Diagram of Figure 2. Pulses from the Radiation Detector first go through a Pre-Amplifier, physically connected to the Radiation Detector. The Pre-Amplifier isolates the following cable and circuit loading from the photomultiplier tube and affixes a known capacitance across the tube output.

These pulses are then fed into an Amplifier. The Amplifier amplifies the signal to a level compatible with the following Level Detector stages.

There are four discriminators or Level Detectors. Level Detector A passes pulses greater than A and less than B for further processing and subsequent output in Channel 1. Pulses less than A are rejected. Level Detector B passes pulses greater than B but less than C for further data processing and subsequent output in Channel 2.

Level Detector C rejects pulses greater than C. Level Detector D operates on the tail of pulses that were passed by the other detectors and operates a Toggle. The Toggle selects the storage elements in which data is to be temporarily stored. Operation of the Level Detectors is shown in the simplified sketch of Figure 3.

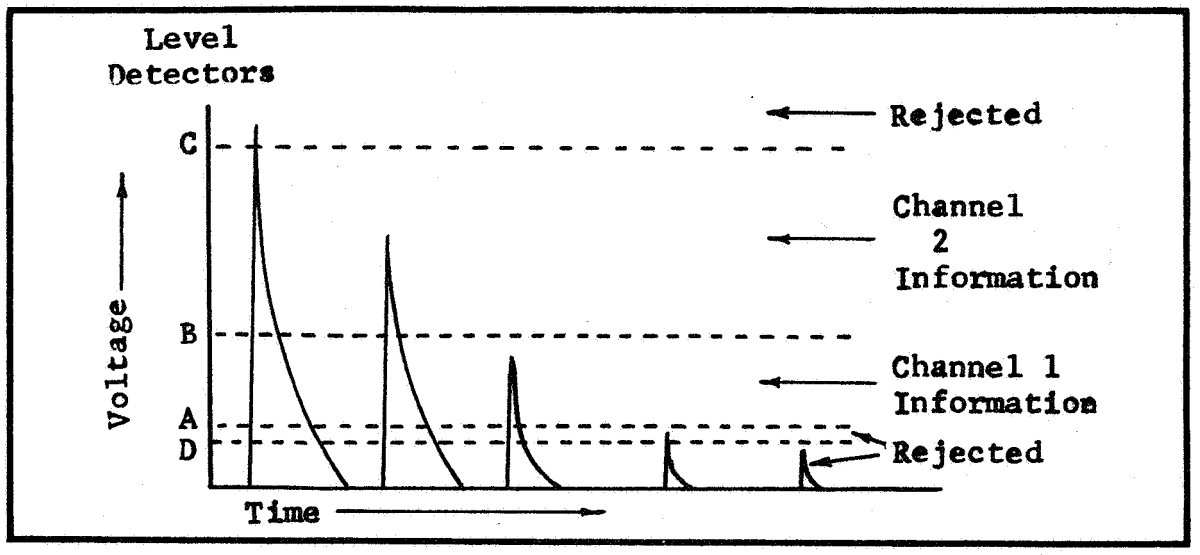

Figure 3. Simplified Sketch of Pulse Train From Amplifier into Level Detectors.

The primary and secondary Storage Elements store incoming pulse data for subsequent read out upon command by the Toggle activated by the tail of the incoming pulse detected by Level Detector D.

The Logic circuits select, by command from the Toggle, which set of storage elements are to be read out.

The one-shot Pulse Generator creates a square wave pulse of known area and magnitude for each incoming pulse from the respective Logic circuits.

The Integrators sum the pulses from the Pulse Generator into a capacitor. Outputs from the Integrators are D.C. voltages proportional to the frequency of pulses coming into the particular channel.

The Signal Processor has no provision to monitor background radiation. The nominal settings of the Level Detectors A and C are .10 and .85 Mev., respectively. These settings detect gamma rays only between the .10 and .85 Mev. energy levels. Background radiation outside of this corridor is rejected. It is believed that the count rate caused by background radiation in this energy corridor would be insignificant when compared to the count rate caused by millicurie flight levels of activity. In support of this belief, insignificant amounts of background radiation in this corridor were detected throughout the ablation testing phases of this contract.

Thus, a provision to monitor radiation background was not included in the Signal Processor.

3.0 SYSTEM DEVELOPMENT

3.1 Design Guidelines

The Dual Ablation Measuring System was designed to continuously measure the recession of both the material surface and char-layer interface of phenolic nylon and phenolic graphite heat shield materials and to be compatible with the performance and environmental requirements of advanced research rocket vehicles such as the NASA's Pacemaker. Design guidelines for the system are presented in Figures 4 and 5 .

	Maximum	Minimum
Ablation material thickness (inches)	2.00	0.25
Virgin material thickness (inches)	2.00	0.25
Char layer thickness (inches)	0.50	0.00
Surface Temperature (^{o}F)	5000	1500
Char Interface Temperature (^{o}F)	1300	750
Isotope Half Life (days)	--	50
Heat shield substructure thickness (Inches of Tungsten alloy Kennertium W2)	0.75	0.00
Size (excluding detector) (in^3)	31.0	--
Weight (excluding detector) (lbs)	1.50	--
Power Required (watts at 28 volts)	1.70	--
Output Impedance (Ohms)	1000	--
System Output: Analog voltage proportional to input count rate. 5 volts maximum.		
Accuracy: System output tracks input count rate within five percent over a range of Ablation rate of 0 to .25 in/sec at a max. rate of change of 0.04 in/sec^2.		

Figure 4 - General Design Guidelines for Dual Ablation Measuring System.

Environment	Specification	Test
Vibration Sinusoidal Random	 15g rms 20-200 cps 25g rms 200-2000 cps 25g rms 20-2000 cps	 3 axes 2 octaves/min. 120 seconds, 3 axes
Acceleration Shock	100g 150g	120 seconds, 6 axes 5-15 milli-seconds, 6 axes
Temperature (Except Detector) (Detector including insulation)	20°F to 160°F 20°F to 200°F	20° steps, 30 min at each step. 20° steps, 30 min at each step. 10 min. at each 20° step above rating of detector.
Altitude	Vacuum equivalent to an altitude of 300,000 feet	30 Min. at 300,000 Ft. 10 min. descent to ground level.

Figure 5 - Environmental Design Guidelines for Dual Ablation Measuring System.

3.2 Sources of Error

3.2.1 General. The Dual Ablation Measuring System is designed to perform a dynamic measurement of a continually decreasing random disintegration rate of radionuclides. Possible sources of error, therefore, fall into three distinct regions: (1) Those errors caused by averaging a random process, (2) Linearity errors, and (3) Tracking errors. A closer look at these possible sources of system errors follows.

3.2.2. Statistical Errors. The errors inherent in averaging a random event are called Statistical errors. The one sigma statistical error, in percent, is defined by the following equation:

$$\text{One sigma statistical error} = 100\ n^{-\frac{1}{2}}$$

Where n is the input counts per time, or integration, constant. The output of the Dual Ablation Measuring System fluctuates around a mean value. The amount of fluctuation is defined by the one sigma statistical error of the particular count rate being integrated. Sixty seven percent of the time the instantaneous output value will be within one sigma of the mean. To minimize output fluctuation, either the count rate must be increased or the system time constant must be increased.

3.2.3. Linearity Errors. Electronic system linearity errors, if present, will be calibrated out by the techniques, presented later, for system calibration.

The linearity of incorporation of radioisotopes into Ablation Sensor Plugs is the prime linearity error that cannot be neglected. Past experience indicated that the limit of linear incorporation of isotopes, by the present techniques, was the inherent local density variation of the parent heat shield material. Measurements were taken of the homogenity of radioisotope incorporation into the phenolic nylon and phenolic graphite heat shield materials used during this contract. Indications were that a linear distribution was obtained plus or minus two percent for the majority of the Ablation Sensor Plugs. It is felt that this linearity may be obtained repeatedly if the techniques of radioisotope incorporation presented in Volume II are followed.

3.2.4 Tracking Errors. The Dual Ablation Measuring System must integrate detected radionuclide disintegration over a finite period past in time. The period is called the system time constant and is defined as the time required for the system output to respond to sixty-three percent of an instantaneous step change in input. Thus system output must lag the instantaneous input by an amount equal to approximately one-half the system time constant. The lag may be decreased by decreasing the system time constant. A decrease in time constant will increase statistical fluctuation, as previously discussed. Therefore, a trade-off exists between desired output fluctuation and speed of system response. This trade-off must be carefully considered when determining requirements for a particular mission. A specific example of the trade-off is considered later under flight mission requirements.

3.3 Source Development

3.3.1 General. Two radiation sources, uniformly incorporated into the Ablation Sensor Plug, are used for the Dual Ablation Measuring System. One source, Indium tri-Chloride in which In^{114m} is the radioisotope, was selected since it depleted at the same rate as the ablative materials' virgin phases. The second source, Zirconium Niobium Oxalate in which $ZrNb^{95}$ is the radioisotope, was selected since it depleted at the same rate as the ablative materials' char surface recession.

Before the selection and use of these particular compounds, other possible compounds were studied in detail. After selection, methods were established to uniformly incorporate the compounds into the parent ablative materials. Criteria for selection, methods of incorporation, and results obtained are presented in the following sections along with pertinent data on the isotopes chosen.

3.3.2 Isotope Selection Criteria. The criteria for selection of the two radioactive compounds were:

1. One compound decomposes at decomposition temperature of the virgin materials, the other will not decompose until oxidized or eroded from the char surface.
2. Compounds must be gamma emitters to penetrate vehicle substructure.
3. Nuclear radiation from the compounds must be sufficiently different to allow discrimination.
4. Commercially available.

Lists of candidate Surface Recession Indicators and Char Interface Recession Indicators were prepared of commercially available radioactive compounds that decomposed in the temperature regimes of interest. These candidate compounds are presented in Figure 6 and Figure 7.

Chemical Compound	Phase Change Temp (°F)	Radio-isotope	Isotope Half Life	Principal Gamma Radiations	
				Energy (Mev)	Abundance (%)
NbC	7000	Nb^{95}	35 days	.77	95
NbO	3800	Nb^{95}	35 days	.77	95
ZrC	6350	Zr^{95}	65 days	.76	43
				.72	55
ZrO	4900	Zr^{95}	65 days	.76	43
				.72	55
CeC	6150	Ce^{144}	285 days	.13	20
EuC	5780	Eu^{152}	--	Many	--
TaC	7010	Ta^{182}	115 days	.10	56
				1.12	61

Figure 6. Candidate Surface Recession Indicators.

Chemical Compound	Phase Change Temp (°F)	Radio-isotope	Isotope Half Life	Principal Gamma Radiations	
				Energy (Mev)	Abundance (%)
NH_4I	750-1025	I^{125}	60 days	.035	100
		I^{131}	8 days	.36	80
NaI	1140	I^{131}	8 days	.36	80
Hg_2Cl_2	750	Hg^{197m}	23 hours	.13	31
HgS	1080	Hg^{197}	65 hours	.08	29
		Hg^{203}	47 days	.28	83
$FeCl_2$	1100	Fe^{59}	45 days	1.29	43
				1.10	57
$InCl_3$	825	In^{114m}	50 days	.19	20
$ScCl_3$	1000	Sc^{46}	84 days	1.12	100
				.89	99
$CoCl_3$	1500	Co^{60}	5.3 years	1.17	100
				1.33	100
SeO_2	800	Se^{75}	120 days	.40	25
				.27	100
				.13	94

Figure 7. Candidate Char Interface Recession Indicators.

The next step was to perform a Thermogravimetric Analysis (TGA) and Differential Thermal Analysis (DTA) on both the phenolic nylon and phenolic graphite heat shield materials. The purpose of these tests was to determine the decomposition temperatures of each of the heat shield materials. These tests were performed on the Deltatherm Analyzer shown in Figure 8.

A Thermogravimetric Analysis (TGA) records the weight of a specimen, by means of a Cahn electrobalance, enclosed in a furnace programmed to increase temperature at a specified rate.

A Differential Thermal Analysis (DTA) measures the difference in temperature between a reference material, Al_2O_3, and the material of interest as they are both heated in a furnace, at a programmed known rate. Al_2O_3 has a linear response to the temperatures in the furnace. Departure of the material of interest from a linear temperature response is magnified by the differential measurement and recorded. A departure indicates a crystal rearrangement or phase change, of the material of interest, that either liberates or absorbs heat.

The results of these tests indicated that both heat shield materials initiated decomposition in the neighborhood of 800°F. The results obtained with phenolic graphite are presented in Figure 9, Thermogravimetric Analysis of Phenolic Graphite, and Figure 10, Differential Thermal Analysis of Phenolic Graphite, and were similar for both heat shield materials.

These results were also similar to those obtained under the previous NASA Contract, NAS 9-2610, where a radioactive indicator compound was provided to measure the virgin material recession of AVCO 5026-39 heat shield material. The decomposition temperature of the AVCO heat shield material was in the same regime.

Previous experience with the AVCO heat shield material indicated that compounds that decomposed above 1000°F, such as Scandium Chloride ($ScCl_3$), depleted at a rate slower than the heat shield virgin material. A compound such as Ammonium Iodide (NH_4I), which decomposes in the regime of interest, has a very weak gamma ray. Thus Indium Chloride ($InCl_3$), which decomposes at 825°F, would probably work as a virgin material recession indicator for phenolic nylon and phenolic graphite. In^{114m}, the radioisotope of Indium Chloride, emits gamma rays primarily at .19 Mev. Thus a char surface indicator that could be discriminated from In^{114m} should be chosen from isotopes that emit primarily above .3 Mev.

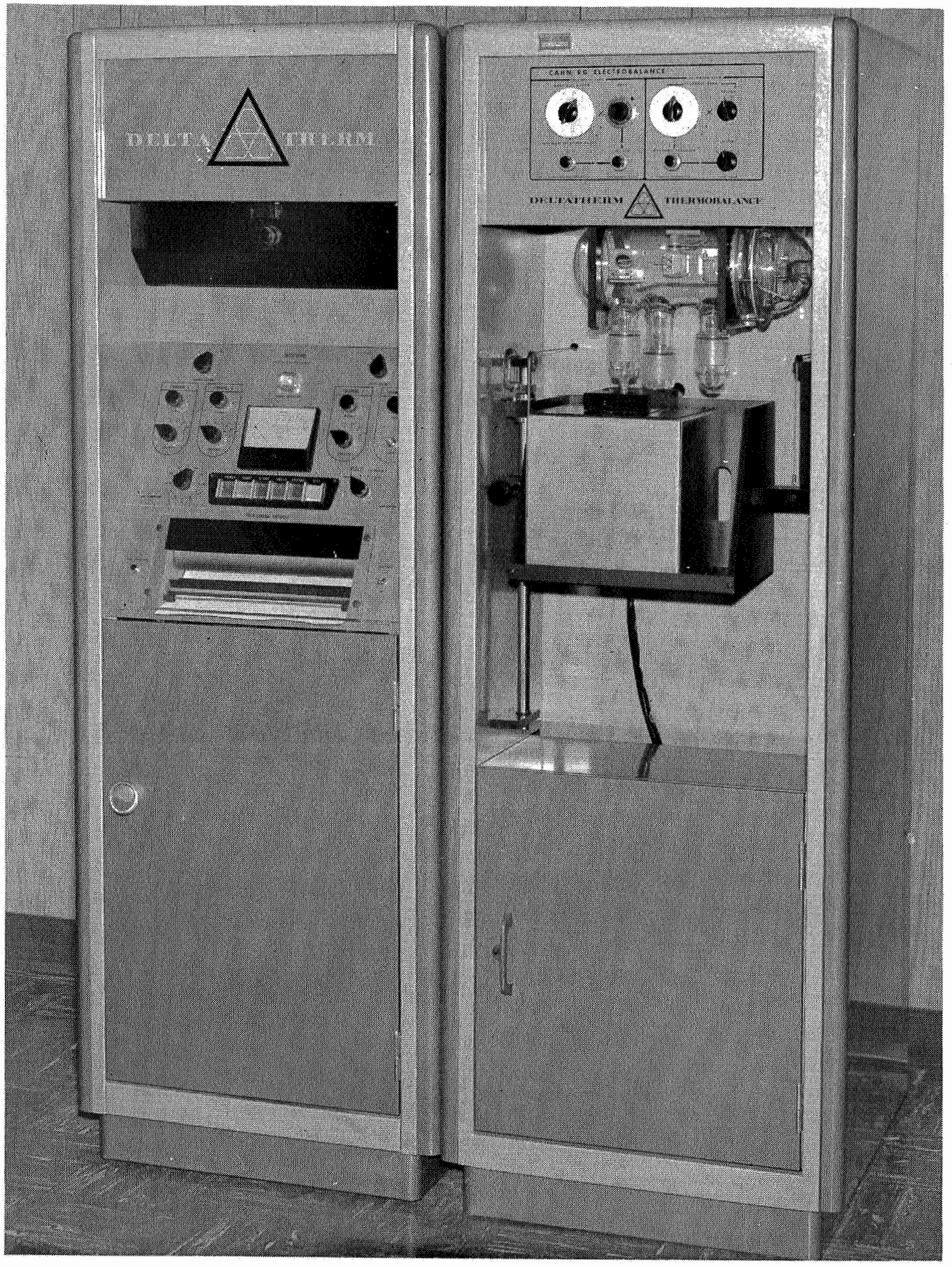

Figure 8. Deltatherm Thermal Analyzer.

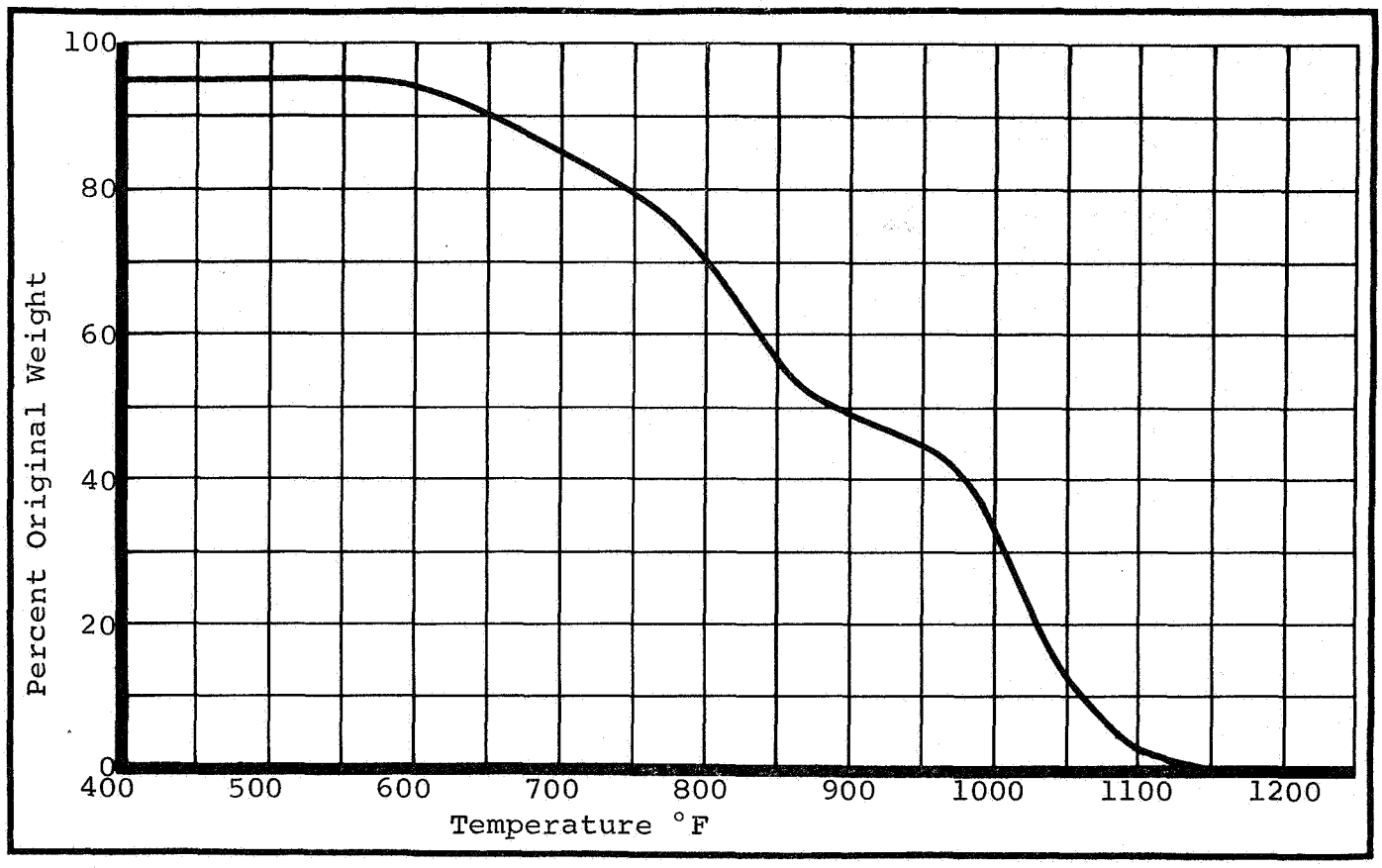

Figure 9. Thermogravimetric Analysis of Phenolic Graphite.

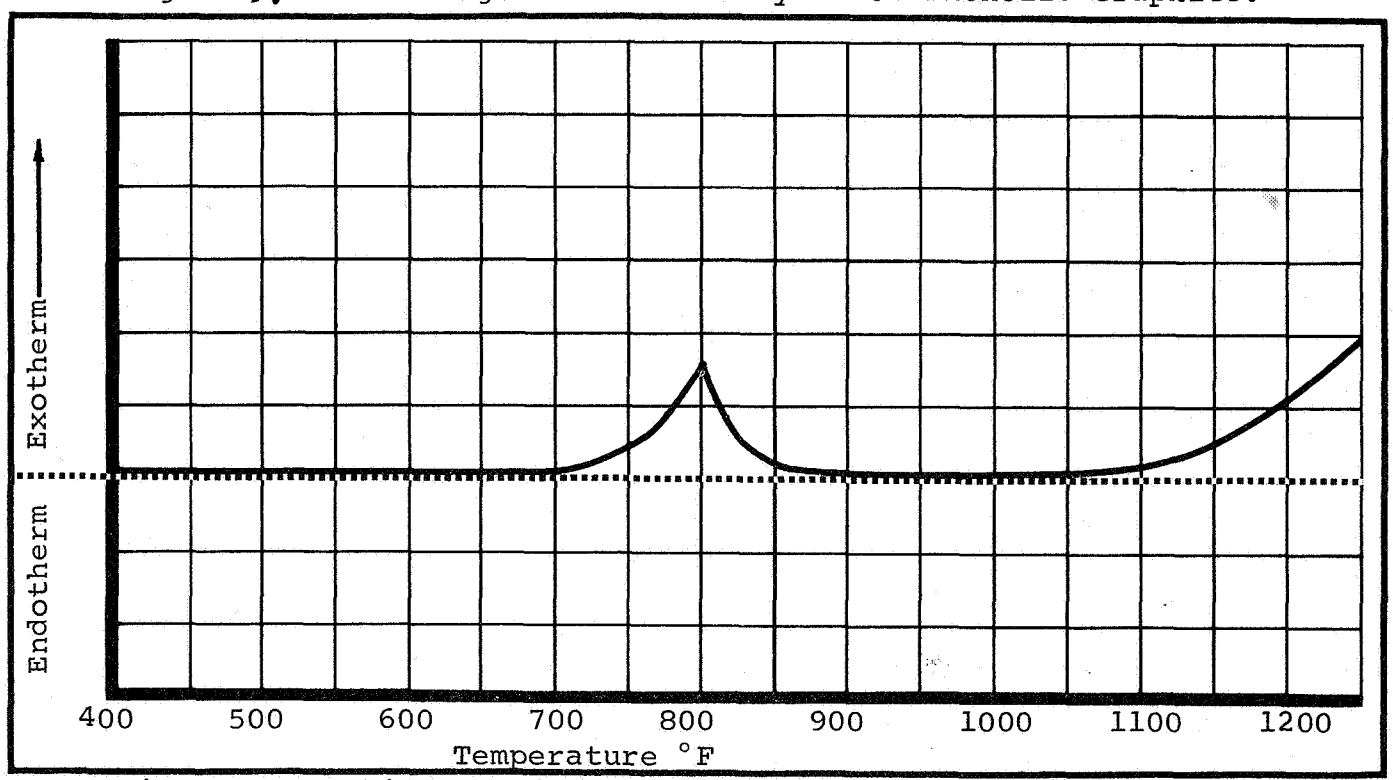

Figure 10. Differential Thermal Analysis of Phenolic Graphite.

The various compounds of Zirconium (Zr) and Niobium (Nb) thus appeared attractive as surface recession indicators. These compounds all decompose at high temperatures and the primary gamma radiation occurs at .75 Mev. Thus Zr and Nb in conjunction with In appeared attractive from both the nuclear and the chemical viewpoints. The commercially available compound of Zirconium is $ZrNb^{95}$, Zirconium Niobium in an oxalate complex. The ZrNb elements appear together since the Nb^{95} is a daughter product of the decay of Zr^{95}. At equilibrium the compound decays with the half life of the parent Zr^{95}, 65 days.

The decay schemes of the isotopes $ZrNb^{95}$ and In^{114m} are presented in Figure 11, Nuclear Decay Schemes of $ZrNb^{95}$ and In^{114m}.

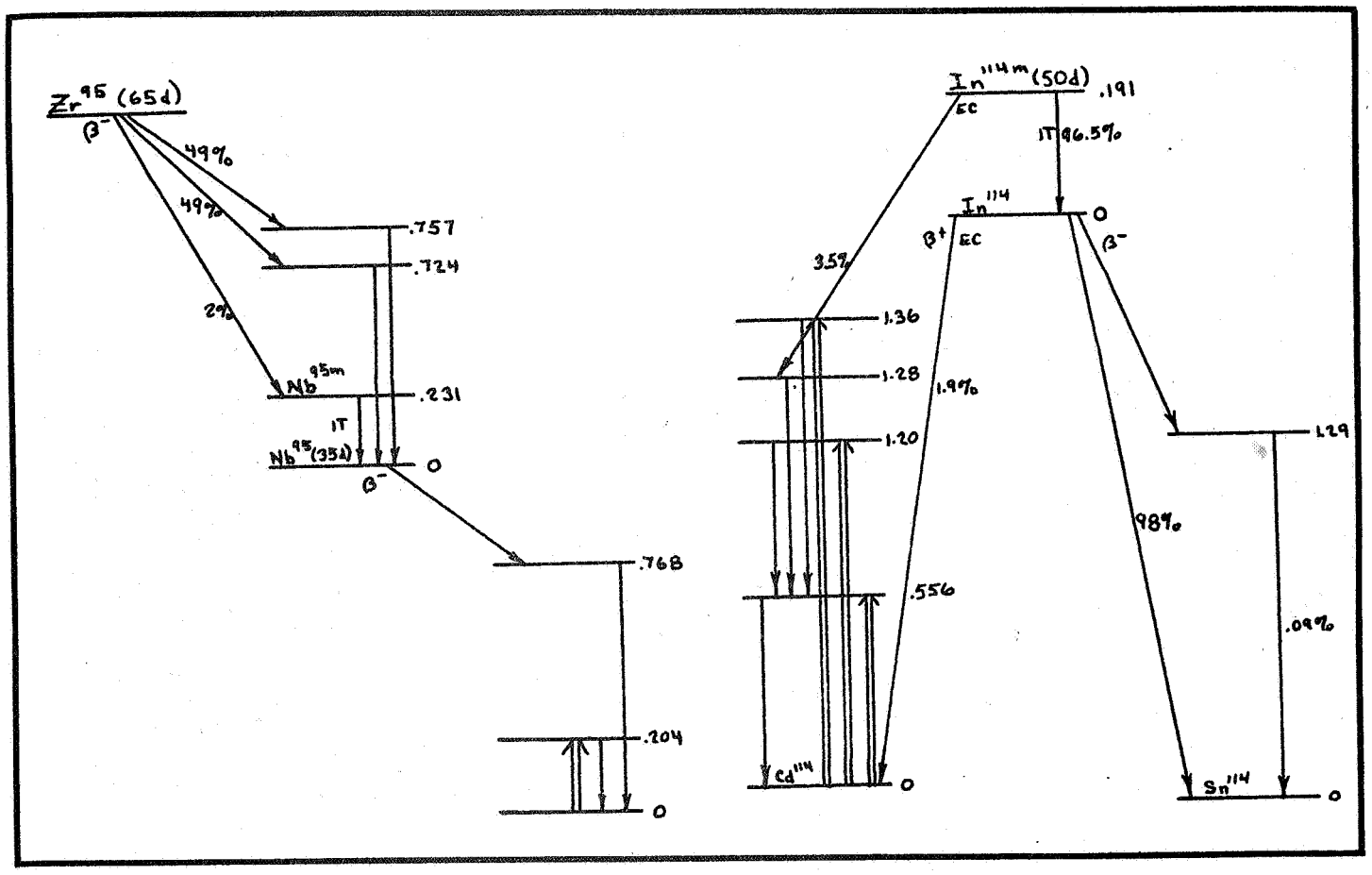

Figure 11. Nuclear Decay Schemes of $ZrNb^{95}$ and In^{114m}.

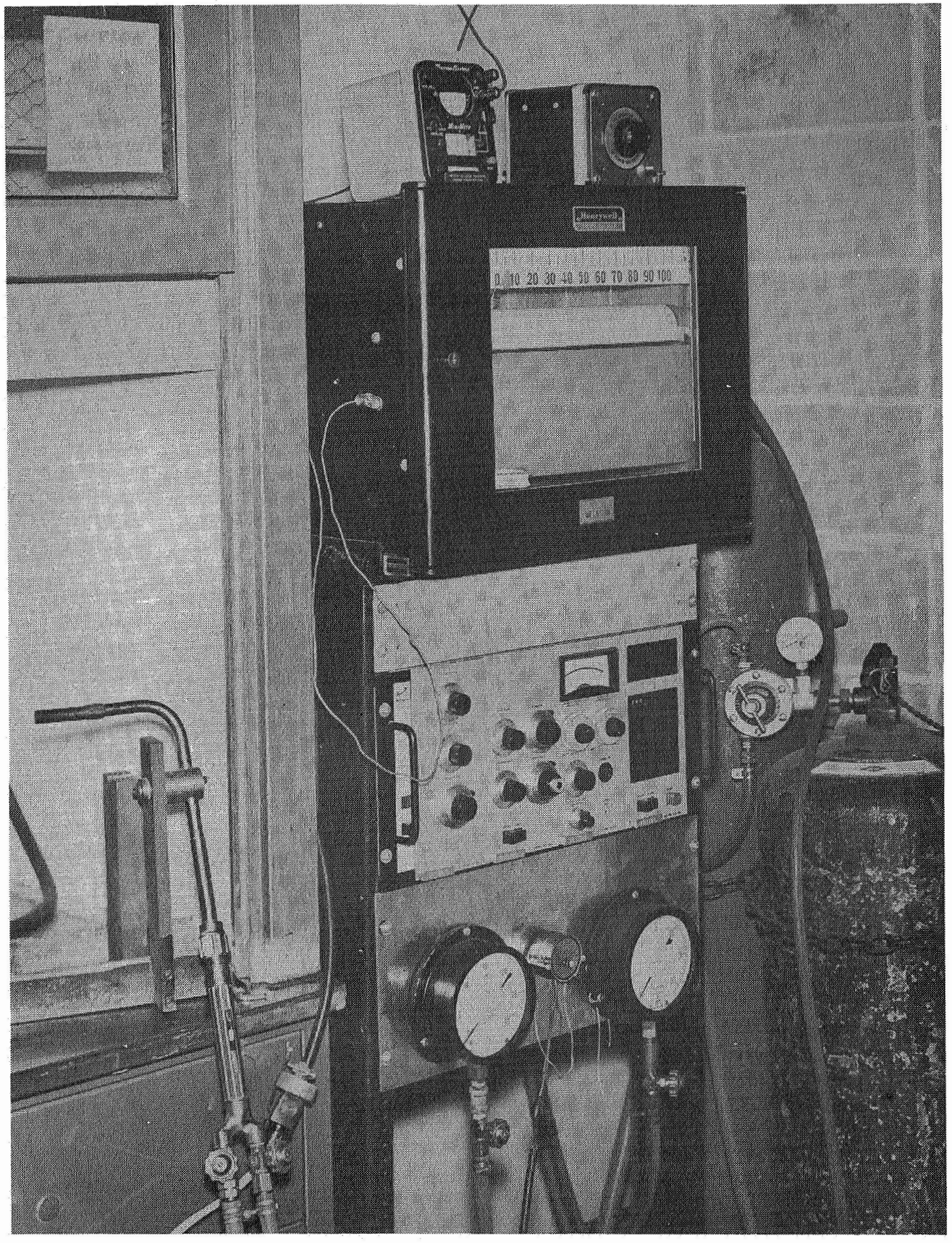

Figure 12. Laboratory Nuclear Counting Equipment.

In the decay scheme of $ZrNb^{95}$ gamma rays are emitted for 95% of the nuclear disintegrations. The .19 Mev gamma from In^{114m} is emitted in only 23% of the nuclear disintegrations. Thus approximately four times as much In^{114m} activity must be introduced into a sensor plug to obtain the same integral count rate as from a given quantity of $ZrNb^{95}$. Gamma ray spectra of In^{114m} and $ZrNb^{95}$ were taken with the single channel analyzer of Figure 12 Laboratory Nuclear Counting Equipment. This equipment consists of:

1. A scintillation probe (Nuclear Chicago, Model DS8-20) containing a ½ inch diameter by 3/4 inch NaI(Tl) crystal, coupled to a 10 stage 3/4 inch diameter photomultiplier tube and preamplifier.

2. A single channel analyzer constructed from RIDL plug-in units containing scaler and ratemeter units.

Figure 13. Superimposed Gamma Ray Spectra of $ZrNb^{95}$ and In^{114m}, presents the gamma ray spectra obtained from an In^{114m} source four times the strength of the $ZrNb^{95}$ source.

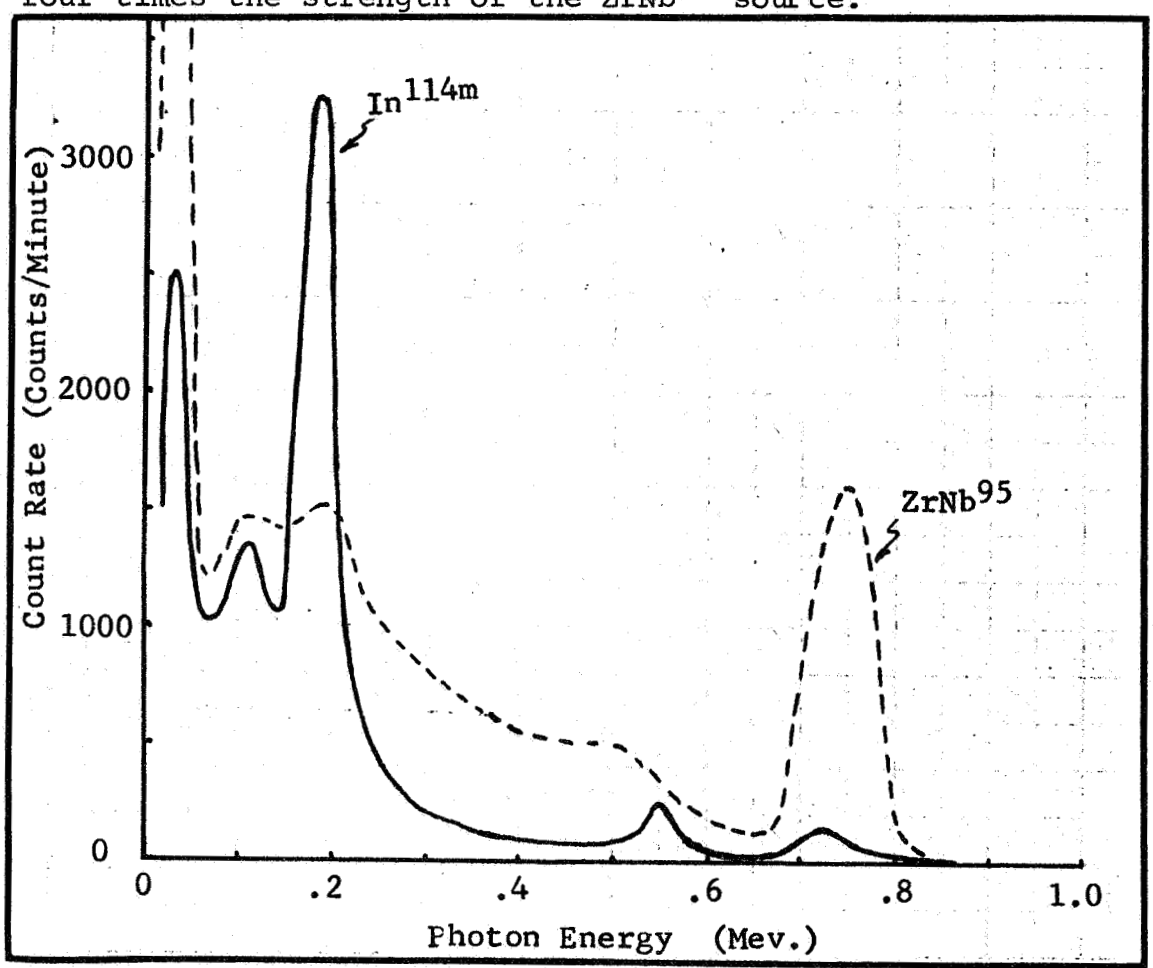

Figure 13. Superimposed Gamma Ray Spectra of $ZrNb^{95}$ and In^{114m}.

Figure 13 spectra indicate that from the nuclear standpoint the radiations of $ZrNb^{95}$ and In^{114m} may be discriminated between after the mutual overlaps are accounted for.

3.3.3 Isotope Selection Tests. Initial measurements indicated that satisfactory preliminary methods had been established to uniformly mix radioisotopes into uncured phenolic graphite and to uniformly impregnate radioisotopes into phenolic nylon.

The DTA and TGA analyses indicated that both heat shield materials decomposed in the same temperature regime as Avco 5026-39 heat shield material. Measurement of the char layer interface of Avco 5026-39 was previously demonstrated, by Emerson, under contract NAS 9-2610. Indium Chloride was used as an indicator compound during this previous contract. No measurements of the total heat shield thickness were required.

Initial tests during this present contract were performed to determine a suitable refractory radioindicator that would provide a measure of total heat shield thickness. Ablation tests were performed in the oxygen-acetylene jet fixture of Figure 14. Ablation tests performed with $ZrNb^{95}$ Oxalate indicated that the amount of this radioisotope remaining in the Ablation Sensor Plug at the end of test as determined by laboratory nuclear counting equipment (a scaler), provided a suitable measure of total heat shield thickness as measured with micrometer calipers. The average end point thickness from isotope data agreed with the physically measured thickness within plus or minus .03 inches. Total heat shield thickness was the only measurement attempted during this "Surface Recession" test series.

Raw data and reduced test results, as well as data on uniformity of incorporation of the radioisotope $ZrNb^{95}$, for this test series is presented in Volume II.

The next test series incorporated both $ZrNb^{95}$ and In^{114m} into the test Ablation Sensor Plugs. The purpose of this test series was twofold: (1) Demonstrate that $InCl_3$ would provide a measure of virgin material remaining, and (2) Demonstrate that both total heat shield thickness and virgin material remaining could be measured on the same Ablation Sensor Plug.

The results from this ablation test series indicated that the amount of $InCl_3$ remaining provided a measure of virgin material

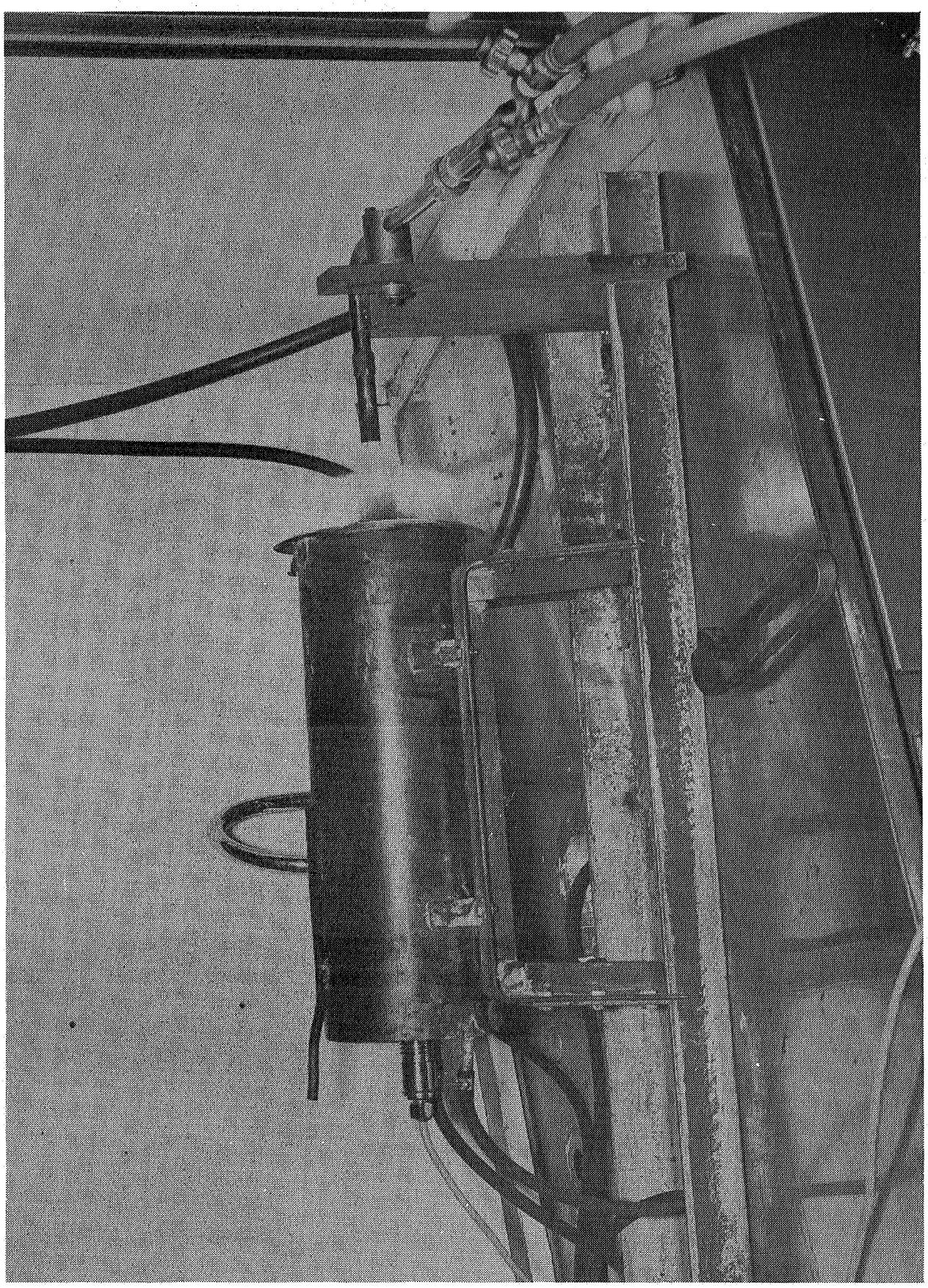

Figure 14 Oxy-Acetylene Jet Fixture.

thickness for both heat shield materials. The results also indicated that it was possible to measure both total heat shield thickness and virgin material remaining on the same Ablation Sensor Plug.

Agreement between the average sensor end point and physical measurements was slightly less than plus or minus .03 inches for these tests.

Data from these tests is presented in full in the Appendix, Volume II.

The chemical compounds $In^{114m}Cl_3$ and $ZrNb^{95}$ oxalate, when incorporated into Ablation Sensor Plugs, thus fulfilled the criteria for surface and virgin material recession indicators on both phenolic nylon and phenolic graphite heat shield materials. The gamma radiations from each were readily discriminated, with laboratory counting equipment, and were of sufficiently high energy to penetrate most vehicle substructures with minimal attenuation. These compounds were selected as indicators for the remainder of the program.

3.3.4 Preparation. Phenolic nylon heat shield material was obtained from the NASA cured, in the form of a billet 4" thick by 12" diameter. The phenolic nylon used during this program had a bulk density of 36 pounds per cubic foot. The composition by weight was 25 percent phenolic resin (Union Carbide type BRP-5549), 40 percent nylon powder (DuPont type Zytel 103) and 35 percent microballoons (Union Carbide type BJO-9030).

Inactive Ablation sensor plugs were machined directly from the billet. The sensor plugs were .25 inch diameter by 1.8 inches long. The porosity of phenolic nylon made it possible to vacuum impregnate the sensor plugs with radioactive solutions. After subsequent drying, the radioactive isotopes remained in the sensor plugs, while the carrier solution, water, was vaporized away. The next step was to trim the sensor plug to 1.00 inch length overall by cutting off both ends, which contained a greater concentration of radioisotopes than did the uniform center of the plug. All procedures with radioactive solutions

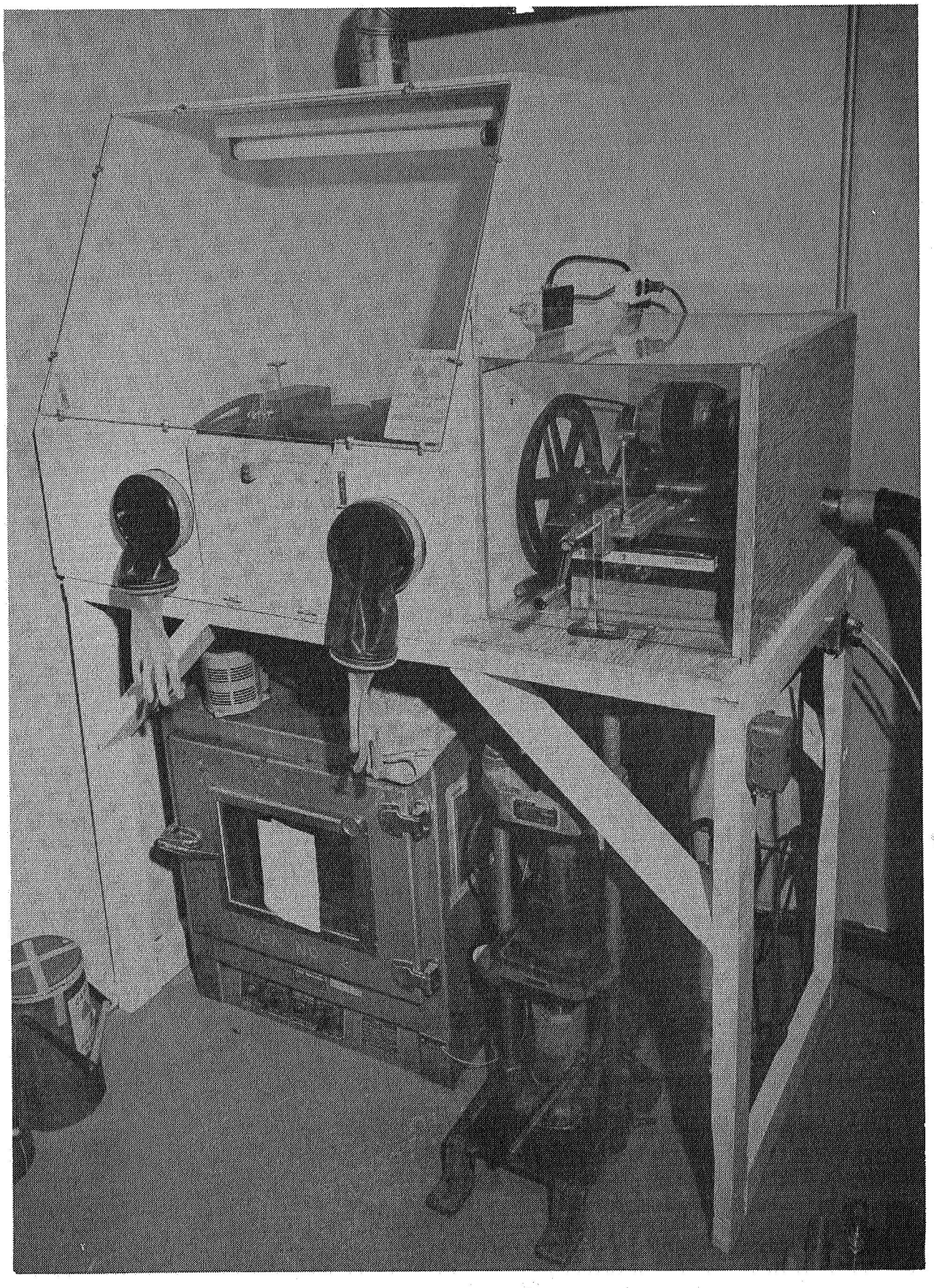

Figure 15 Glove Box for Handling Radioactive Materials.

were carried out in the glove box of Figure 15. Ablation Sensor Plugs were machined to 1.00 inch final length in the saw fixture of Figure 16.

Preliminary experiments indicated that the cured phenolic nylon sensor plugs would absorb 62 percent of their weight of water when vacuum impregnated. A one inch long sensor plug of phenolic nylon ½ inch in diameter weighs .462 gm. Sixty two percent of this is .287 gm or .287 cm^3 of water. Therefore, the radioactive impregnating solutions were mixed so that .287 ml of solution contained the amount of radioisotopes that were desired to be incorporated into a completed 1.0 inch long sensor plug.

The method used to mix, impregnate, dry, and machine phenolic nylon sensor plugs was the same whether one or ten sensor plugs were impregnated at a time. When ten sensor plugs were impregnated at a time a 70 milliliter straight sided glass vial was used as the impregnating vessel. When only one sensor plug was impregnated, a 5 milliliter cylindrical graduate was used as the impregnating vessel. During impregnation the impregnating vessel was contained in a covered 500 milliliter reaction kettle equipped with a stopcock and connected to a vacuum line. An example of the entire procedure is contained in the Appendix Volume of this report.

The phenolic graphite heat shield material was obtained in the raw (uncured) state. The phenolic graphite used during this program was Narmco 4028. Narmco 4028 is a carbon fiber reinforced heat shield material consisting of 50 percent, by weight, phenolic resin and 50 percent ¼ inch long carbon fibers. The bulk density of a molded piece is 87 pounds per cubic foot. The uncured phenolic graphite was stored at 40°F until use to prolong its shelf life.

The relatively high density of phenolic graphite made it impractical to try to incorporate the radioactive compounds into a finished ablation sensor plug by vacuum impregnation. For this reason the radioactive compounds were mixed into the uncured material. The material was dried under vacuum at room temperature. The radioactive compounds remained in the uncured material and the carrier solution, water, vaporized off. A disk was then molded from which sensor plugs were machined. Each disk, from an available two inch I.D. mold, yielded six sensor plugs. Figure 17 shows a picture of the lathe equipped to machine radioactive Ablation Sensor Plugs.

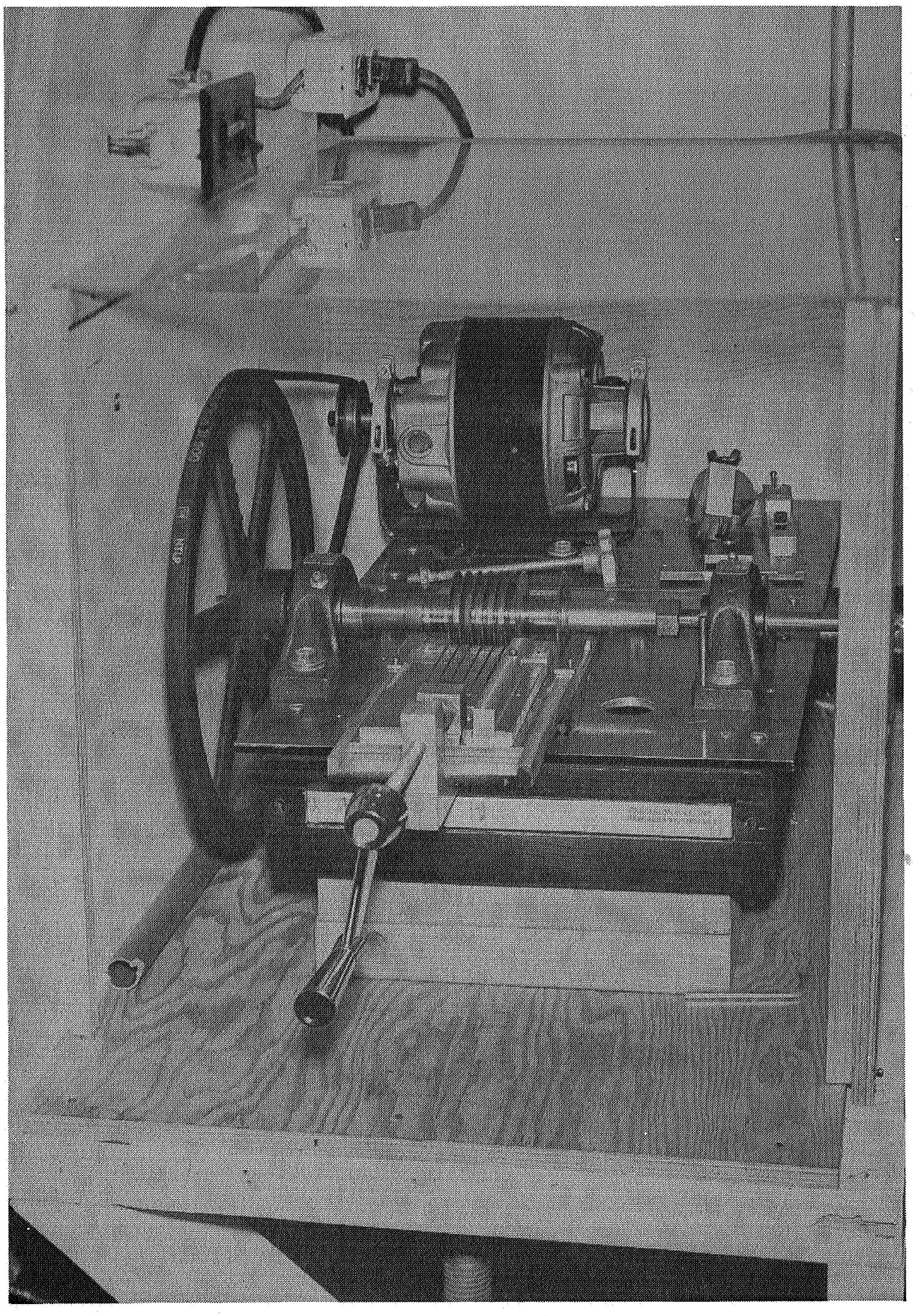

Figure 16. Saw Fixture for Machining Ablation Sensors.

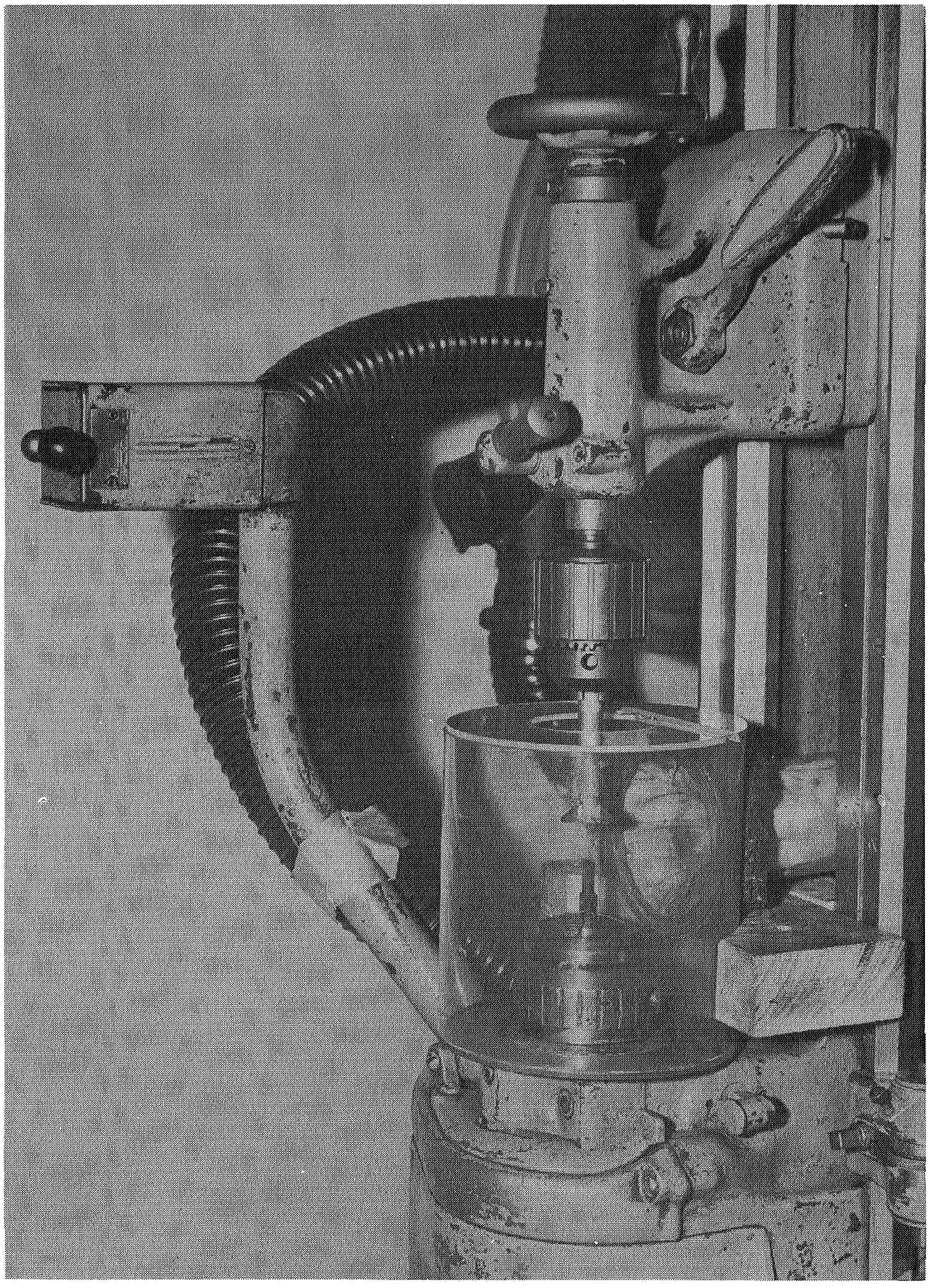

Figure 17 Lathe Equipped to Machine Ablation Sensors.

An example of the entire procedure is contained in the Appendix, Volume II, of this report.

3.3.5 Uniformity Measurement. The uniformity with which radioactive ablation indicator compounds can be incorporated into an Ablation Sensor Plug directly influences system measurement accuracy. For this reason various modifications of the basic methods of incorporating the radioactive compounds into an Ablation Sensor Plug were tried. The techniques that yielded the most uniform results were standardized and used throughout the System Operational Test phase of the contract.

Two basic methods of uniformity measurement were used. One was a destructive method while the preferred technique was non-destructive.

The destructive method was to slice an Ablation Sensor Plug into .1 inch thick disks. The radioactivity contained in each disk was measured with the laboratory counting equipment. A plot was then made of the radioactivity of each disk as compared to the mean radioactivity of the disks measured. The disadvantage of this method was that the Ablation Sensor Plug was destroyed and could not be used for system test purposes.

The preferred non-destructive method of uniformity measurement offered several advantages. First, the Ablation Sensor Plug was not destroyed and could be used for system test purposes. Second, the uniformity record obtained provided an unique pedigree for each Ablation Sensor Plug. Third, the uniformity record was presented in a manner that could directly be related to overall system measurement accuracy.

Non-destructive uniformity measurements were made using the equipment and set-up shown in the sketch of Figure 18.

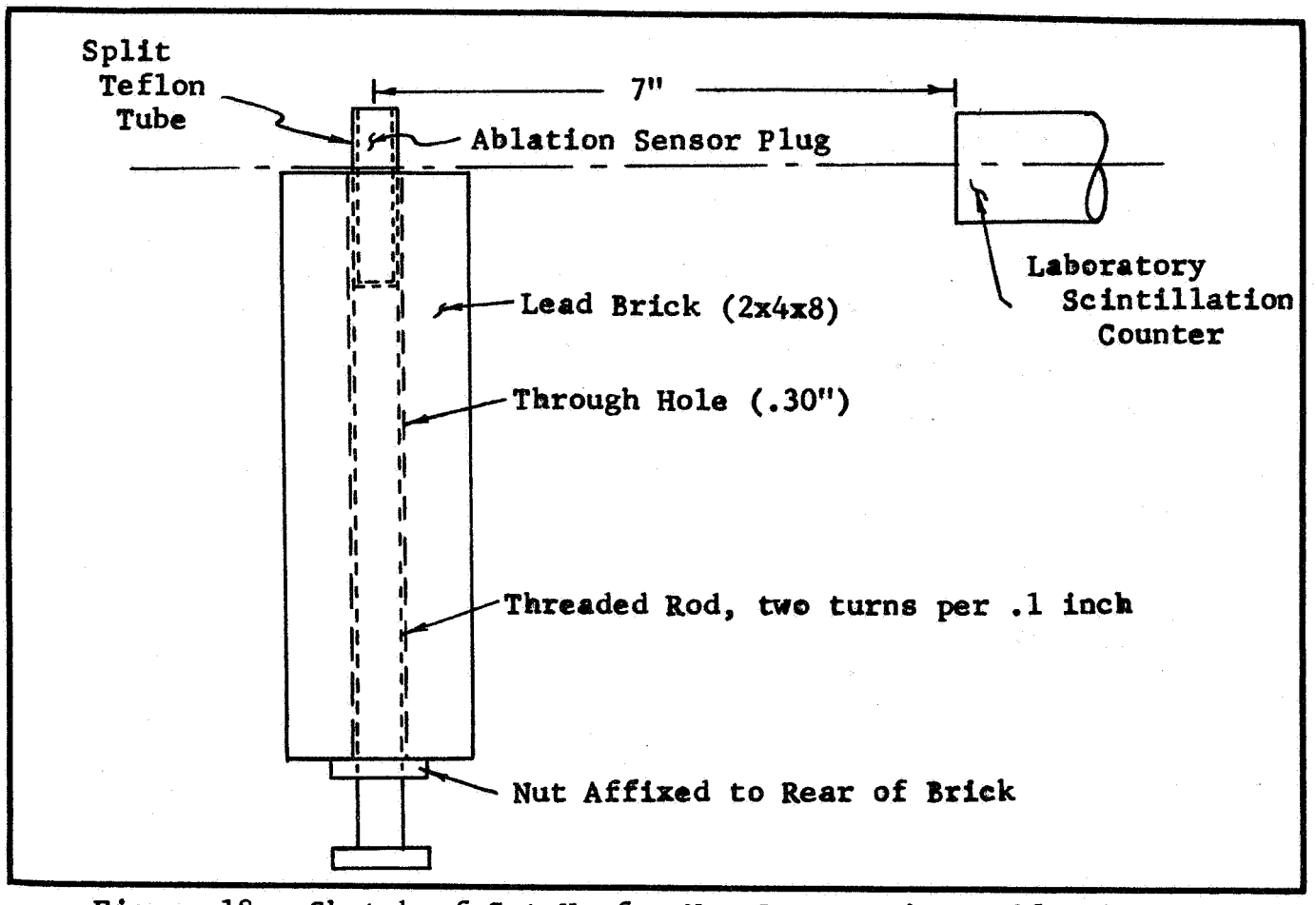

Figure 18. Sketch of Set-Up for Non-Destructive Uniformity Measurements.

Non-destructive uniformity tests were performed in the following manner. An Ablation Sensor Plug was placed in a split ¼ inch diameter by 1 inch long piece of Teflon tubing. The tube and sensor were inserted into the hole in the lead brick flush with the front surface. The threaded rod was advanced until it touched the rear of the Ablation Sensor Plug. The position of an indexing device on the rear of the threaded rod was noted.

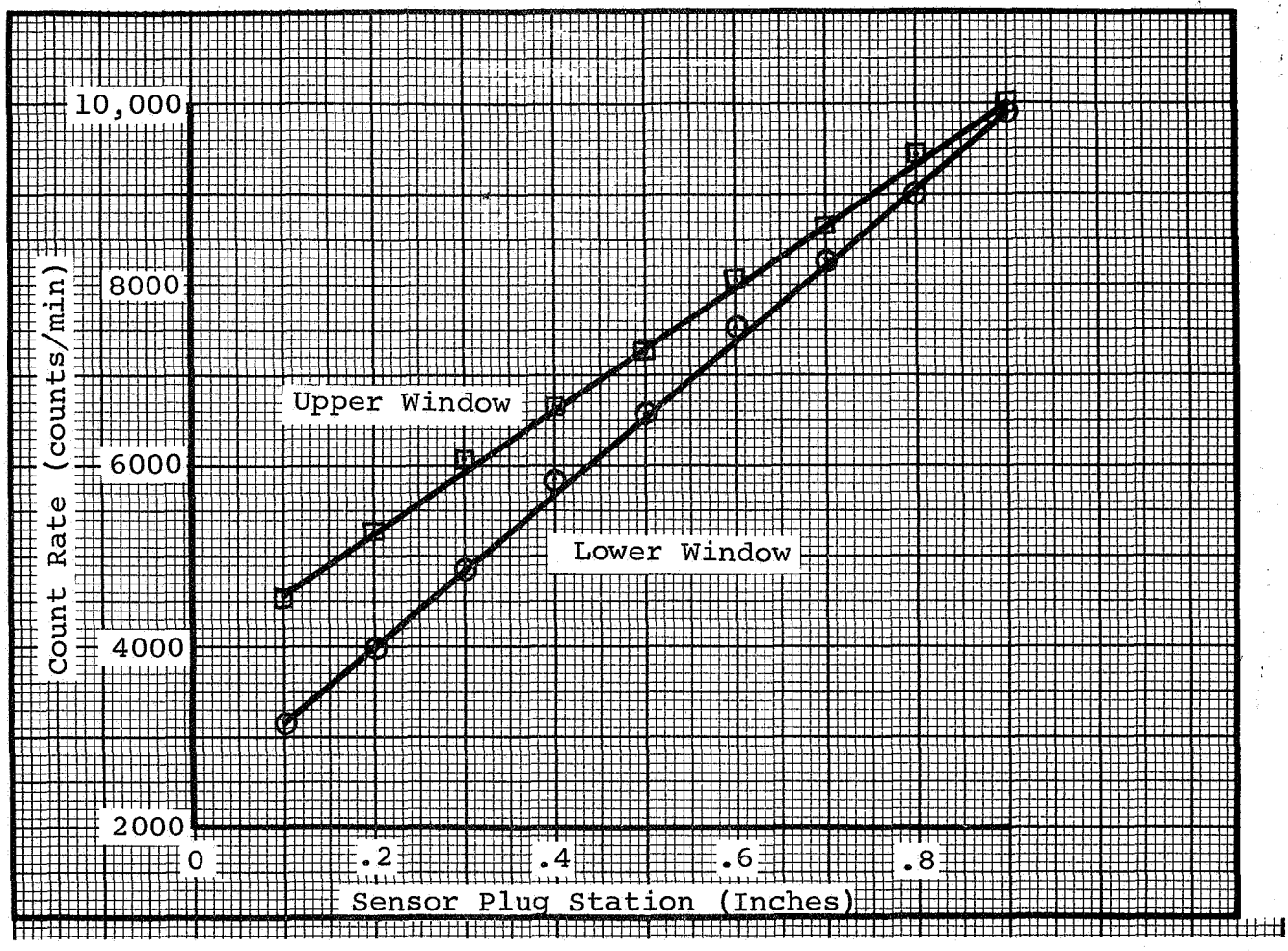

Figure 19. Typical Linearity Data, Phenolic Graphite Sensor Plug #5.

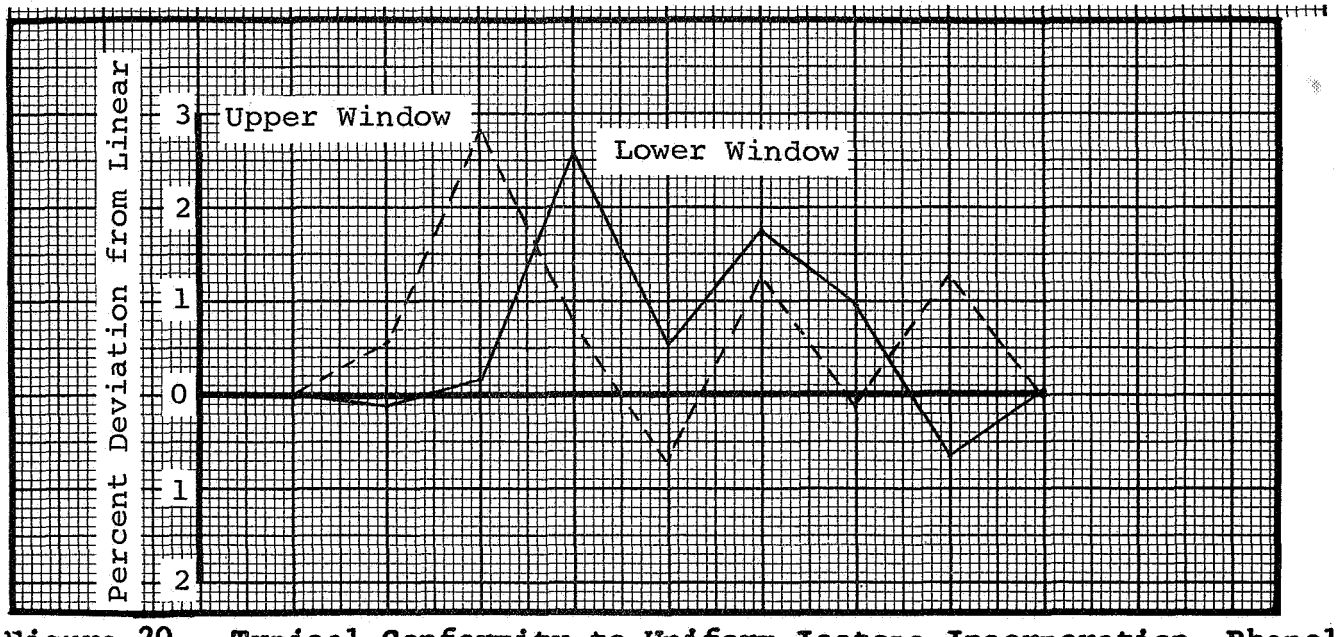

Figure 20. Typical Conformity to Uniform Isotope Incorporation, Phenolic Graphite Sensor Plug #5.

A one minute count was taken on the laboratory nuclear counting equipment. Window settings were used that counted and discriminated between the higher energy radiation, from $ZrNb^{95}$, and the lower energy radiation, from In^{114m}. The threaded rod was advanced two full revolutions (.1 inch), and the procedure was repeated. This process continued until the Ablation Sensor Plug protruded fully from the lead brick.

Figure 19 presents a plot of typical data taken in this manner superimposed upon the ideal straight line of uniform radioactive incorporation. Figure 20 is an analysis of Figure 19 and indicates the degree of conformity to uniform radioactive compound incorporation that was obtained. Figure 18 was obtained by dividing the difference between the actual data point and the straight line by the count rate obtained when the ideal Ablation Sensor Plug protrudes fully from the lead brick (The maximum value of the ideal straight line at full extension). This value was then expressed as a percentage at the various measurement stations of the Ablation Sensor Plug.

Typical uniformity values obtained, for both heat shield materials, were plus or minus two percent. These values were obtained using the impregnation and mixing procedures presented in the Appendix, Volume II.

3.3.6 Quality Control Methods. A quality control procedure was set up to demonstrate the uniformity of incorporation to be expected from each batch of Ablation Sensor Plugs prior to individual uniformity measurement and test. The procedure utilized here should form the backbone of any future procedures implemented for use during flight missions.

The basic parameters demonstrated are typical uniformity to be expected from a particular batch, typical calibration curves to be expected from a particular batch, and total activity incorporated into the randomly picked Ablation Sensor Plug.

The procedure is illustrated here for a typical phenolic graphite Ablation Sensor Plug, but it was similar for phenolic nylon. Six phenolic graphite Ablation Sensor Plugs can be made from each disk molded. One of these Sensor Plugs is selected at random and sliced into .1 inch disks .25 inch in diameter. These disks were then stacked together in the slotted teflon tube and non-destructively measured for uniformity by expulsion from the lead shield. The resulting plot of activity versus

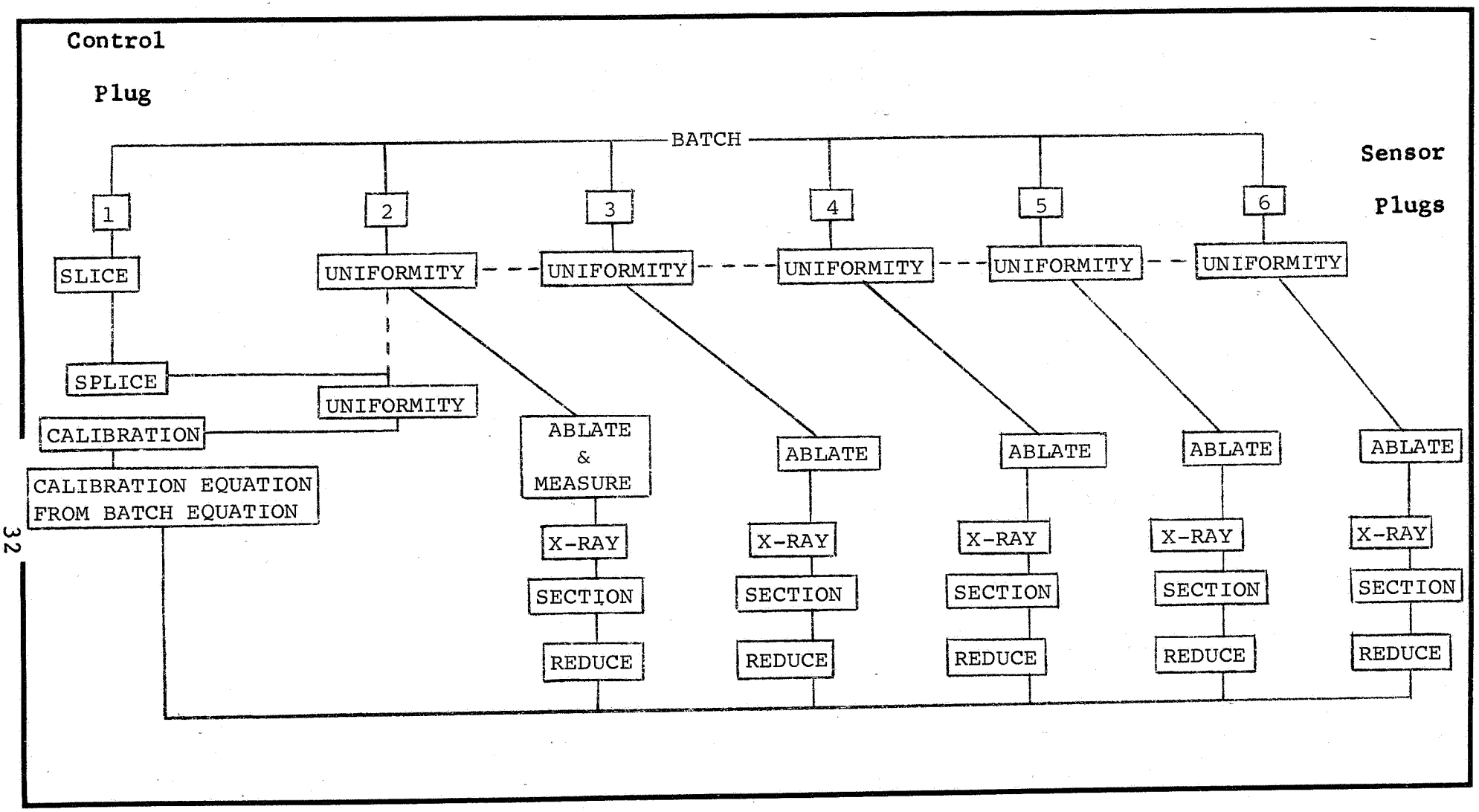

Figure 21. Ablation Sensor Plug Quality Control Flow Diagram.

exposed stack length provides a typical example of the uniformity to be expected from that batch.

The individual slices were then stacked in front of the radiation detector in proper position for an ablation test. A count was taken at each nuclear energy level. One slice was removed and the process repeated until no slices remained. The resulting data reduction and plot of count rate versus stack length provided an Ablation Sensor Plug calibration curve typical of the particular batch. The count rate obtained with all slices present is a typical representation of total activity incorporated into a random sample of a particular batch. This provides a measure of batch to batch uniformity.

Figure 21 presents a diagram of the procedure as applied to the test programs performed under this contract. In this diagram sensor plug one was the random sample selected. The other sensor plugs were tested, in this diagram, since no serious non-uniformity was spotted on the random sample.

3.3.7 Isotope Accuracy Tests. A series of ablation tests was performed with laboratory nuclear counting equipment to determine the accuracy of total and virgin material thickness measurements attainable with the isotopes chosen for the radioactive Ablation Sensor Plug. Forty ablation tests were performed with each heat shield material. Raw data, recorder traces, sensor plug uniformity data, and results for all of these tests are presented in the Appendix, Volume II.

After the tests were performed, each test model was X-rayed to provide a non-destructive indication of the virgin material remaining. Then each test model was sectioned. Total heat shield thickness and virgin material remaining were then visually measured. (In the case of phenolic graphite, density measurements were made along the length of the Ablation Sensor Plug to determine the virgin material measured location. This data is presented and explained in Volume II.)

The results of this test series of eighty ablation tests, at heat fluxes from 400 BTU/ft^2-second to 100BTU/ft^2-second, are presented in Figure 22. The average agreement between the total thickness at the end of the test from isotope data and the physically measured thickness was plus or minus .01 inches. The average agreement between the virgin material thickness at the end of the test from isotope data and the physically measured thickness was plus or minus .02 inches.

Model Number	Measurement		Predicted		Percent Counts		Deviation **	
	Total	Virgin	Total	Virgin	Total	Virgin	Total	Virgin
640-27-2	.37	.27	.37	.28	49.5	40.5	.00	.01
640-28-1	.34	.28	.35	.29	47.4	41.5	.01	.01
641-102-1	.25	.17	.23	.18	33.5	26.8	-.02	.01
641-102-3	.28	.19	.27	.21	37.9	30.9	-.01	.02
640-30-2	.56	.44	.58	.45	69.1	57.9	.02	.01
641-103-1	.53	.49	.51	.50	63.0	62.2	-.02	.01
641-101-3	.60	.48	.60	.49	70.3	61.5	.00	.01
641-105-3	.71	.66	.71	.69	79.2	78.9	.00	.03
641-31-1	.91	.76	.91	.77	93.8	85.2	.00	.01
640-20-2	.89	.77	.89	.77	92.7	85.7	.00	.00
640-30-1	.84	.71	.84	.58	89.2	70.5	.00	-.13
640-34-1	.85	.78	.86	.78	90.5	86.5	.01	.00
640-35-2	.44	.37	.44	.41	56.5	54.3	.00	.04
641-102-2	.37	.31	.36	.32	47.9	44.7	-.01	.01
641-101-2	.77	.65	.78	.67	84.2	77.2	.01	.02
640-37-1	.73	.60	.74	.58	82.2	69.9	.01	-.02
640-36-1	.56	.47	.59	.49	69.9	62.4	.03	.02
640-35-1	.58	.48	.57	.49	68.7	61.5	-.01	.01
640-32-1	.26	.17	.26	.17	36.7	26.0	.00	.00
641-101-4	.27	.19	.27	.20	38.3	30.6	.00	.01
641-106-3	.42	.33	.42	.33	54.3	45.2	.00	.00
641-104-4	.40	.33	.39	.34	51.8	46.2	-.01	.01
641-100-1	.96	.89	.95	.93	96.2	95.2	-.01	.04
641-106-1	.95	.87	.94	.88	95.5	91.8	-.01	.01
640-23-1	.86	.76	.87	.60	91.5	71.9	.01	-.16
640-35-1	.84	.71	.85	.68	90.2	78.5	.01	-.03
641-103-2	.68	.63	.67	.65	76.3	75.5	-.01	.02
640-21-1	.74	.61	.75	.61	82.5	73.1	.01	.00
640-22-1	.59	.47	.60	.49	71.1	62.4	.01	.02
640-18-2	.57	.45	.57	.44	68.1	57.5	.00	-.01
641-106-2	.63	-	.64	.51	73.7	63.1	.01	-
641-104-2	.62	.52	.62	.52	72.4	64.4	.00	.00
640-18-1	.93	.79	.94	.76	96.2	84.5	.01	-.03
641-105-1	.93	.87	.93	.88	94.4	92.0	.00	.01
641-104-1	.81	.67	.81	.69	86.2	79.0	.00	.02
641-22-2	.78	.70	.80	.74	85.8	83.5	.02	.04
641-103-3	.97	.91	.95	.92	96.3	94.5	-.02	.01
641-24-1	.97	.86	.98	.84	98.6	90.2	.01	-.02
641-22-1	.70	.60	.70	.62	79.2	74.1	.00	.02
641-24-2	.69	.55	.69	.53	78.4	65.9	.00	-.02

** - Deviation - (Predicted - Measurement)

Figure 22. Composite Data Summary, Phenolic Nylon **Isotope Accuracy Tests.**

Model Number	Measurement		Predicted		Percent Counts		Deviation **	
	Total	Virgin	Total	Virgin	Total	Virgin	Total	Virgin
641-112-1	.80	.23	.80	.21	87.2	32.3	.00	-.02
641-109-3	.78	.25	.78	.23	85.8	35.3	.00	-.02
641-107-4	.86	.42	.86	.42	91.0	56.7	.00	.00
641-111-2	.84	.48	.83	.46	89.2	60.2	-.01	-.02
641-111-3	.95	.70	.92	.67	94.8	78.0	-.03	-.03
641-107-1	.94	.74	.90	.72	94.0	81.8	-.04	-.02
640-94-2	.60	.10	.61	.12	72.5	18.8	.01	.02
640-95-2	.64	.00	.64	.05	75.1	8.1	.00	.05
640-92-2	.47	.00	.51	.07	64.0	11.2	.04	.07
640-91-1	.37	.00	.36	.00	49.2	00.0	-.01	.00
641-108-2	.84	.47	.84	.45	90.2	59.5	.00	-.02
641-107-3	.87	.48	.87	.50	92.0	64.4	.00	.02
640-43-1	.98	.77	.95	.75	96.5	84.5	-.03	-.02
641-110-3	.95	.66	.97	.65	97.8	76.6	.02	-.01
640-40-1	.80	.34	.75	.34	83.5	47.7	-.05	.00
641-111-1	.76	.32	.77	.31	84.8	44.3	.01	-.01
640-104-1	.51	.05	.50	.07	63.6	12.0	-.01	.02
640-103-2	.55	.00	.54	.00	67.0	00.0	-.01	.00
641-110-4	.28	.00	.31	.00	42.8	00.0	.03	.00
641-109-4	.36	.00	.40	.00	53.3	00.0	.04	.00
641-110-1	.94	.65	.88	.66	92.6	77.1	.06***	.01
640-93-2	.84	.80	.83	.78	39.6	86.5	-.01	-.02
641-108-1	.88	.40	.88	.41	92.6	55.5	.00	.01
640-92-1	.87	.44	.84	.46	90.1	60.9	-.03	.02
641-109-1	.83	.25	.85	.22	90.4	33.6	.02	-.03
640-41-2	.81	.15	.80	.17	87.4	27.0	-.01	.02
641-109-2	.64	.00	.64	.00	74.8	00.0	.00	.00
640-40-2	.63	.10	.62	.05	73.9	8.2	-.01	-.01
641-113-2	.32	.00	.31	.00	43.2	00.0	-.01	.00
640-39-2	.46	.00	.42	.00	55.3	00.0	-.04	.00
641-113-4	1.0	.79	.98	.81	98.4	88.7	-.02	.03
641-111-4	.99	.80	.95	.82	96.7	89.1	-.04	.02
641-108-4	.95	.57	.97	.55	98.0	68.3	.02	-.02
641-113-3	.96	.55	.96	.53	97.0	66.6	.00	-.02
641-112-4	.87	.14	.90	.11	93.8	17.7	.03	-.03
640-101-2	.87	.10	.86	.09	91.4	14.7	-.01	-.01
641-113-1	.72	.00	.74	.00	83.0	00.0	.02	.00
640-98-1	.72	.08	.71	.09	80.8	14.9	-.01	.01
640-99-2	.44	.00	.41	.00	54.2	00.0	-.03	.00
640-38-1	.46	.00	.45	.00	58.3	00.0	-.01	.00

** Deviation - (Predicted - Measurement)
*** Plug expanded during ablation tests

Figure 22 Cont'd. Composite Data Summary, Phenolic Graphite Isotope Accuracy Tests.

Material thickness predictions were made from scaler measurements of the radioactive intensity of each isotope remaining in each Ablation Sensor Plug at the end of test. These predictions were compared to the visual measurements, at test end, to determine the error of measurement. From the results of the Isotope Accuracy tests it was concluded that the chosen isotopes did leave the heat shield at the proper time and could be used to measure heat shield ablation.

3.4 Detector Development

3.4.1 General. The Radiation Detector was selected based on an evaluation of available detectors at the time of contract award. The detector chosen consisted of a ruggedized photomultiplier tube, including an encapsulated wrap around high voltage power supply, coupled to a Cesium Iodide (Sodium activated) 1¼ inch diameter by 1 inch long scintillation crystal. These components were assembled and encapsulated in an aluminum outer package provided with a mounting bracket. Figure 23 shows a picture of the entire detector package. The scale in the picture is in inches.

3.4.2 Selection Criteria. The detector had to be capable of detecting and discriminating between gamma photons of two different nuclear energy levels. In addition, the detector had to be presently available and had to:

1. Operate satisfactorily within the temperature constraints of the specified environmental criteria.
2. Operate satisfactorily when exposed to the shock, acceleration, and vibration constraints of the specified environmental criteria.
3. Be of minimum size.
4. Operate with resolution and noise requirements compatible with system measuring requirements.
5. Use a minimum of power.
6. Be as efficient as possible to minimize required radiation levels.

3.4.3 Solid State Detector. Two separate types of Radiation Detectors, solid state and scintillation, have attractive features with respect to the specific nuclear measuring task at hand. The solid state detector is basically a transistor. It therefore appeared attractive from the size, weight, shock, and power criteria. However, it is an order of magnitude less

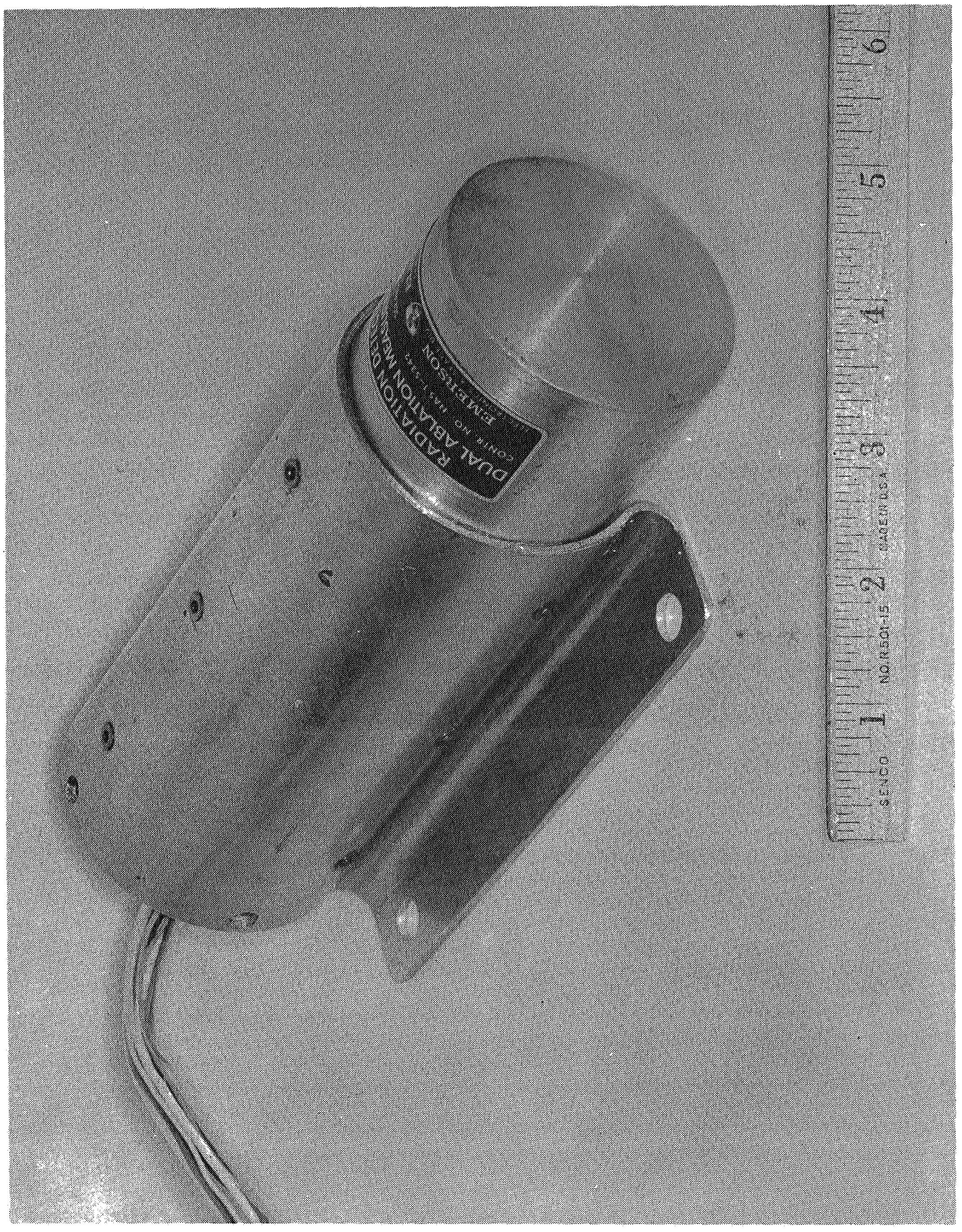

Figure 23. Radiation Detector for Dual Ablation Measuring System.

efficient than a scintillation detector. In addition, the resolution of available solid state detectors was known to decrease with an increase in temperature and the noise output increase. A silicon surface barrier detector (ORTEC SBEI-050-500) was tested to determine if its output noise level was too severe to permit successful use in the system. The results of these tests are presented in Figure 24.

Figure 24 shows the nuclear energy spectra of $ZrNb^{95}$ and In^{114m} taken with the ORTEC detector at 75°F, room temperature. Each source was placed five inches away from the detector. The In^{114m} source was 1.2 millicuries and the $ZrNb^{95}$ source was 0.4 millicuries. The superimposed data points and lines show the noise spectra taken at the temperatures indicated. The noise spectras were obtained with no radiation source present. The results clearly indicated that it would not be possible to discriminate, and thus measure, the two nuclear energy levels being emitted from an Ablation Sensor Plug at temperatures even slightly above room temperature.

A steady state temperature of 120°F in a research vehicle nose cone has been measured before launch, and is not at all unreasonable. Under these thermal conditions, detectors such as the ORTEC-050-500 silicon surface barrier solid state detector could not perform the discrimination necessary to accurately measure ablation.

These thermal tests were qualitatively repeated with a Lithium Drift solid state detector (SSR No. 5x5 - LID-2000-100A) with similar results.

These tests indicated that at this time a solid state detector would not perform adequately at steady state temperatures not unreasonable in the nose cone of research vehicles before launch.

3.4.4 Scintillation Crystal Photomultiplier Detector. Thermal noise is not so much a problem with scintillation detectors. However, other environmental criteria such as shock and vibration pose quite a problem. A scintillation detector is composed of a scintillation crystal optically coupled to the glass face of a photomultiplier tube. The majority of available photomultiplier tubes are of glass construction. The exception is the RCA C 70144 venetion blind tube which is ceramic.

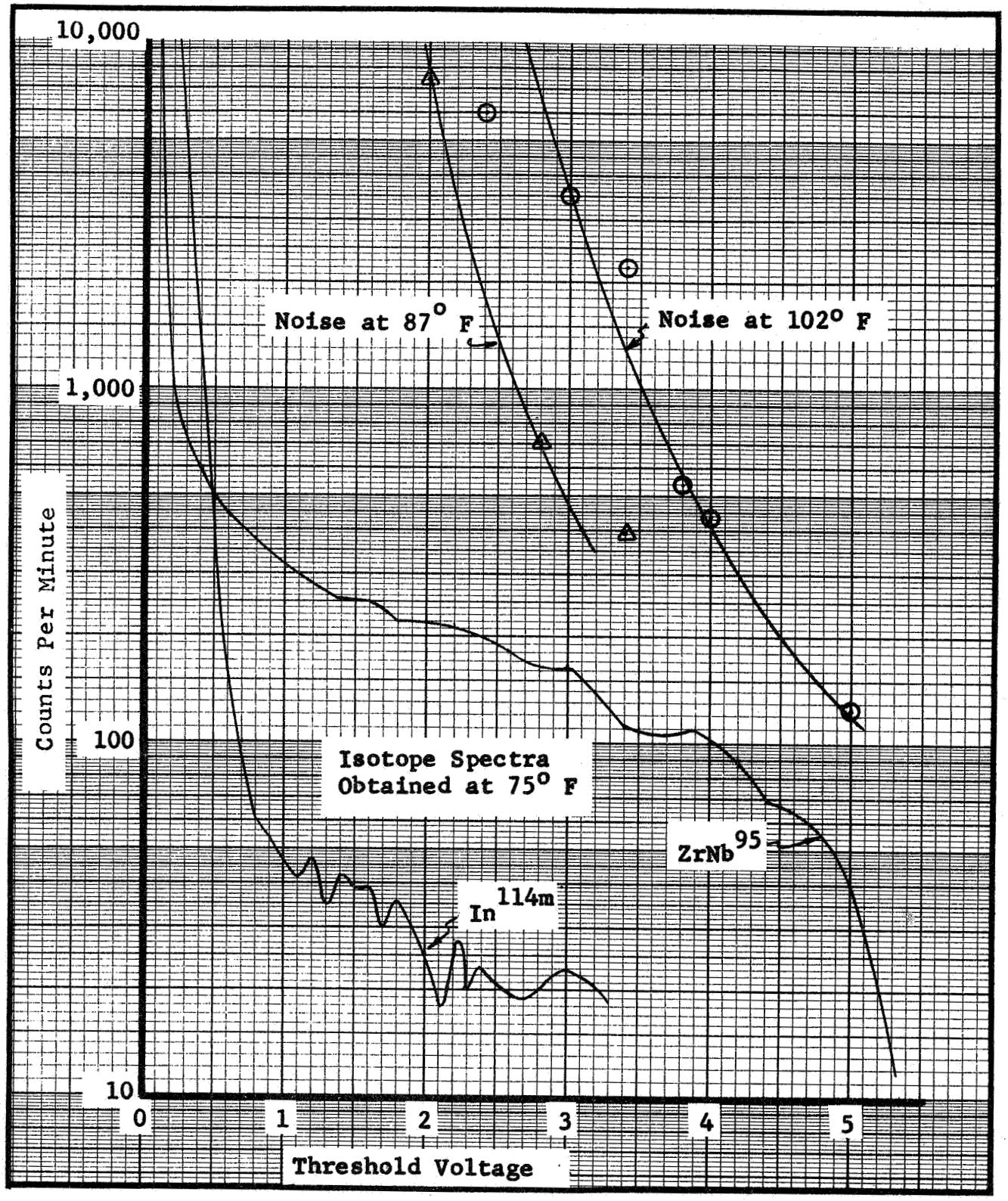

Figure 24. Signal and Noise Levels of an ORTEC SBEI-050-500 Silicon Surface Barrier Radiation Detector at Different Temperatures.

Shock and vibration pose problems to the scintillation crystal, to the glass photomultiplier faceplate, to the glass photomultiplier tube itself, and to the multiplying dynodes within the photomultiplier tube.

Specification of a more rugged Cesium Iodide crystal, instead of the standard Sodium Iodide, alleviated the crystal fracture problem at the expense of a slower maximum counting rate and lower light output (thus increasing system noise interference). A Cesium Iodide Sodium activated crystal, a new development at the time of this contract, was finally specified. The sodium activated Cesium Iodide crystal had a light output twice that of the more standard Thallium activated Cesium Iodide scintillation crystal, and its pulse decay was twice as fast as the Thallium activated crystal.

Figure 25 presents a list of the ruggedized photomultiplier tubes available at the time of this contract along with pertinent performance and environmental figures.

No environmental data were available for the RCA venetian blind tube. The EMR, Electro Mechanical Research, tubes were the only available tubes that might meet the contract shock and environmental specifications. Note that the RCA 8571 tube, which is quite small, would be adequate for use with many launch vehicles.

An EMR phototube was selected for use in the radiation detector. With the wrap-around high voltage power supply, this is called out as EMR model 601A-M4 integrated photoelectric sensor. This package meets Emerson's specification XES2922 Revision A, dated January 17, 1966, which is included in the Appendix Volume. The integrated package consists of an EMR model 541D-01-14 multiplier phototube and an EMR 652A wrap-around high voltage power supply.

The EMR type photomultiplier is a ruggedized tube employing Venetian blind structure of the Lallemand type (i.e., with a spherically shaped focusing screen in front of each Venetian blind dynode). The slatted circular dynodes are welded to Kovar rings which in turn are sealed to the glass tube proper. The Kovar rings protrude outside of the glass envelope. Resistors are welded to the rings to provide the dynode voltage divider. The high voltage power supply is wrapped around this structure. The assembly is potted in a fiberglass tube.

Manufacturer Model Type	EMR 541 A Venetian Blind	EMR 541 D Venetian Blind	RCA C 70144 Venetian Blind	RCA 8571 Cage	ITT F 4028 Box	Dumount KM 2356 Box
Performance						
Window Index	7056 Glass	7056 Glass	1.78	NA	1.5	1.5
Quantum Eff.	15%	5%	NA	6%	NA	5%
Power (Approx.)	2.6 watt	.78 watt	2.25 watt	.07 watt	.63 watt	.5 watt
Voltage (Approx)	2600 Volts	2600 Volts	1500 Volts	750 Volts	2600 Volts	1000 Volts
Dark Current at 10^6 gain	2.0×10^{-9} A at 20°C & 10^6 gain	3×10^{-11} A at 20°C & 10^6 gain	5.5×10^{-9}A at 20°C & 1.7×10^5 gain	1×10^{-9} A at 20°C & 3×10^5 gain	1×10^{-9} A at 150°C & 10^6 gain	5×10^{-8} A at 25°C & 2×10^5 gain
Cathode Material	SbCs	Bi-Alk	Bi-Alk	SbCs	Bi-Alk	NA
Cathode Size	1" Dia.	1" Dia.	1.8" Dia.	.06x.357"	1" Dia.	
Physical						
Size Dia.	1¼"	1¼"	2"	.53"	1¼"	2"
Length	4½"	4½"	4"	1.37"	4½"	4-5/8"
Weight	4½ Oz.	4½ Oz.	7 Oz.	.17 Oz.	4 Oz.	6 Oz.
Environmental	100g 11ms gu.					
Shock G's	2500	2500	NA	30	60	200
Duration	5 ms	5 ms	NA	11 ms	11 ms	3 ms
Vibration G's	30	30	NA	20	30	25
Frequency	20-2000 cps	20-2000 cps	NA		@ 2000 cps	50-2000 cps
Max. Temp.	75°C	150°C	75°C	75°C	150°C	75°C

Figure 25. Performance Specifications of Photomultipliers.

The entire integrated photoelectric sensor was then mated with the Cesium Iodide scintillation crystal and re-potted inside an aluminum assembly provided with a mounting bracket. Crystal mounting and package assembly was performed by Harshaw Chemical Company. The completed package meets Emerson's specification XES2935, Revision A, dated May 2, 1966, which is included in the Appendix, Volume II.

3.5 Signal Processor Development

3.5.1 General. The function of the Signal Processor is to receive electronic pulses from the Radiation Detector (actually the pre-amplifier mounted on the Radiation Detector), separate them according to two levels of amplitude, momentarily store, and then create D.C. output voltages proportional to the input frequency of each pulse amplitude. It is basically a two channel nuclear pulse height analyzer.

Figure 26 presents a picture of the Signal Processor. The scale is in inches. The six switches provide a degree of flexibility to allow full scale, 5 volt, output for a range of input frequencies, and to change system time constant to provide adequate data smoothing at low count rates, such as checkout in a laboratory with low level radioactive sources.

3.5.2 Design. Figure 27 presents a detailed system block diagram. Operation may be understood by reference to this diagram and to the following block descriptions.

The power supply consists of two voltage regulators that regulate the 28 ± 3VDC input and provide outputs of + 10 ± .1 and -10 ± .1 VDC, with respect to a 0 VDC return, to all circuit blocks. Power is also supplied to the high voltage wrap-around power supply in the Radiation Detector.

The pre-amplifier module is located on the Radiation Detector. The pre-amplifier is an emitter follower located in the output circuit of the photomultiplier tube. This circuit functions to isolate the following circuit loadings from the photomultiplier and affix a known capacitance across the tube output. The pre-amplifier module contains a temperature compensation network to minimize pulse amplitude changes due to thermal effects on the high voltage power supply, photomultiplier tube, and scintillation crystal.

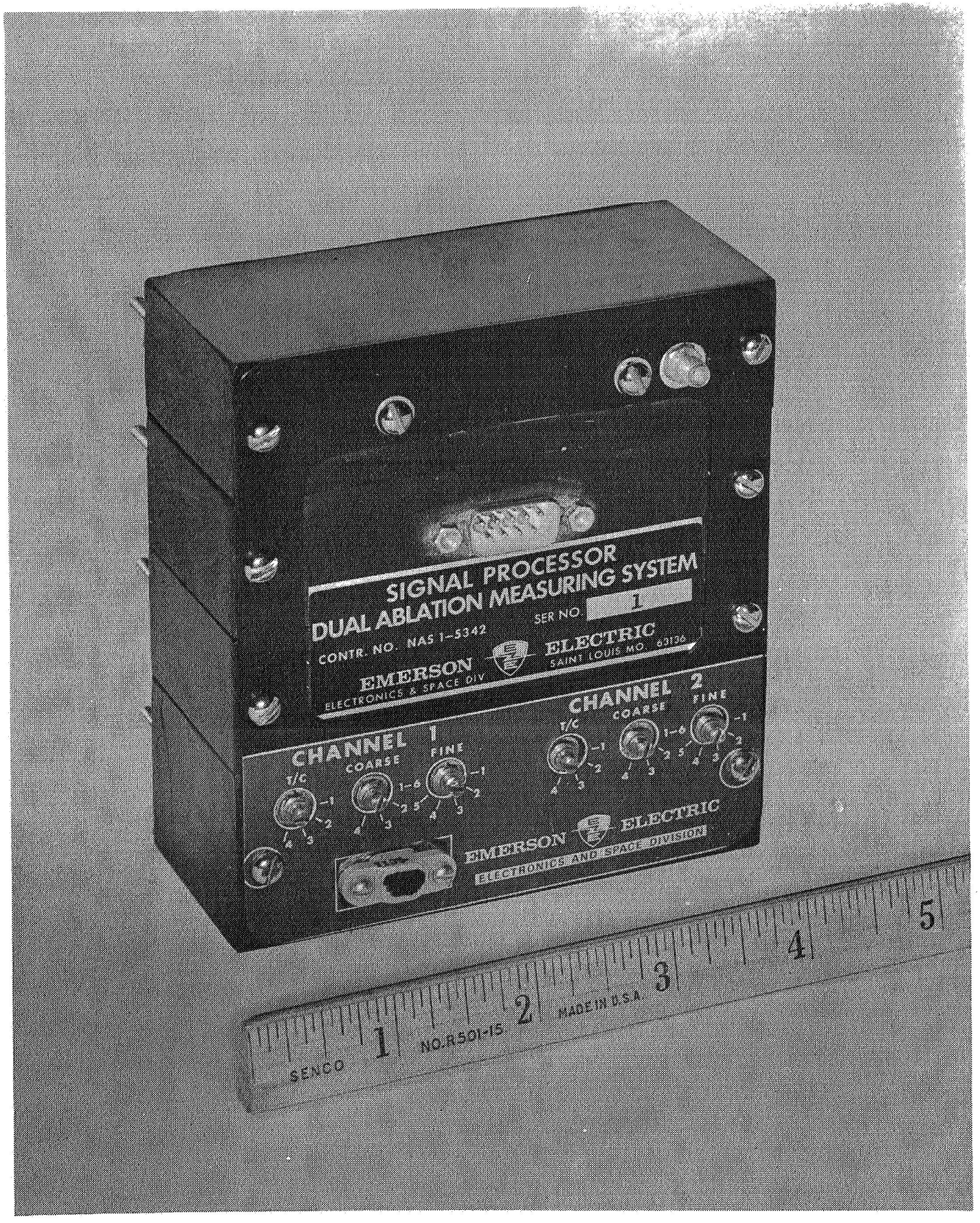

Figure 26. Signal Processor for Dual Ablation Measuring System.

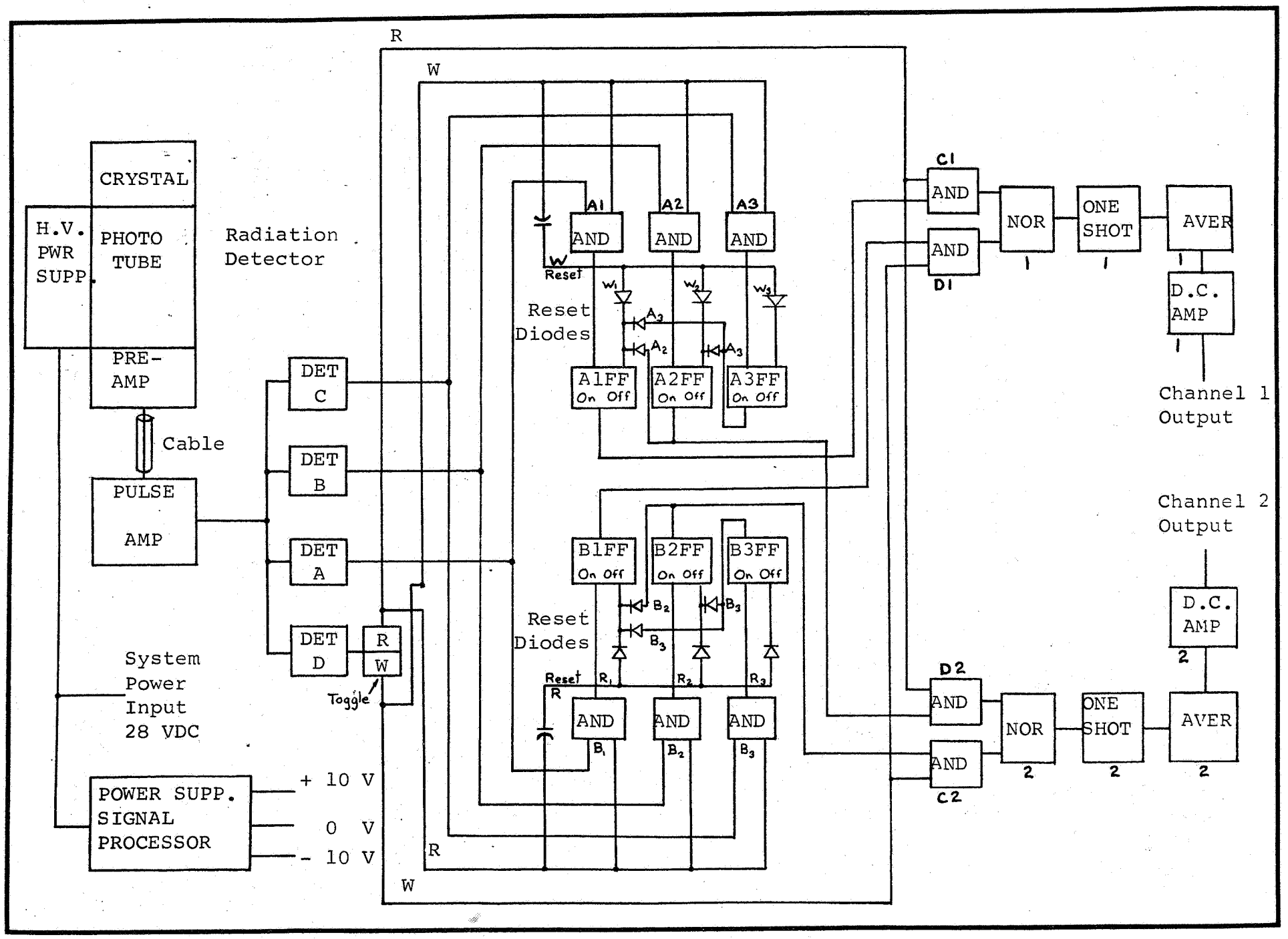

Figure 27. Dual Ablation Measuring System Block Diagram.

Figure 28 shows a typical pre-amplifier output pulse.

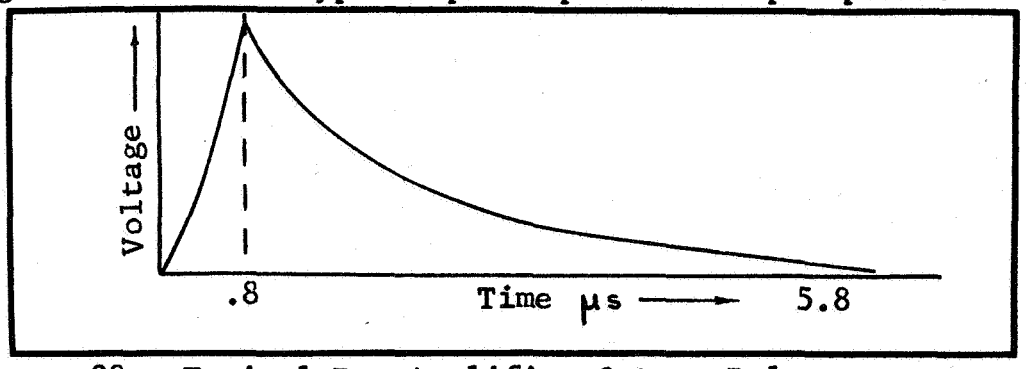

Figure 28. Typical Pre-Amplifier Output Pulse.

The pulse amplifier is a direct coupled, fed-back, operational amplifier. Pulses are amplified and shaped at this stage to: (1) Provide a reasonable voltage level so that temperature drifting of the following level detectors will have less effect on system output, (2) Provide a shape that will minimize pulse pile up at high counting rates. A schematic representation of the pulse amplifier output pulses is shown in Figure 29.

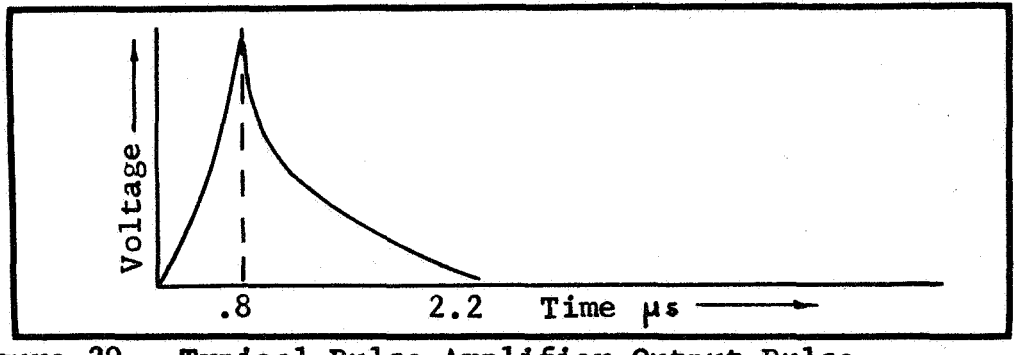

Figure 29. Typical Pulse Amplifier Output Pulse.

The toggle circuit is a monostable multivibrator with steering circuitry. This circuit toggles at every falling edge of detector D pulses to provide the alternate timing pulses. These pulses determine which set of logic circuits pulses from detectors A, B, and C are read into or written out of.

Four level detectors are provided. These are hybrid Schmitt Trigger circuits with base fed back hysteresis instead of emitter hysteresis. A differential amplifier is used to provide greater temperature stability than a conventional Schmitt Trigger.

Level detector D is set at the lowest voltage level and provides the command for the Toggle circuit to change state.

Level detectors A, B, and C are set at ascending voltage levels in that order. Pulses greater than A but less than B are

channel 1 information. Pulses greater than B but less than C are channel 2 information. Pulses greater than C or less than A are rejected.

Diode Transistor Logic circuits are used throughout to provide a minimum of components. Two sets of storage and logic circuits are provided. This provision increases reliability and allows the circuits to operate at lower frequency. Storage elements are chosen by the state of the Toggle circuit.

The One Shot multivibrator creates an output pulse of constant magnitude and width for each input pulse in its particular channel. The One Shot circuit is an hybrid design providing two transistors charging a capacitor to minimize recovery time between the random nuclear events.

The Averaging circuit is a current averaging or integrating, device to provide linear D.C. output as a function of input frequency.

The D.C. Amplifier is an emitter fed back operational amplifier held to a gain equal to one. This provides a high input impedance for the Averager circuits while providing an output impedance compatible with specifications.

3.5.3 Operation. Operation of the system will be described based on Figure 27, System Block Diagram, Figure 30, Definition of Symbols, Figure 31, Representative Detector Output Pulses, and Figure 32, Waveforms Sequence.

Figure 30, Definition of Symbols, presents the symbols used in this section to refer to various circuit blocks.

Symbol	Meaning
PULSE AMP	Pulse Amplifier
DET. D	Detector D
DET. A	Detector A
DET. B	Detector B
DET. C	Detector C
TOGGLE	Bistable Multivibrator
R	Toggle State Read
W	Toggle State Write
FF	Bistable Multivibrator
ON	Rising Pulse
OFF	Falling Pulse
AND	AND Gate
RESET	A short fast rising pulse
NOR	NOR Gate
ONE SHOT	Monostable Multivibrator
AVER.	Averaging Circuit
D.C. AMP.	Direct Current Amplifier

Figure 30. Definition of Symbols

Figure 31, Representative Detector Output Pulses, shows five levels of pulses input to the pulse amplifier. The four level detectors, A, B, C, and D, are superimposed on this diagram. System operation will be explained with pulse #4. Assume that all level detectors are initially OFF.

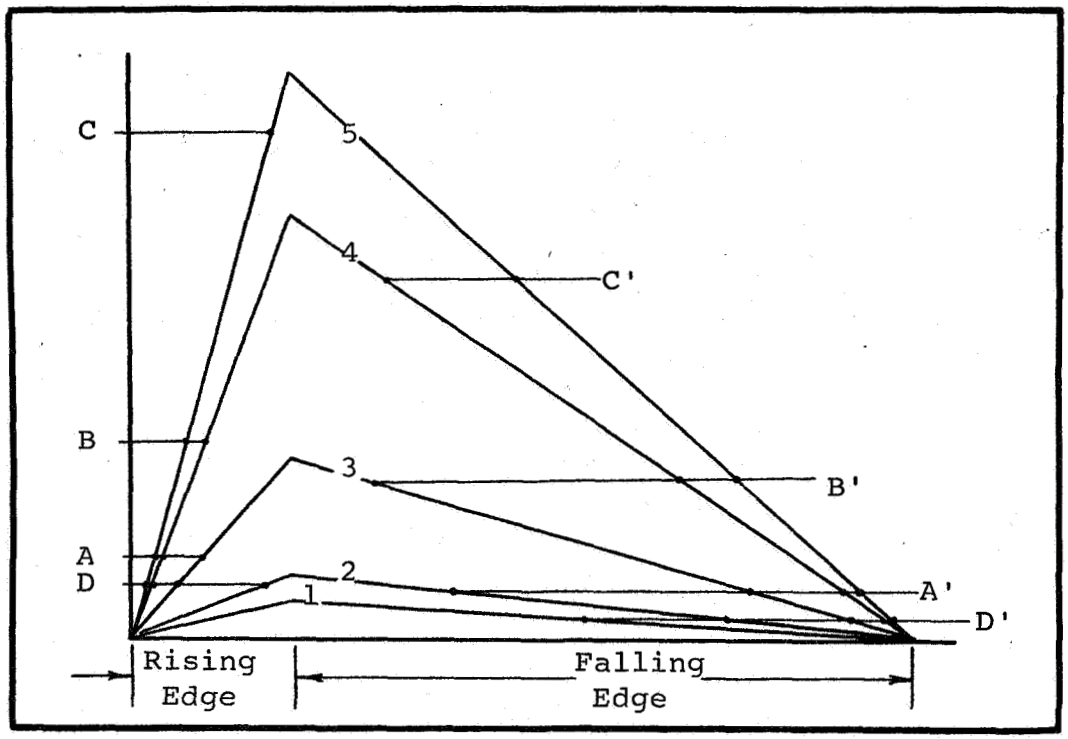

Figure 31 Representative Detector Output Pulses.

Pulse height detection is done by the D, A, B, and C detectors, shown on Figure 27. Dual Ablation Measuring System Block Diagram. Detector levels are represented by D, A, B, C, D', A', B', and C'. These symbols also represent the magnitude of the pulse height needed to operate the detectors. The unprimed symbols represent detector threshold levels which must be exceeded by the rising edge of an input pulse I in order to turn ON a corresponding detector. The primed symbols represent detector levels for which the falling edge of the input pulse I must be less than in order to turn the corresponding detector OFF. The difference between A and A', B and B', and C and C' is due to hysteresis effects in the corresponding detectors. This hysteresis is useful in order to generate finite width detector pulses, especially for pulses in which the threshold is barely exceeded.

For pulse #4, the input pulse I is greater than D, A, and B, but less than C. Detector thresholds D, A, and B have been exceeded so D, A, and B detectors are turned ON in that order. When the pulse height falls to less than B' but greater than A', the B detector is turned OFF. When the pulse height falls to less than A' but greater than D', the A detector is turned OFF. When the pulse height falls to less than D', the D detector if turned OFF. Although this pulse falling edge also passed

through level C', nothing additional happened because detector C had not previously been turned ON.

The input pulse I may be traced through the Signal Processor by reference to Figure 27 , Dual Ablation Measuring System Block Diagram, and Figure 32 , Waveforms Sequence. Cross reference to the actual circuit board drawings and the interconnection drawings is also helpful.

Detector D functions to operate the TOGGLE after each input pulse has completed its lifetime. Thus, the falling edge of D detector pulse always changes the state of the TOGGLE. TOGGLE States are R and W. R to W changes of the TOGGLE are made to generate W RESET pulses. W to R changes of the TOGGLE are made to generate R RESET pulses.

Detector A pulse rising edge and TOGGLE W state pulse enter A_1 AND gate. The combination generates A_1 AND pulses. A_1 AND pulses turn A_1FF ON. W RESET pulses turn A_1FF OFF. A_1FF ON pulse and TOGGLE R state pulse rising edge enter C_1 AND gate. The combination generates C_1 AND pulses. Detector A pulse rising edge and TOGGLE R state pulse enter B_1 AND gate. The combination generates B_1 AND pulses. B_1 AND pulses turn BIFF ON. R_1 RESET pulse turns BIFF OFF. BIFF ON pulse and TOGGLE W state pulse falling edge enter D_1 AND gate. The combination generates D_1 AND pulses. C_1 AND and D_1 AND pulses enter 1 NOR. The combination generates 1 NOR pulses. 1 NOR pulses operate 1 ONE SHOT.

1 ONE SHOT pulses have the same frequency as Input Pulses I. The ONE SHOT pulses enter 1 AVER. circuit. The 1 AVER. circuit converts the pulse repetition frequency into a DC voltage proportional to this frequency. The DC voltage enters 1 DC AMP which amplifies the voltage. The voltage is connected to Channel 1 Output terminal.

Detector B pulse rising edge and TOGGLE W state pulse enter A_2 AND gate. The combination generates A_2 AND pulses. A2 AND pulses turn A_2FF ON. A2FF OFF to ON pulse rising edge is connected through Reset Diode A_2 to A1FF. This arrangement functions to turn A1FF OFF. A1FF had been turned ON because A Detector had also been turned ON. W_2 RESET pulse turns A2FF OFF. A2FF ON pulse and TOGGLE R state pulse rising edge enter D2 and gate. The combination generates B2 AND pulses. B2 AND pulses turn B2FF ON. B2FF OFF to ON pulse rising edge is

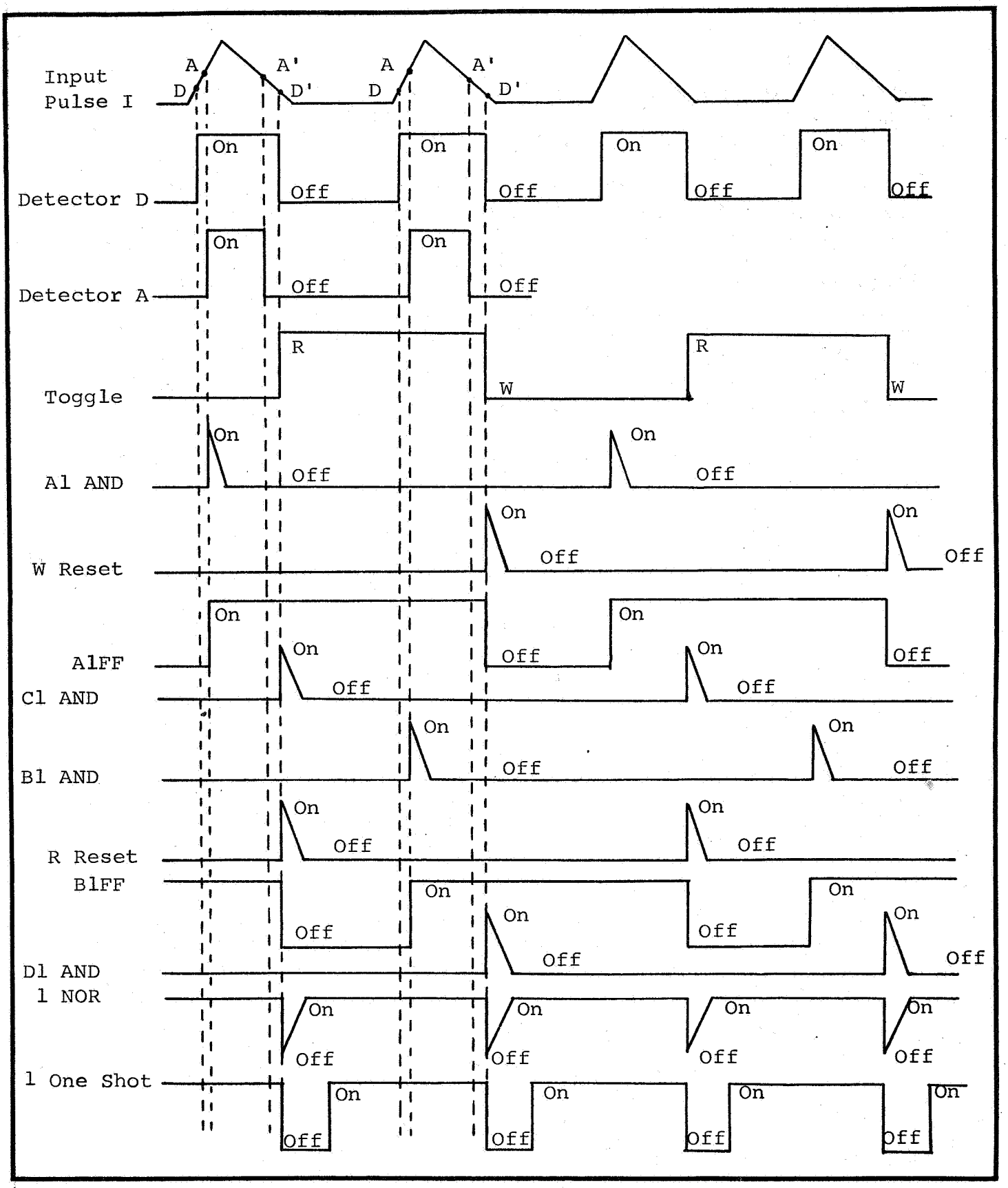

Figure 32. Waveforms Sequence.

connected through Reset Diode B_2 to B1FF. This arrangement functions to turn B1FF OFF. B1FF had been turned ON because A detector had been turned ON also.

R_2 RESET pulses turn B2FF OFF. B2FF ON pulse and TOGGLE W state pulse rising edge enter C2 AND gate. The combination generates C2 and pulses. D2 AND and C2 AND pulses enter 2 NOR. The combination generates C2 AND pulses. D2 AND and C2AND pulses enter 2 NOR. The combination generates 2 NOR pulses. 2 NOR pulses operate 2 ONE SHOT. The 2 ONE SHOT pulses enter 2 AVER. circuit. The 2 AVER. circuit converts the pulse repetition frequency into a DC voltage proportional to this frequency. The DC voltage enters 2 DC AMP which amplifies the voltage. The voltage is connected to Channel 2 Output terminal. This is Detector B information. Detector C pulses function in a manner similar to those of Detectors A and B.

There are three differences between the sequence of operation following the C Detector and the sequence following A and B detectors. The first difference is that A3FF OFF to ON pulse rising edge acts through two Reset Diodes A_3 to turn both A2FF and A1FF OFF. The second difference is that B3FF OFF to ON pulse rising edge acts through two Reset Diodes B_3 to turn both B2FF and B1FF OFF. See Example pulse number 5 of input pulses to Detectors. A1FF, B1FF, A2FF, and B2FF have been turned ON because A and B Detectors had been turned ON. The third difference is that both A3FF and B3FF ON state is not brought out to other circuits. Detector C pulse serves to turn OFF pulses from Detectors A and B that have reached A1FF, B1FF, A2FF and B2FF's. Thus, Detector input pulses I representing Radiation and noise energy above C threshold are rejected.

3.5.4 Fabrication. The Dual Ablation Measuring System circuit blocks were individually breadboard and tested to prove the functional operation of each. The resulting breadboard system is shown in Figure 33.

System fabrication includes the Signal Processor, Pre-Amplifier, and Radiation Defector. The Signal Processor consists of the following four individual, potted modules:

1. Power Supply, Pulse Amplifier - Toggle
2. Level Detectors

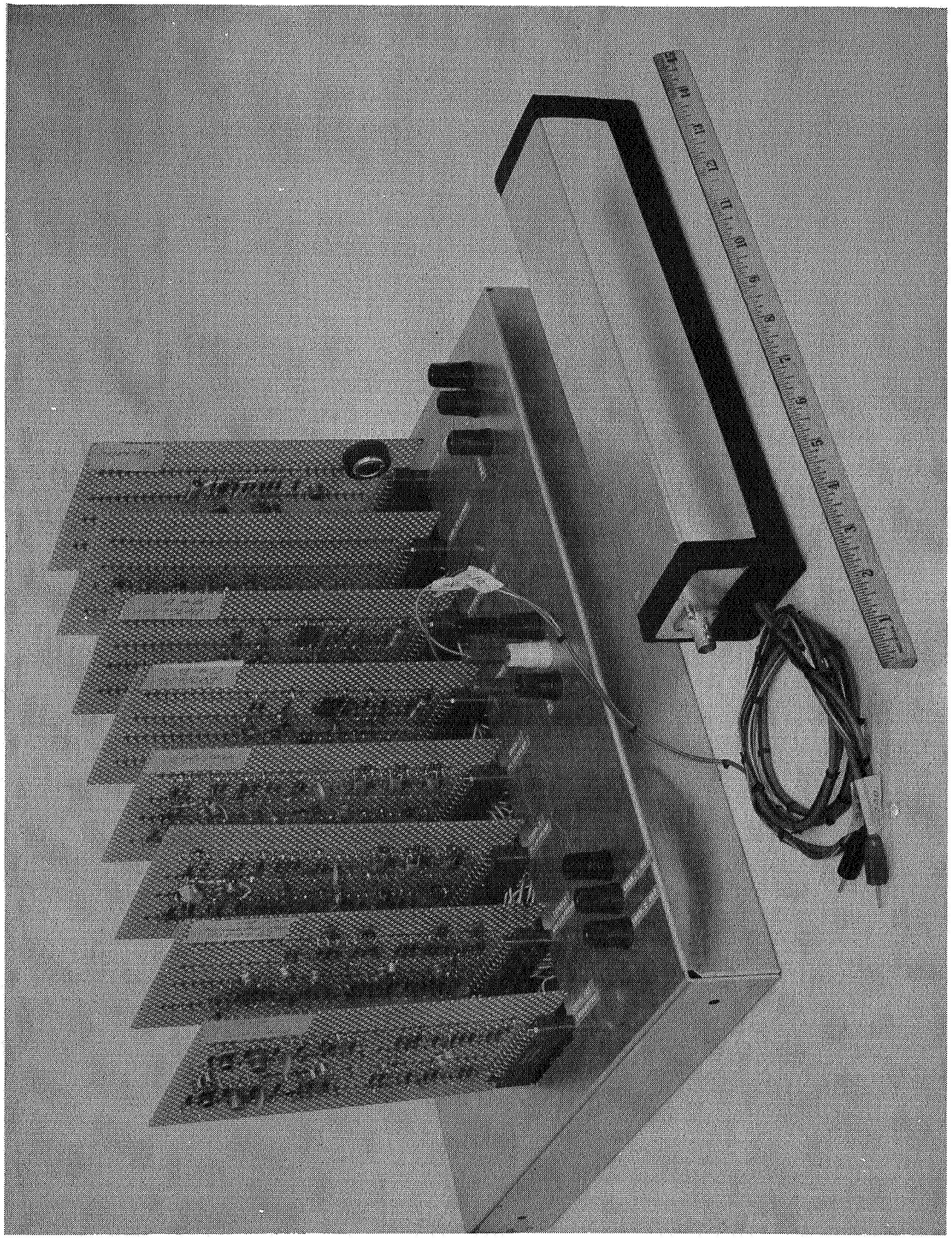

Figure 33. Dual Ablation Measuring Breadboard System.

3. Flip-Flops and AND Gates
4. AND AND NOR, One Shots, and Averaging

Each module consists of at least two printed circuit boards with the discrete components soldered to them. Standard fabrication procedures applicable to printed circuit board-soldered discrete components are used throughout. After the boards are wired, each diode is coated with RTV 102 silicone rubber to protect the diode glass from fracture during curing of the primary epoxy embedding compounds.

The boards of a module are wired together, staked to a header, and embedded in an epoxy potting compound. Each module is then finished to proper size and shape.

Emerson chose the embedded module approach because of its inherent ability to withstand severe shock, vibration, acoustic, and acceleration inputs. Protection from these environments is principally provided by the epoxy embeddment material which prevents relative motion between components thus reducing fatigue action.

The modules are then assembled in final system form and the individual headers wired together according to the interconnection diagram. This header is then embedded in a soft potting compound thereby providing repairability to an individual module level. The modules are held together by top and bottom metal cover plates to which each module is bolted. The eight through bolts provide the means by which the Signal Processor is hard mounted to a test or rocket vehicle structure.

The pre-amplifier module is separate and is attached to the rear of the Radiation Detector. Fabrication and wiring of the circular printed circuit board follows standard procedures. Circuit components are then embedded, in epoxy, into the annular space between two concentric potting shells. After attachment to the rear of the Radiation Detector, and wiring, the hole in the center small potting shell is filled with RTV102.

Fabrication of the Radiation Detector is performed by the suppliers, EMR and Harshaw Chemical Co. The photomultiplier tube with wrap around high voltage power supply is supplied by EMR potted in an epoxy fiberglass tube. Harshaw Chemical Co. then bands a Cesium Iodide crystal to the phototube faceplate. This assembly is then potted inside an aluminum can fitted with a

mounting bracket.

3.5.5 Testing. The initial functional, temperature, and linearity testing was performed on the breakboard circuits. Functional tests to 100 Kc were performed on the logic circuits at room temperature and insured proper action.

Output linearity versus input pulse frequency tests were performed on the entire breakboard. Input pulses were supplied with a laboratory pulse generator. For tests at various frequency ranges, to 100 Kc, and room temperature, the results indicated the system was linear to within ½% of full scale reading. For tests to 100 Kc over a temperature range of 20 to 160°F, the results indicated linear operation to within 1% of full scale reading. For tests at room temperature to 100 Kc varying the supply voltage from 23 to 31 volts, the results indicated linear output to within ½% of full scale.

Threshold and hysteresis levels were tested as a function of temperature from 20 to 160°F. The results indicated a 5% change of levels between 120 and 160°F. The detector frequency limits were over 500 Kc.

Amplifier linearity was checked to 100 Kc with various input pulse widths from .6 to 2.2 microseconds. The results indicated linear performance.

Output voltage and One Shot pulse width were tested from 20 to 160°F at 100 Kc. The results indicated a 40% decrease in pulse width as the temperature increased from 20 to 160°F and a similar 15% decrease in system D.C. output.

These tests indicated that the overall system design was sound enough to initiate fabrication of the prototype system.

When the prototype systems were completed and integrated with their respective Radiation Detectors, but before final embeddment, the systems were again subjected to thermal tests. Based on the results of these tests thermistor compensation networks were designed and incorporated into the pre-amplifier, One Shot, and Averaging circuits.

Output linearity tests, as a function of input frequency at room temperature, were performed on the system. Pulse input was from a laboratory pulse generator. The results indicated linear operation to a maximum frequency of 100 Kc, over various frequency ranges.

3.6 Reliability

A detailed reliability analysis is contained in the Appendix, Volume II. Pertinent results of the analysis, performed after the breadboard system was fabricated, are presented here.

The analyses showed that six resistors were utilized in circuits where they would be expected to dissipate 200 percent of their power ratings. These resistors were changed.

Parts were selected such that they would be subjected to a stress ratio of 30 percent or less. In most cases this stress ratio was held to 10 percent or less.

The significance of this can be seen by the fact that the failure rate at 50°C for the particular type capacitors and resistors used in the Ablation Meter triples as the stress ratio is raised from 30 percent to 100 percent. The failure rate for diodes and transistors under the same conditions is increased by a factor of 5 or more. The necessity of maintaining low stress ratios in order to obtain a high MTBF is thus quite apparent.

These analyses assured the selection of MIL-STD silicon diodes and silicon NPN transistors wherever possible due to low failure rates of these devices compared to germanium or PNP devices.

The maximum temperature to which parts would be exposed on a mission was held to 50°C. This was effected by a power supply design which provides thermal heat sinks for two power transistors and a power resistor. Not only was the temperature of the high power dissipating parts lowered, but also the temperature of all surrounding parts were lowered and resulted in a 50 percent increase in the MTBF of the power supply.

A reliability prediction was made utilizing the failure rates and procedures of MIL-HDBK-217A (1 December, 1965). Component failure rates were adjusted using the recommended K factors for missile applications as specified.

Reliability is expressed as a probability of failure free operation over the specified mission interval. Certain standard assumptions were made to allow this calculation.

1. The Ablation Meter failure is constant for the 120 hour hour checkout period and the 10 minute mission length. This is a good assumption since infant mortality failures will be removed during checkout at Emerson and part wearout times are for greater than 120 hours.

2. Any discrepancies noted during the 120 hours of checkout are repaired prior to launch.

With these assumptions, using the exponential expression relating mission reliability (success probability) and failure rate:

$$R = P_S = e^{-ft.}$$

	Name of Unit	No. of Units	Failure Rate (Each)	Failure Rate (Total)
1.	Pre-Amplifier	1	.5493	.5493
2.	Amplifier	1	3.5903	3.5903
3.	Detector A, B, C, or D	4	3.8678	15.4712
4.	AND Gate	6	.6885	4.1310
5.	Flip-Flop	6	2.6315	15.7890
6.	AND-AND-NOR Gate	2	1.9155	3.8310
7.	1 Shot and Averaging	2	6.4577	12.9154
8.	Toggle	1	5.9830	5.9830
9.	Power Supply	1	10.5287	10.5287
10.	Chassis	1	4.1601	4.1601
11.	Photomultiplier Tube (EMR)	1	2.0000	2.0000
12.	Photomultiplier Tube (EMR) Pwr. Supp.	1	12.4845	12.4845
	Total System Failure Rate =			$\overline{91.4335}/10^5$Hrs.

P_S (For 10 minute mission) = .99985 (probability of successfully completing a 10 minute mission.)

MTBF = 1090 hours

3.7 Flight Mission Requirements

3.7.1 General. Flight mission requirements are governed primarily by: (1) distance from source to detector, and (2) maximum expected ablation rate.

The distance from Ablation Sensor Plug to the Radiation Detector is the major consideration in determination of source strength. Source strength required for a given system output increases as the square of the distance between source and detector. This effect is presented in Figure 34, which shows calculated source strength as a function of distance from source center to detector face.

The maximum expected ablation rate determines the appropriate system time constant to be set on the Signal Processor. In actual usage the system will be monitoring a continually depleting heat shield thickness thus a continually decreasing disintegration rate. Since the system averages the disintegration rate it sees over an interval that is past in time, it will always lag the instantaneous disintegration rate by approximately one half a system time constant.

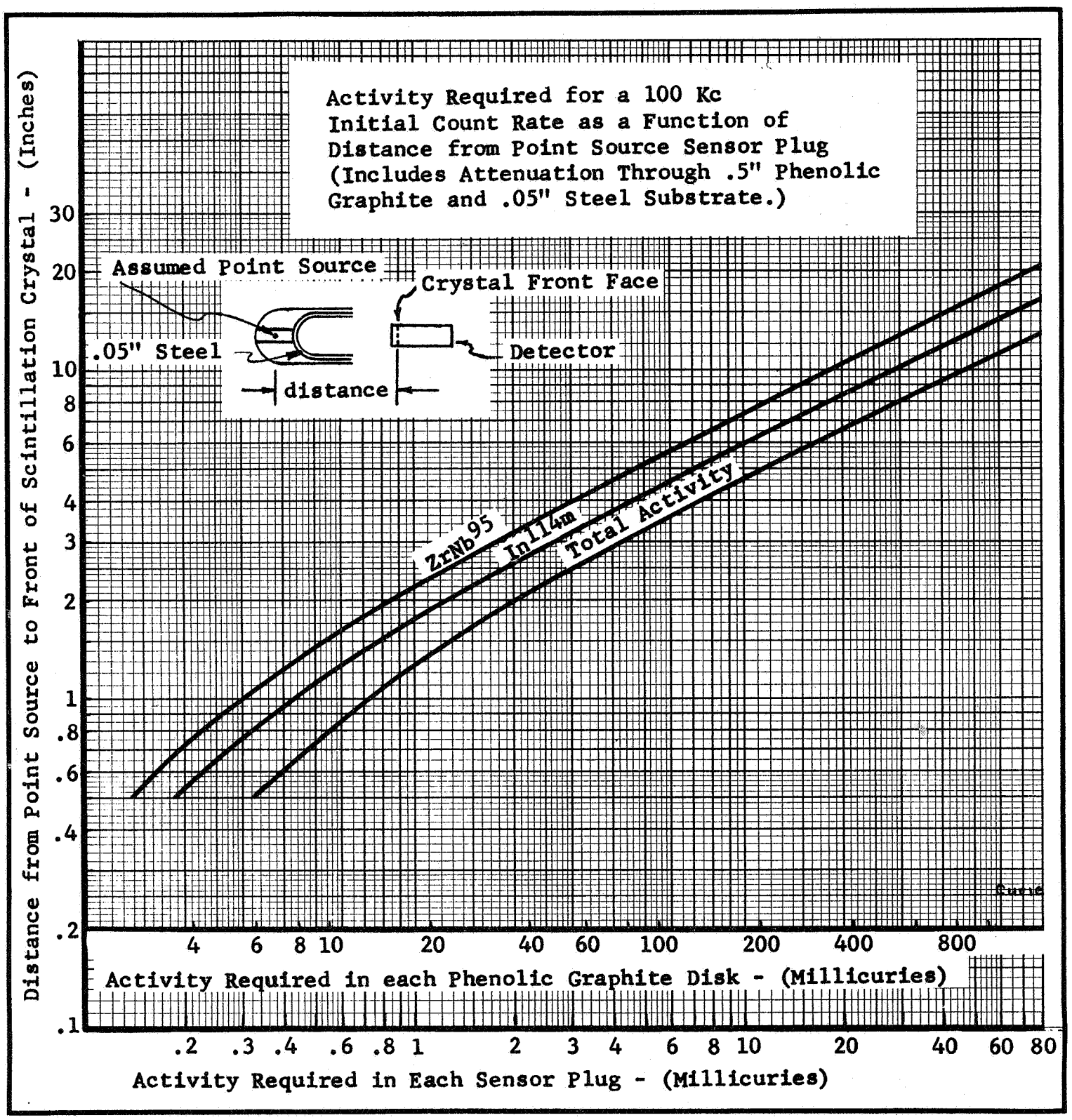

Figure 34. Calculated Source Strength as a Function of Distance.

Nuclear disintegrations are random in nature, however, and the smoothness of data output also depends on the time interval (system time constant) over which the disintegration rate was averaged.

Therefore, in the specification of the system time constant to be used for a particular flight mission, a trade-off must be considered between output data smoothness and the magnitude that the system lags the instantaneous, decreasing, disintegration rate.

As an example of flight mission requirements, source strength calculations as well as trade-off effects of specified system time constant will be presented with reference to a specific flight mission.

3.7.2 Example Flight Mission Parameters. These example flight mission parameters were obtained from the NASA-LRC letter of June 23, 1966, to Mr. J. D. Bartley, Jr., of Emerson Electric. The recession rates were obtained from flight test data of one type of research vehicle. The flight mission parameters were:

1. Radioactive source at flight payload stagnation point.
2. Radiation detector on axial centerline of payload.
3. 1.0 inch ablator (Narmco 4028) thickness.
4. 0.05 inch steel substructure thickness.
5. 1-1/16 inches from face of scintillation crystal to substructure.
6. Maximum surface recession rate of 0.030 inches/second.
7. The above maximum rate to occur after a surface recession of 0.5 inches.
8. Maximum pyrolysis-interface recession rate of 0.045 inches/second.
9. The above maximum rate to occur after a pyrolysis-interface recession of 0.7 inches.
10. The assumption of point sources of radiation 0.5 inch from the ablator-substructure interface and on the detector axial centerline.

Additional parameters that entered into the calculations were:

1. CsI scintillation crystal 1 1/4" diameter by 1" thick.
2. Measuring isotopes were In^{114m} and $ZrNb^{95}$.
3. Electronic windows at .1, .25, and .85 Mev.

3.7.3 Substructure Attenuation. A small percentage of the photons emitted from the radioactive ablation sensor plug will be absorbed and scattered in both the steel substrate and the ablator. The equation used to calculate absorption is:

$$I/Io = Be^{-\mu x}$$

where: I = intensity at thickness x
I_o = original intensity
B = dose build up factor
μ = absorption coefficient

For this calculation the dose build up factor will be assumed to be 1.0. Dose build up occurs by scattering within the absorber. The resultant scattered photons appear at lower energy levels. This measuring system needs photons in the proper windows for counting therefore B assumed = 1.0.

The absorption coefficients for steel were found from the Nucleonics Data Sheet "Gamma Ray Absorption Coefficients". The absorption coefficients for Narmco 4028 were found from the NBS Radiological Health Handbook assuming that carbon was the major constituent. The resulting attenuation was calculated by assuming that all photons emitted travel through .5" of ablator and .05" of steel. These attenuation figures, presented below, are subsequently used in the calculation of source strength.

Material	Absorption Coefficient (In^{-1})		(%) Fraction Transmitted	
	.2 Mev	.75 Mev	.2 Mev	.75 Mev
.05" Steel	3.01	1.51	86.0	92.7
.5" Narmco	.426	.237	80.9	88.8

Figure 35 presents calculations of percent of incident of gamma photons transmitted through steel and tungsten substructures using dose build up factors recommended in the NBS handbook previously mentioned.

3.7.4 Overall Counting Efficiency. Overall counting efficiency is a function of incident gamma ray energy, scintillation crystal size and type, and source-crystal geometry. Figure 36 presents these relationships for a 1" diameter by 1" thick NaI scintillation crystal. Figure 35 presents the relationship of geometry change alone for different detector sizes. Overall counting efficiency is the percent of total gamma disintegrations that interact with the scintillation crystal.

The Radiation Detector of the Dual Ablation Measuring System uses a 1 1/4" diameter by 1" thick cesium Iodide scintillation crystal. However, the 1" diameter by 1" long curves of Figure 34 were used to calculate required source strength to provide a conservative (i.e. large) estimate.

The flight mission parameters indicate that the assumed point sources are (1.0625) + (.5) + (.05) = 1.61 inches from the face

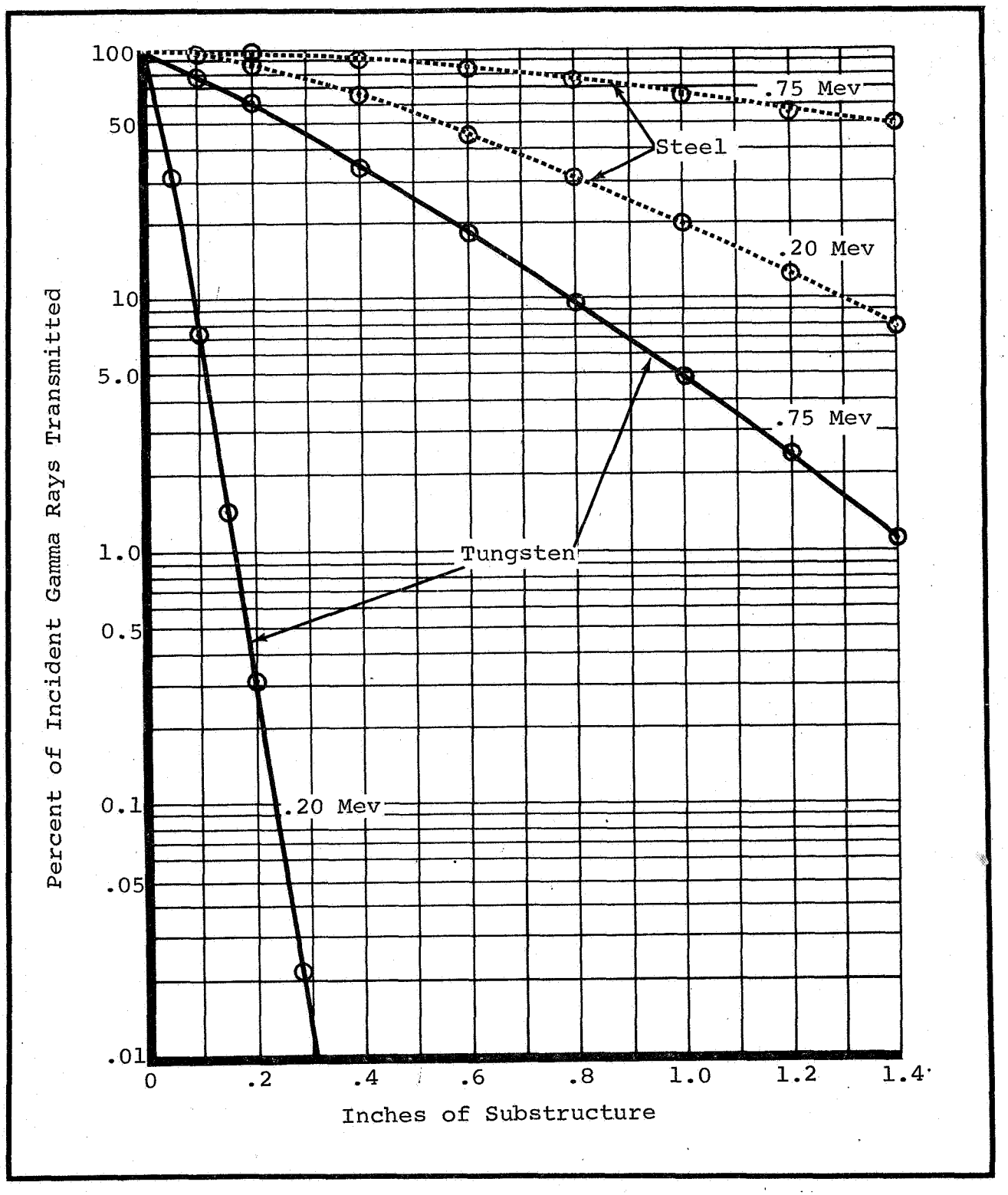

Figure 35. Calculated Percent of Incident Gamma Rays Transmitted Through Substructure, Including Dose Build Up Factors.

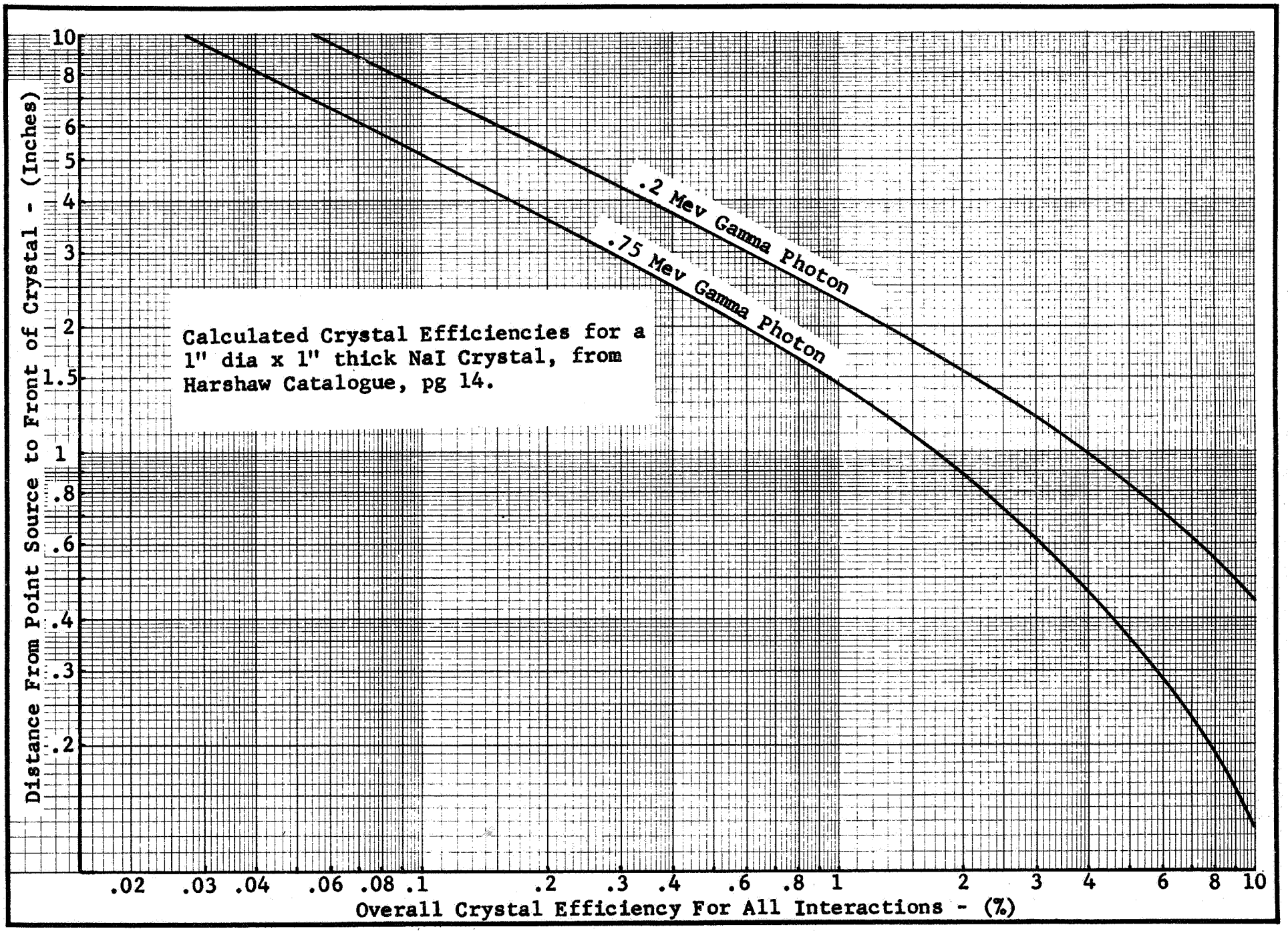

Figure 36. Calculated Overall Crystal Efficiencies for a 1" dia by 1" NaI Crystal.

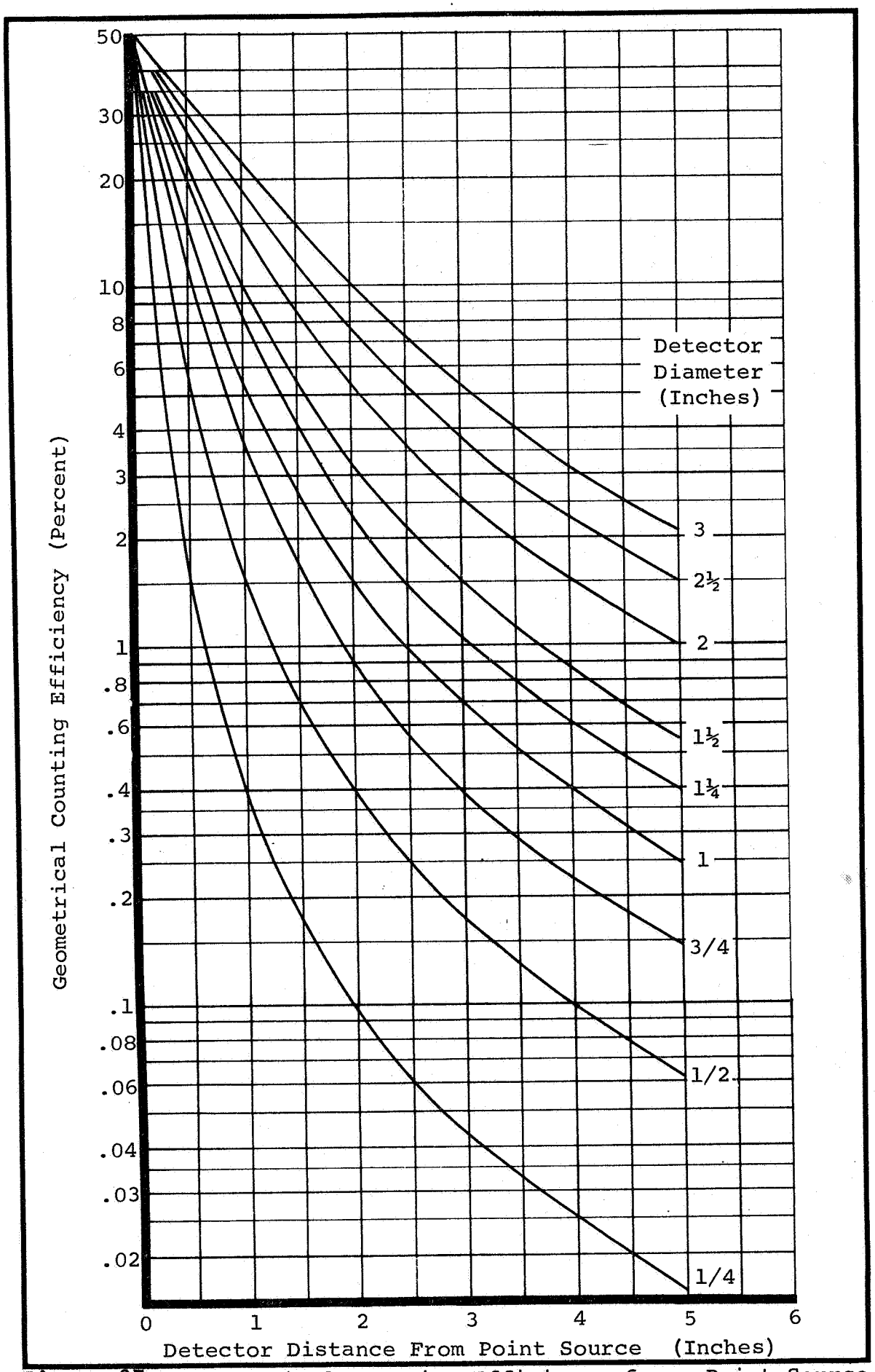

Figure 37. Geometrical Counting Efficiency for a Point Source and Various Sizes of Detectors.

of the scintillation crystal. From Figure 36, the overall counting efficiencies for a Sodium Iodide crystal are:

.85% for a .75 Mev photon
1.90% for a .20 Mev photon

Cesium Iodide (a higher density crystal than Sodium Iodide) is 20% more efficient than Sodium Iodide for photons of .75 Mev, and 6% more efficient than Sodium Iodide for photons of .2 Mev. Therefore the overall counting efficiencies for a Cesium Iodide crystal are:

1.03% for a .75 Mev photon
2.03% for a .20 Mev photon

3.7.5 Electronic Window Restrictions. Figure 38 presents the nuclear gamma spectrum of In^{114m} and $ZrNb^{95}$ with the system electronic windows superimposed. (These spectra were obtained at the NASA-LRC with a 2" diameter by 2" thick Sodium Iodide scintillation crystal.) The important point to note is that not all detected disintegrations appear at the nominal energy level of the particular isotope. This is called spectrum overlap. Integration under the curves of Figure 38, in the proper electronic windows, yields the following restrictions:

1. 59.2% of total crystal interactions from an In^{114m} source will be counted in the lower window.
2. 42.3% of total crystal interactions from a $ZrNb^{95}$ source will be counted in the upper window.
3. 32.4% of In^{114m} counts in the lower window will fall in the upper window.
4. 46.4% of $ZrNb^{95}$ counts in the upper window will fall in the lower window.

These percentages would change if the windows were not positioned as shown or if the spectra were not positioned in the windows as shown.

3.7.6 Source Strength Calculation. The following source strength calculation is based on count rates of 100 Kilocycles per channel. It is desireable to use the system at maximum count rate to provide the smoothest output data consistent with maximum tracing accuracy.

80 Kilocycles actual $ZrNb^{95}$ counts and 63 Kilocycles actual In^{114m} counts will overlap to give a 100 Kilocycle count rate in each channel. (Calculated from the figures presented in the Electronic Window Restrictions section.)

The total counting efficiency is determined by multiplying all

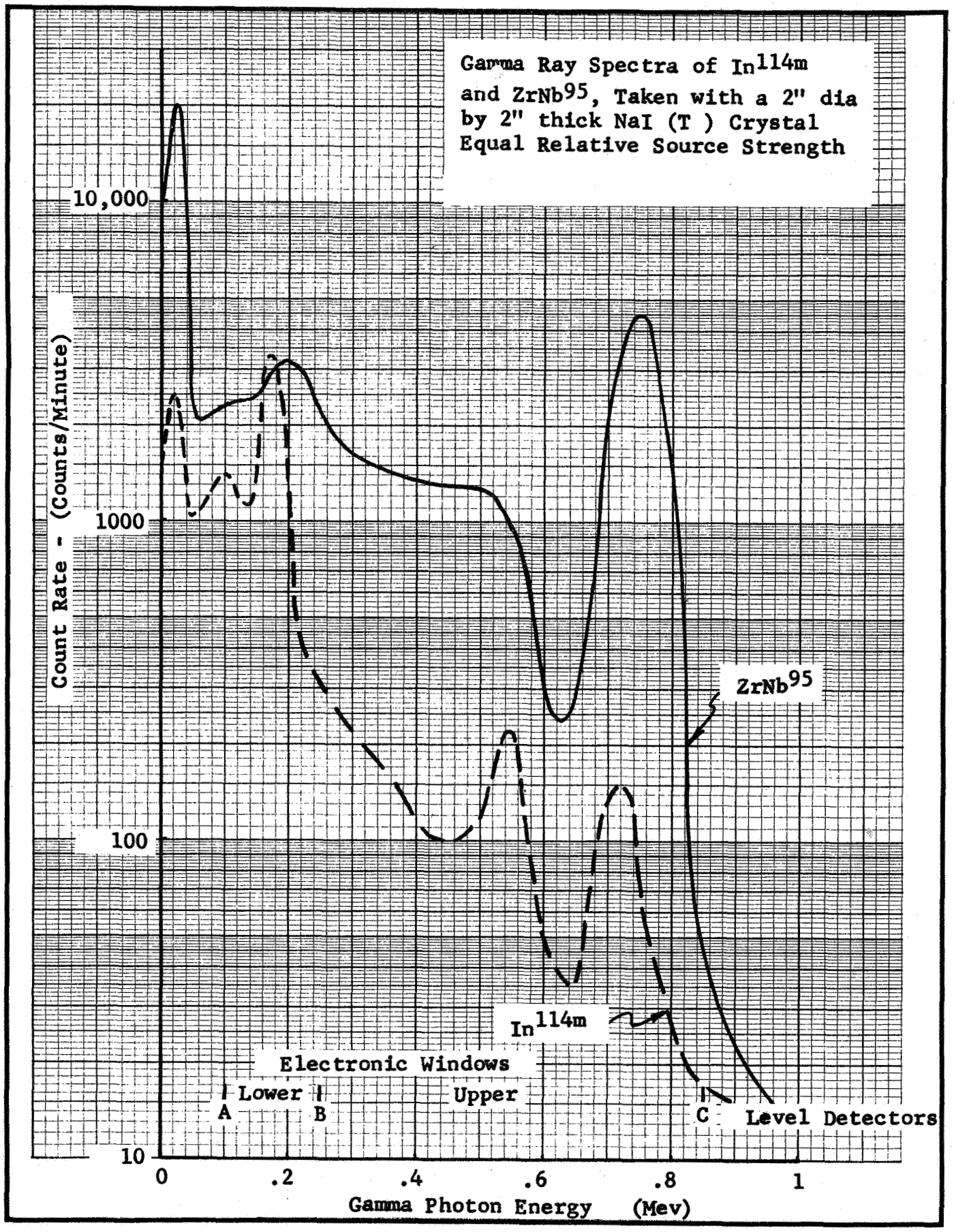

Figure 38. Gamma Ray Spectra of In^{114m} and $ZrNb^{95}$

efficiencies together. Thus for In^{114m} the total efficiency is:

$$(.0203)(.592)(.860)(.809) = .835\%$$

And the total efficiency for $ZrNb^{95}$ is:

$$(.0103)(.423)(.927)(.888) = .359\%$$

In^{114m} emits one gamma photon for every 4.2 beta particles. The Dual Ablation Measuring System will detect only gamma rays; thus the calculated amount of In^{114m} must be multiplied by 4.2 to put it on an equal gamma emission basis with $ZrNb^{95}$ which emits one gamma ray per disintegration.

Each millicurie of activity disintegrates at the rate 3.7×10^7 disintegrations per second.

Therefore we need:

$$ZrNb^{95} = \frac{(8.0 \times 10^4 \text{ counts/second})}{(3.59 \times 10^{-3})(3.7 \times 10^7 \text{ counts/millicurie-second})} = .603 \text{ millicuries}$$

$$In^{114m} = \frac{(6.3 \times 10^4 \text{ counts/second})(4.2 \text{ electrons/count})}{(8.35 \times 10^{-3})(3.7 \times 10^7 \text{ counts/millicuries-second})} = .858 \text{ millicuries}$$

Or a total activity of 1.46 millicuries per Ablation Sensor Plug. These figures were plotted on Figure 34 to show source strength requirements as a function of distance from the Radiation Detector.

3.7.7 System Time Constant Determination. The maximum expected ablation rate, 0.45 inches per second for the example flight mission, determines the proper system time constant. The Dual Ablation Measuring System has four built in time constants: .05, .1, .25, and 1. seconds. Figure 39 shows that specification of a .05 second time constant would provide system tracking accuracy of approximately .2% for an ablation rate of .045 inches per second. This means that the system would lag the instantaneous reading by .2% of the original reading or .002 inches.

Figure 40 shows system output data smoothness as functions of system time constant and count rate. The random disintegration of radioisotopes cause the statistical fluctuation around the mean or true instantaneous disintegration rate. For the .05 second time constant, specified above, Figure 40 indicates that output data would fluctuate less than ±2% around the mean value at a count rate of 80 kilocycles per second.

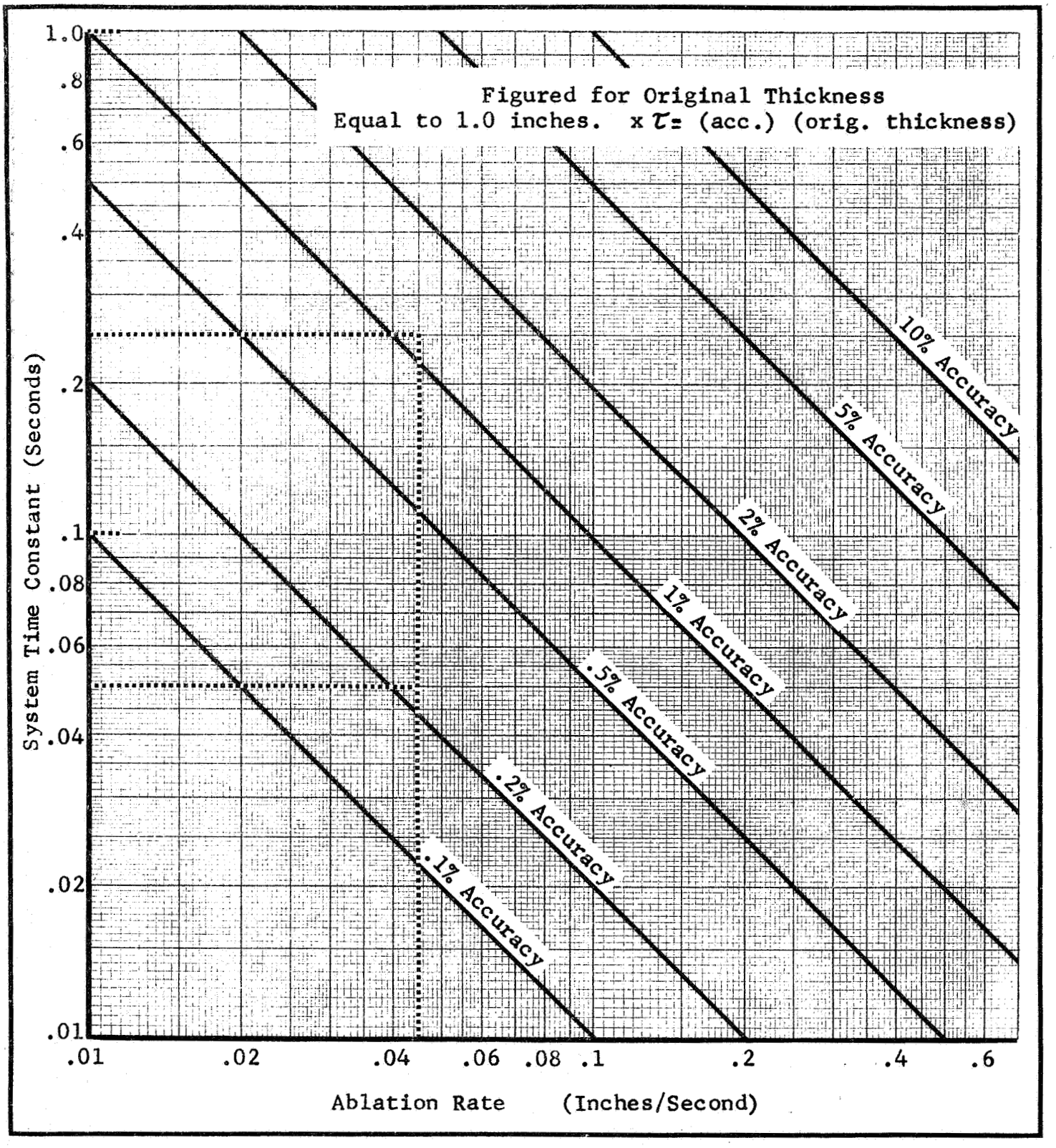

Figure 39. System Tracking Accuracy As A Function of Time Constant And Ablation Rate

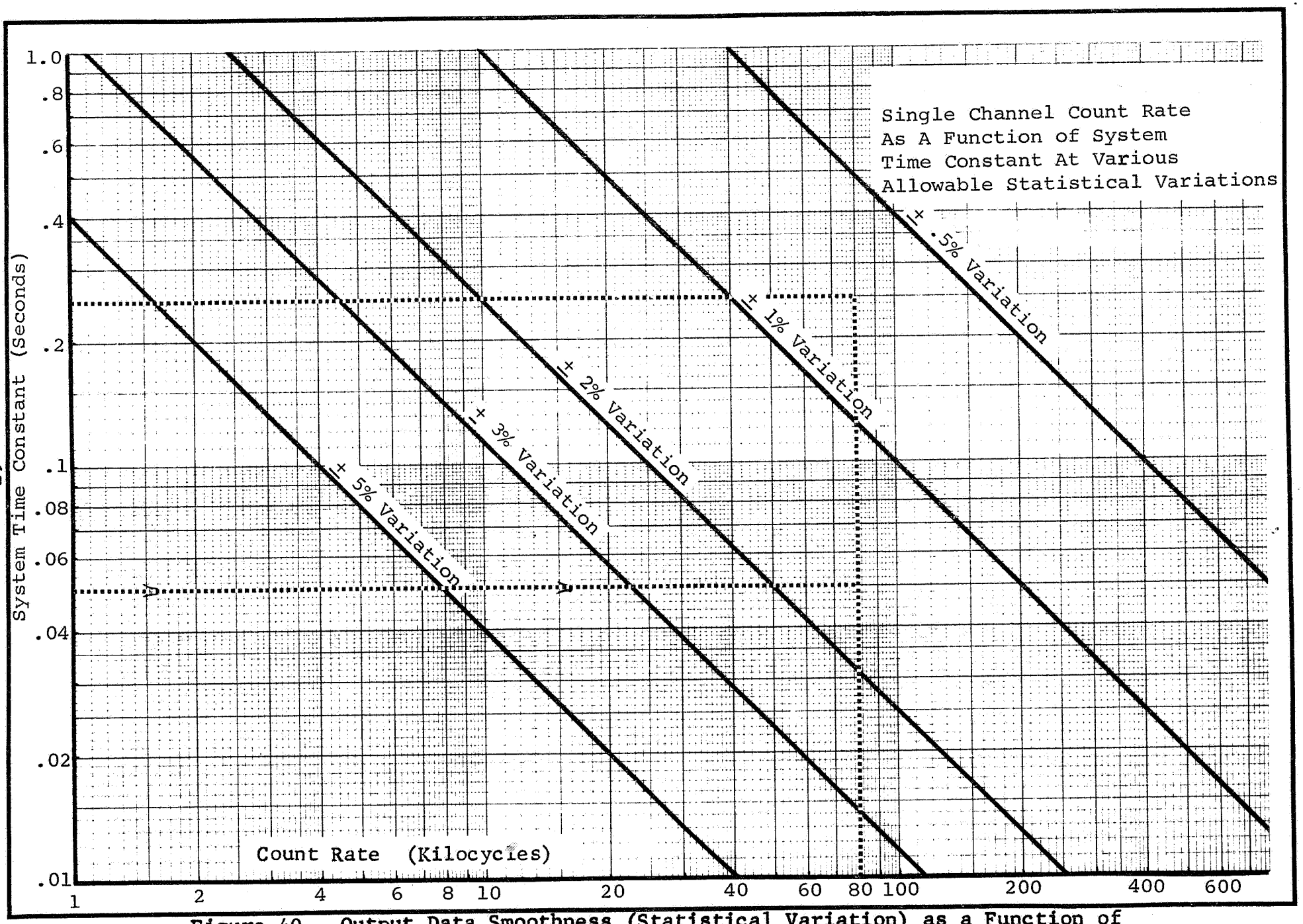

Figure 40. Output Data Smoothness (Statistical Variation) as a Function of System Time Constant and Single Channel Count Rate.

It is desirable to have minimum output data fluctuation, statistical variation, consistent with acceptable system accuracy or resolution. For the example flight mission, specification of a .25 second time constant would minimize output data fluctuation to less than ±1%, at an 80 Kilocycle count rate; system resolution (from Figure 37) would then become approximately 1%, or .01 inches, at an ablation rate of .045 inches per second.

Thus a trade-off exists between desired output fluctuation and system resolution. For the example flight mission a time constant of .25 seconds should be specified. This value minimizes output data fluctuation without sacrificing system resolution beyond the point of accurate data retrieval.

3.7.8 Summary. The various parameters that must be defined to determine flight mission requirements of the Dual Ablation Measuring System have been presented along with a brief discussion and example calculation. Calculations were based on a 100 kilocycle single channel count rate. This was done to provide the smoothest data consistent with maximum accuracy. Many flight missions will not require this high degree of accuracy. In that case, after careful study of the trade-off points, it is possible to use the system at a lower maximum single channel count rate. It is possible, by means of the built in output gain switches, to use the system with source levels that provide a maximum single channel count rate of 10 kilocycles. For laboratory use capacitors may be added externally to provide full scale, five volt, output at even lower source levels.

3.8 System Characteristics.

The Dual Ablation Measuring System was designed to be compatible with the performance and environmental requirements of advanced research rocket vehicles such as the NASA's Pacemaker. The design guidelines of paragraph 3.1 were followed as closely as possible. The resulting system has the performance, environmental, and electrical requirements presented in **Figures 41** through **43.**

	Maximum	Minimum
Ablation material thickness (inches)	2.00	0.25
Virgin material thickness (inches)	2.00	0.25
Char layer thickness (inches)	0.50	0.00
Surface Temperature (^{o}F)	5000	1500
Char Interface Temperature (^{o}F)	1300	750
Isotope Half Life (days)	--	50
Heat shield substructure thickness (Inches of tungsten alloy Kennertium W-2).	0.75	0.00
Size	33 In^3 (excluding detector)	
Weight	1.90 pounds (excluding detector)	
Power	3.6 Watts at 28 volts	
System Output	Analog voltage proportional to input count rate	
Output Impedance	Less than 100 ohms	
Accuracy	System output tracks the input count rate within five percent over a range of ablation rate of 0 in/sec to .25 in/sec at a max. rate of change of 0.04 in/sec^2	

Figure 41. Dual Ablation Measuring System Performance Specifications.

Environment	Specification	Test
Vibration		
Sinusoidal, Fig 514-3 Curve B, 5-10 Hz-.20" DA, 10-18Hz-1g, 18-40Hz-.06" DA, 40-2000Hz-5g	MIL-STD-810A Method 514-1 Equipment Class 4	30 min Logarithmic Sweep 5-2000-5 Hz in 15 minute 3 axes
Random Fig 514-4 Curve B, $.04g^2/Hz$ 7.5g rms	MIL-STD-810A Method 514-1 Equipment Class 4	30 minute 3 axes
Acceleration	MIL-STD-810A 30 g	60 seconds 6 axes
Shock	MIL-STD-810A 20 g Fig 516-1	10 milliseconds Sawtooth
Temperature	55° F to 95° F (including Detector)	20° Steps 30 minutes at each step

Altitude	Vacuum equipvalent to an altitude of 300,000 Feet	30 Min at 300,000 Ft. 10 Min descent to ground level

Figure 42. Dual Ablation Measuring System Environmental Specifications

Input Power: 28 ± 3 VDC, 120 Milliamperes maximum
Input Radiation: Channel 1: $Indium^{114m}$
Channel 2: $Zirconium\ Niobium^{95}$

Output Signals

Channel 1: 5VDC maximum at 100 Khz
Channel 2: 5VDC maximum at 100 khz

Time Constants: .05, .1, .25, 1.0 second each channel
Output Level: Impedance 1 Kohm, short circuit proof;
4 Coarse adjust, 6 fine adjust each channel

External One-Shot Capacitor

The One-Shot timing capacitor may be externally paralleled to lengthen the One Shot pulse width. This allows operation at low radiation levels. Note: This capability is not short circuit protected. For values of external capacitance greater than .001 microfarad, a factor of .0014 Khz per microfarad may be used to size the capacitor for full scale voltage.

Figure 43. Dual Ablation Measuring System Electrical Specifications

4.0 SYSTEM PERFORMANCE TESTS

4.1 Tracking Accuracy.

The Dual Ablation Measuring System must integrate detected radionuclide disintegration over a finite time period. This period is called the system time constant and is defined as the time required for the system output to respond to 63 percent of an instantaneous step change in input.

The design guidelines state that desired tracking accuracy is 5% of input signal for a maximum rate of change of 100% of input signal per second. (Maximum ablation rate of .25 in/sec at minimum thickness .25 inches). The system will always lag the instantaneous input by a value less than one time constant. Assuming that the system lags by one full time constant, a system time constant of .05 seconds would fulfill the design guidelines. (.05 seconds x 100%/sec)

A series of tests were performed to check the actual system performance.

Measurements were made of system tracking accuracy in the following manner. The Dual Ablation Measuring System output was connected to a recorder. A parallel connection from the Radiation Detector was made to a multichannel analyzer in the multiscaling mode. The multiscaling mode caused the analyzer to dwell on each channel during its all channel scan for one second. Detected pulses from the radiation detector were those sequentially stored in separate channels of the analyzer during the one second dwell.

A radioactive source was placed in front of the Radiation Detector. The source was connected to the paper movement reel of a Brush recorder in such a manner as to cause the source to move away from the detector at a constant speed of .5 cm/second.

The recorder and multichannel analyzer were turned on. As the radioactive source moved away from the Radiation Detector, the output of the Dual Ablation Measuring System was recorded on the recorder, and the Radiation Detector output was simultan-

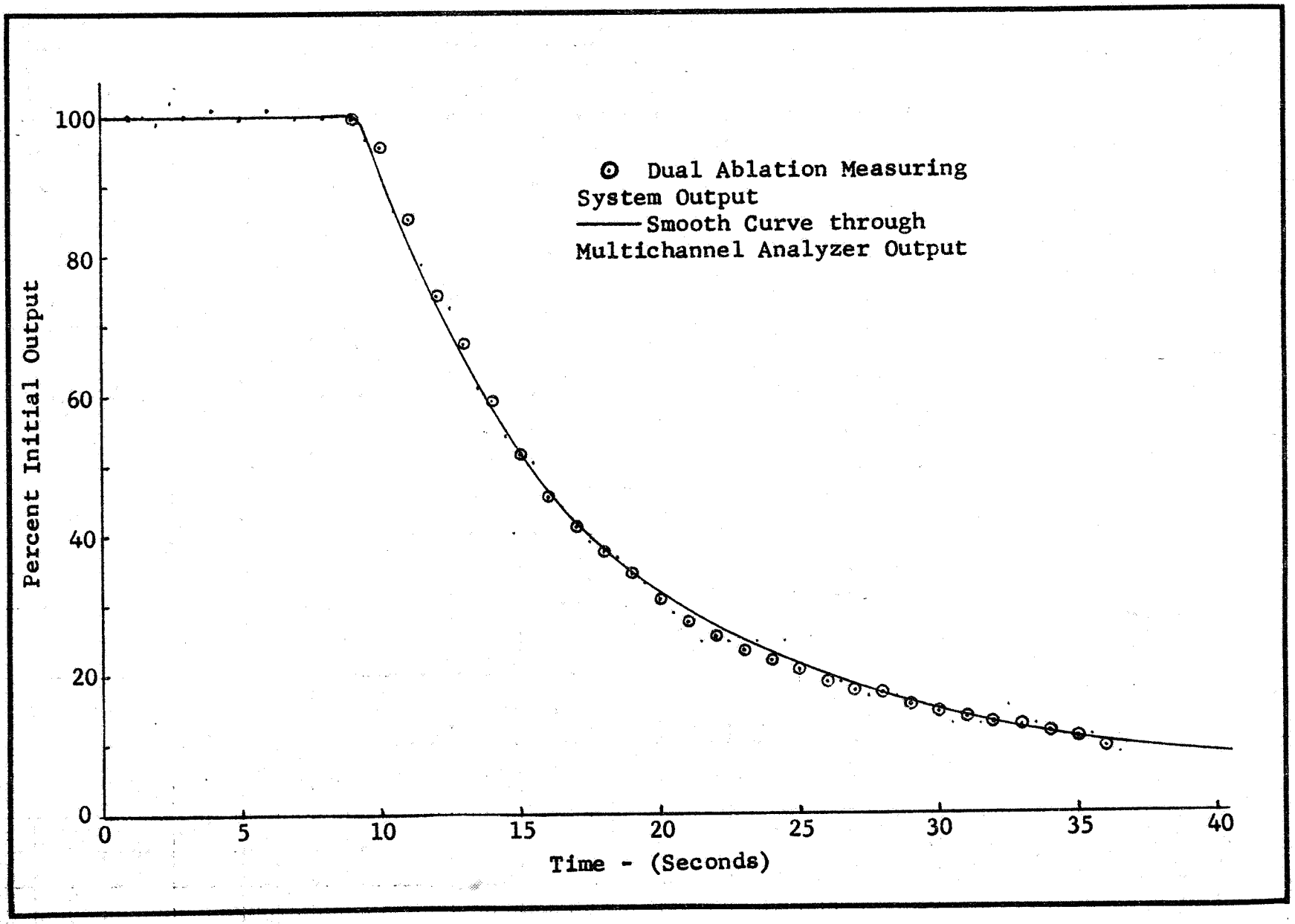

Figure 44. Results of System Tracking Accuracy Tests.

eously stored in the multichannel analyzer in sequential channels.

When the results are plotted to the same scale a plot of system analogue output is obtained from the recorder and system digital input from the multichannel analyzer. A smooth curve drawn through the multichannel analyzer data represents true input. Data points from the recorder may be superimposed to show how accurately the Dual Ablation Measuring System tracks a changing input signal.

The results from one of these tests are presented in Figure 44. The results indicate that the Dual Ablation Measuring System will track input well within the specified 5 percent during the period of most rapid signal change.

The circled data points represent Ablation Meter Output. Other data points are the Multichannel analyzer output through which the smooth curve was drawn. On this test statistical variation of the input signal increased until at about 30 percent of initial input signal the statistical variation in the multichannel analyzer data overshadows any tracking errors.

The method of interpreting this curve is the following. At ten seconds the rate of signal change is 14.8% per second of input signal. At eleven seconds the rate of signal change is 11.8% per second of input signal. With the .25 second time constant used for test, if we assume that the system lags input by a full time constant, the Dual Ablation Measuring System output should be 3.7% and 2.95% behind the input signal. The actual data points indicate a lag of 3.2% and 3.0%.

Thus the system performs as predicted if lagging by one full time constant is assumed. Extending these results to the ca e of a .05 second time constant with a signal rate of change of 100% per second, it may be seen that system design guidelines, with respect to tracking accuracy, have been met.

4.2 Ablation Tests.

4.2.1 General. A series of forty ablation tests were performed using the pre-production Dual Ablation Measuring System Serial Number 1. External capacitance was added to the system to provide full scale output at the low counting rates necessarily used in the laboratory. Ablation Sensor Plugs were fabricated of phenolic nylon and phenolic graphite heat shield materials; each contained 40 microcuries of $ZrNb^{95}$ and 160 microcuries of In^{114m}.

The ablation tests were performed in the oxy-acetylene jet facility for varying durations at heat fluxes from 100 to 400 BTU/ft^2-second. System calibration, test procedure, data reduction

method, and test results are discussed in the following paragraphs.

4.2.2 System Calibration Procedure. Calibration of the Dual Ablation Measuring System is similar for either a flight mission or laboratory usage. Three Ablation Sensor Plugs must be fabricated. One contains both radioisotopes. The other two are composed of stacks of disks containing only one radioisotope in each stack. The overall stack length is equal to that of the Sensor Plug with both radioisotopes. The diameter of these Sensor Plugs is slightly smaller than that for the test. The Sensor Plugs are used in conjunction with the Radiation Detector to provide system calibration curves and spectrum overlap curves.

The one Sensor Plug that contains both radioisotopes should contain the amount of radioactivity that will be present in the test specimen on date of test. The ratios of one radioisotope to the other must also be the same as desired on test date.

The quantities of isotopes in the two stacks of slices, containing only one isotope each, are calculated to give at least eighty percent of full scale deflection in one channel or the other. The number of slices depends on the desired accuracy of calibration and on ease of production. **For a one inch thick heat shield, ten .1 inch thick slices are convenient.**

The Radiation Detector of the Dual Ablation Measuring System must be placed in the test model (or a model exactly the same shape and material as the **test model) in exactly the** same position with relation to the Ablation Sensor Plug location as it will be placed during the test. Accurate system calibration depends on precise geometric repetition of the relative locations of Ablation Sensor Plug and Radiation Detector.

Calibration procedure is quite simple. The system is turned on. Time constant switches are placed in the longest time constant position (#4). Gain switches are placed in the smallest gain position (#1).

The Sensor Plug containing both radioisotopes, of the strength to be expected on test date, is placed in the receiving hole in the test model. Gain switches in both output channels are adjusted to give the desired full scale outputs. The Sensor Plug is removed.

Both stacks of slices containing only one radioisotope go through the following operation.

One stack of slices containing only one radioisotope is inserted into the receiving hole in the test model. Readings are taken

of the output in both channels. One slice is removed from the stack. Output readings in both channels are taken and recorded again. This process is repeated until no slices remain in the test model. The process is repeated for the other stack of slices.

Data from this operation is plotted up in the form of two curves for each stack of slices containing one radioisotope. For the stack of slices containing $ZrNb^{95}$ the following curves are plotted: (1) Dual Ablation Measuring System Output in channel #2, expressed as a percent of output with all slices present, versus percent of total stack length (this is the calibration curve for total heat shield thickness); (2) Output in channel #1 as a percent of output in Channel #2 versus percent of total stack length (this is the spectrum overlap curve used in the determination of actual count rate from In^{114m} in the lower channel). For the stack of slices containing In^{114m} the following curves are plotted: (1) Dual Ablation Measuring System output in Channel #2 as a percent of output in Channel #1 versus percent of total stack length (this is the spectrum overlap curve used in the determination of actual count rate from $ZrNb^{95}$ in the upper channel); (2) Output in Channel #1 expressed as a percent of output with all slices present, versus percent of total stack length (this is the calibration curve for virgin material thickness remaining).

Smooth lines drawn through these data points provide the calibration and nuclear spectrum overlap curves. This method of calibration compensates for any system non-linearities that may be present in addition to the normal non-linearities that are introduced by system source-detector geometrical considerations.

Figures 45 and 46 present some of the calibration and spectrum overlap curves obtained during Isotope accuracy testing.

4.2.3 Test Procedure. The test procedures used for this series were essentially the same as those used previously during the Isotope Accuracy test series. The prime differences were in the equipment used: (1) A dual channel recorder was used instead of a single channel recorder; (2) The Dual Ablation Measuring System was used instead of laboratory radiation counting equipment; and (3) Predictions of total heat shield thickness and virgin material remaining were made from an average of the particular recorder traces end points instead of scaler readings.

Ablation test procedure was as follows. The Radiation Detector was placed in a fixture, behind a water-cooled fron face, similar to the fixture shown before. The system was connected properly, proper gain and time constant settings checked, and power applied to the system and recorder amplifiers. A test model, with radioactive Ablation Sensor Plug installed, was afixed to

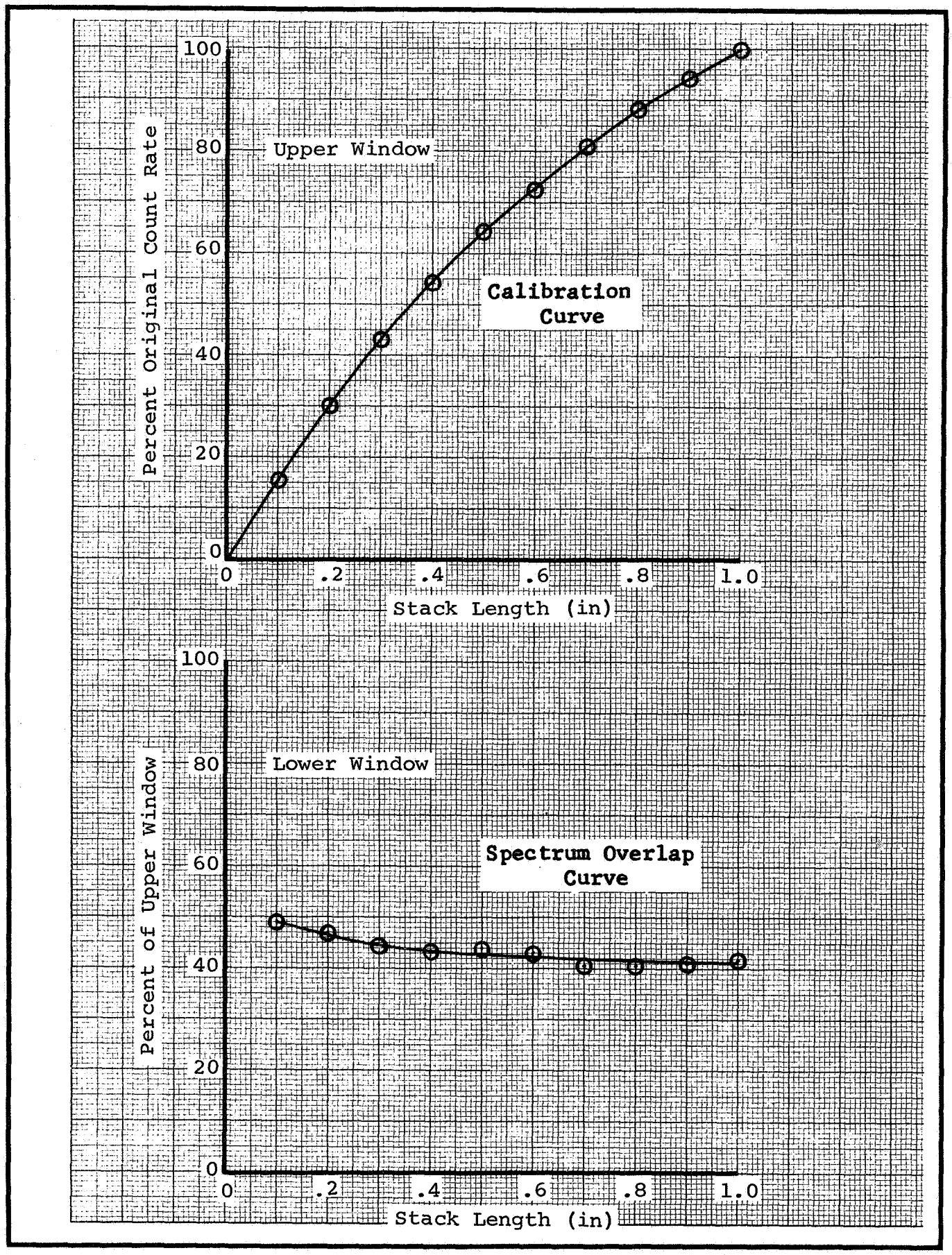

Figure 45. Example Calibration and Spectrum Overlap Curves, $ZrNb^{95}$ Only.

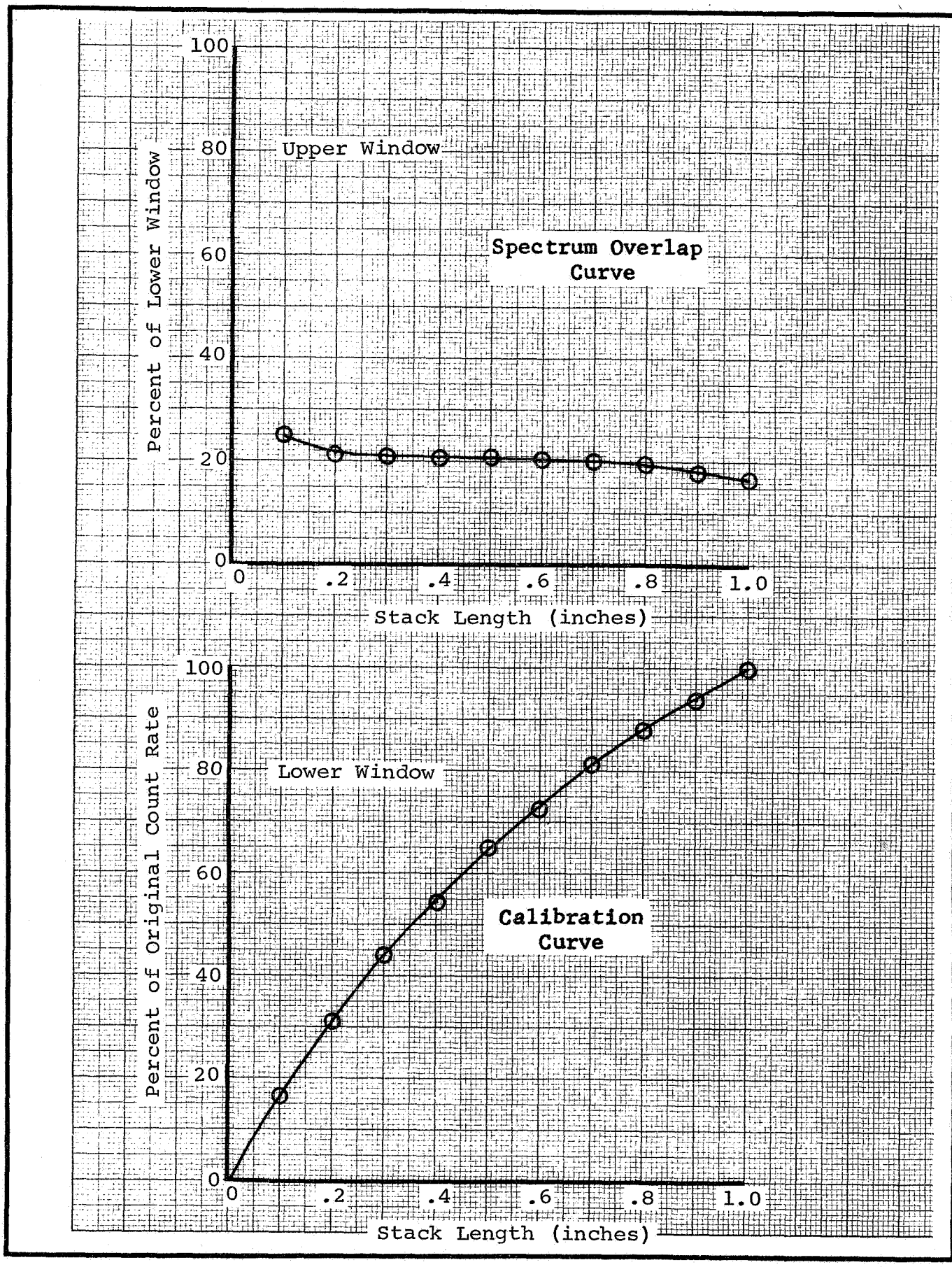

Figure 46. Example Spectrum Overlap and Calibration Curves, In^{114m} Only.

the front of the water-cooled test fixture. The proper distance between oxy-acetylene jet tip and test model front face was set. The recorder was turned on and allowed enough time to set a 100% signal base line. The jet was ignited, swung in front of the test model for the proper test duration, and swung out. Test start and stop were marked on the recorder traces. During the test the model front face temperature was obtained with an optical pyrometer.

After the test the Ablation Sensor Plugs were X-rayed, sectioned, and the locations of surface and virgin material were visually measured and recorded.

Raw data from these tests as well as X-rays and post test model photographs are presented in the Appendix, Volume II.

4.2.4 Data Reduction Procedure. The recordings of a test present observed system output in each channel versus time. This data is reduced in the following manner to achieve total and virgin material recession as a function of time.

Because of the nuclear spectrum overlap obtained with these two isotopes, the test raw data does not directly yield percent of original radioactivity remaining of nuclear energy level characteristic of each output channel. The output in Channel #1 is composed of detected disintegrations from In^{114m} plus a certain percentage of Compton scatter from the disintegrations of $ZrNb^{95}$ in the higher energy channel #2. Similarly the output of Channel #2 is composed of disintegrations from $ZrNb^{95}$ plus the higher energy disintegrations from In^{114m}. Thus to obtain the disintegration rate of either $ZrNb^{95}$ or In^{114m}, it is necessary to subtract the percentage overlap from the other output channel. The nuclear spectrum overlap curves indicate the correct percentage to subtract.

For example: at any time the observed output in the upper ($ZrNb^{95}$) window is represented by

$$U_o = U_a + f(La)$$

where the subscripts refer to observed and actual, U and L refer to upper and lower window respectively, and f refers to the percent overlap of an In^{114m} signal into the upper $ZrNb^{95}$ window (expressed as a percent of lower window count rate, or output voltage).

A similar condition exists for the lower window observed output.

Solution of the simultaneous equations thus formed gives the output in each channel due to disintegrations of the isotope that emits primarily in the window of interest. This output is

then expressed as a percent of original output. Entering the calibration curves with percent original output yields percent original length.

Reference to the example Spectrum Overlap curves, presented in paragraph 4.2.2, indicates that overlap is not a constant but has been observed to be some function of Ablation Sensor Plug length. This fact makes it necessary to iterate on the solutions, to the simultaneous equations, first obtained. (Iteration is necessary since the value for overlaps used in the solution of the equations may not correspond to the overlap for the Ablation Sensor Plug length determined as a solution to the equations.) A computer program was written to solve and iterate on these equations and is presented in the Appendix, Volume II.

If the same data reduction procedure be followed for both channels, two plots are obtained: (1) Heat shield total thickness and (2) Virgin material remaining. Both plots versus test time.

Data was reduced only at the test end points for this test series. The end points provided the only time when the total and virgin material thicknesses could be measured. Thus an average of the recorder traces at end of test was compared to the average at beginning of test to predict heat shield thicknesses remaining from the measured radioactive intensity at the two nuclear energy levels of interest.

4.2.5 Test Results. The results from this System Operational Ablation test series are presented in Figure 47 in tabular form. From the end point measurements made, the overall average error of total heat shield thickness measurement was .01 inches. The overall average error of virgin material thickness measurement was .015 inches.

It should be noted that the test results presented were based on analysis of the average sensor reading at the end of the test compared with physical measurements of test specimen thickness. No attempt was made to determine the specimen thickness from sensor data continuously during a test.

Additional analysis of the raw test data by the NASA-LRC showed that the instantaneous thickness obtained from sensor data fluctuated widely during the test. It is felt that these fluctuations were primarily statistical in nature, caused by uncertainties in the low count rate which resulted from the limited amounts of activity (microcurie quantities) which could be placed in the laboratory test specimens.

TEST MODEL NUMBER		Total Thickness Measurement			Virgin Material Measurement		
		Computed	Measured	Error*	Computed	Measured	Error*
633-12-2	Phenolic Graphite	.85	.88	-.03	.57	.55	.02
633-12-1		.93	.91	.02	.60	.58	.02
633-11-4		.93	.93	.00	.67	.68	-.01
633-11-3		.96	.97	-.01	.78	.78	.00
633-11-2		.98	.98	.00	.86	.85	.01
633-11-1		.91	.92	-.01	.59	.57	.02
633-10-1		.95	.95	.00	.71	.70	.01
633-9-4		.97	.98	-.01	.85	.83	.02
633-9-3		.99	.98	.01	.86	.88	-.02
633-9-2		.99	.99	.00	.92	.91	.01
633-9-1		.91	.91	.00	.38	x	-
633-7-3		.92	.92	.00	.52	.50	.02
633-7-2		.96	.95	.01	.69	.69	.00
633-7-1		.98	.99	-.01	.86	.84	.02
633-6-4		.99	.99	.00	.91	.89	.03
633-6-3		.96	.94	.02	.49	x	-
633-6-2		.96	.95	.01	.57	.55	.02
633-6-1		x	.97	-	x	.72	-
633-5-2		1.0	.99	.01	.80	.81	-.01
633-5-1		.99	1.0	-.01	.92	.90	.02
633-18-1	Phenolic Nylon	.22	-	-	.19	.17	.02
633-17-3		.37	.38	-.01	.35	.33	.02
633-17-2		.54	.54	.00	.50	.48	.02
633-17-1		.71	.71	.00	.66	.63	.03
633-16-4		.88	.88	.00	.80	.81	-.01
633-19-4		.16	.17	-.01	.08	.07	.01
633-19-2		.38	.40	-.02	.27	.29	-.02
633-19-1		.54	.54	.00	.43	.45	-.02
633-18-3		.67	.68	-.01	.58	.58	.00
633-18-2		.82	.85	-.03	.77	.77	.00
633-14-2		.49	.48	.01	.40	.42	-.02
633-14-1		.64	.63	.01	.52	.53	-.01
633-13-4		.73	.76	-.03	.69	.69	.00
633-13-3		.84	.83	.01	.76	.74	.02
633-13-2		.95	.94	.01	.88	.86	.02
633-16-3		.64	.66	-.02	.57	.56	.01
633-16-2		.73	.75	-.02	.66	.67	-.01
633-16-1		.83	.85	-.02	.73	.75	-.02
633-14-4		.92	.92	.00	.84	.82	.02
633-14-3		.99	.96	.03	.85	.87	-.02

*Error - (Computed - Measured)

Figure 47. Composite Results, System Operational Tests.

Thus, it was impossible to determine the absolute accuracy with which the sensor could continuously measure ablation. Additional tests are recommended as a follow on to this contract to demonstrate that higher activity levels will smooth out the data fluctuations that occurred during laboratory tests under this contract. These tests should be conducted in a facility capable of handling levels of radioactivity which would be required in a flight system (millicurie quantities).

4.3 Environmental Tests.

In addition to the System Development tests performed at Emerson, the NASA, Langley Research Center, has performed certain environmental tests on the system and Radiation Detector. The Dual Ablation Measuring System was subjected to thermal environmental tests; the Radiation Detector was subjected to mechanical and vacuum environmental tests as well as thermal tests. The NASA thermal tests demonstrated that the system was not properly thermally compensated.

However, the Radiation Detector passed the following environments with no failures observed, and no degradation of performance.

Sinusoidal Vibration: 15g rms, 20-2000 cps; 25g rms, 200-2000 cps; - three axes, two octaves per minute.

Random Vibration: 25g rms, 20-2000 cps - 120 seconds, three axes.

Acceleration: 100g - 120 seconds, 3 axes.

Shock: 150g; 5-15 milliseconds, 3 axes.

These conditions were originally specified as design guidelines and representative of the environments encountered by advanced research vehicles.

In addition, the Radiation Detector was subjected to the vacuum environment specified as a design guideline, vacuum equivalent to 30 minutes at 300,000 feet followed by a 10 minute descent to ground level. The Radiation Detector, when coated with a coat of epoxy paint, passed this test with no degradation of performance.

4.4 Functional Tests

4.4.1 Type of Testing. Functional tests were conducted with millicurie level radioactive Indium and Zirconium isotopes. Fixed strength sources were used and geometric separation controlled the radiation level at the Radiation Detector. Details of the

technique and tabulation of the data are contained in Appendix T, Volume II.

Tests were conducted to demonstrate the system calibration capability; static linearity, and obtain an estimate of detector dead time.

4.4.2 Calibration. The results of the two calibration tests conducted on the Prototype System #2 are shown in Figures 48 and 49. The curves of constant Zirconium input (identified Zr1, Zr2, etc.) with varying Indium input are uniform in spacing and have a minimum tendency to curve upward and move closer together as the counting rate increases because of detector dead time. The lines of constant Indium input (identified In1, In2, etc.) with varying Zirconium input are also uniformly spaced but have a marked tendency to move closer together as the counting rate increases. This indicates a dead time loss and a spilling over of counts from Channel 1 into Channel 2 because of pulse pile up. At high counting rates, low energy pulses occurring immediately following high energy pulses are superimposed on the trailing edge of the high energy pulse. If the pulses occur sufficiently close in time, the lower energy pulse may be lifted above the Channel 1 window and move into the Channel 2 window causing a change in the relative overlap of the signals.

Comparison of the general shape of the curves in the figures displays the influence of changes in the gain setting of each channel. Increasing the gain in Channel 1 (Figure 49) causes the lines of constant Indium level to be skewed to the right.

The System #2 tests conducted 12/1/67 (Figure 48) utilized counting rates of 90,000 counts per second for a Channel 1 output of 5 volts (10 Divisions) and 84,000 counts per second for the Channel 2 output of 5 volts (10 Divisions).

A corresponding test was conducted on the Breadboard System and the results plotted in Figure 50. The curves of constant input show a more pronounced curvature as the input level is increased. The lines of constant Indium input reverse their curvature for Zirconium inputs greater than position 6 (about 45,000 counts per second) and Indium inputs greater than position 8 (about 61,000 counts per second). This indicates that significant portions of the normal Channel 1 counts are spilling over into Channel 2 because of pulse pile up and window positioning. A slight change in the upper level of the Channel 1 window and a corresponding shift in the lower level of the Channel 2 window would improve the performance.

Dual Ablation Measuring System #2
System Ch2 T/C 4 Fine 2 Coarse 2
Switches Ch2 T/C 4 Fine 5 Coarse 2
Output 5 VDC = 10 Divisions

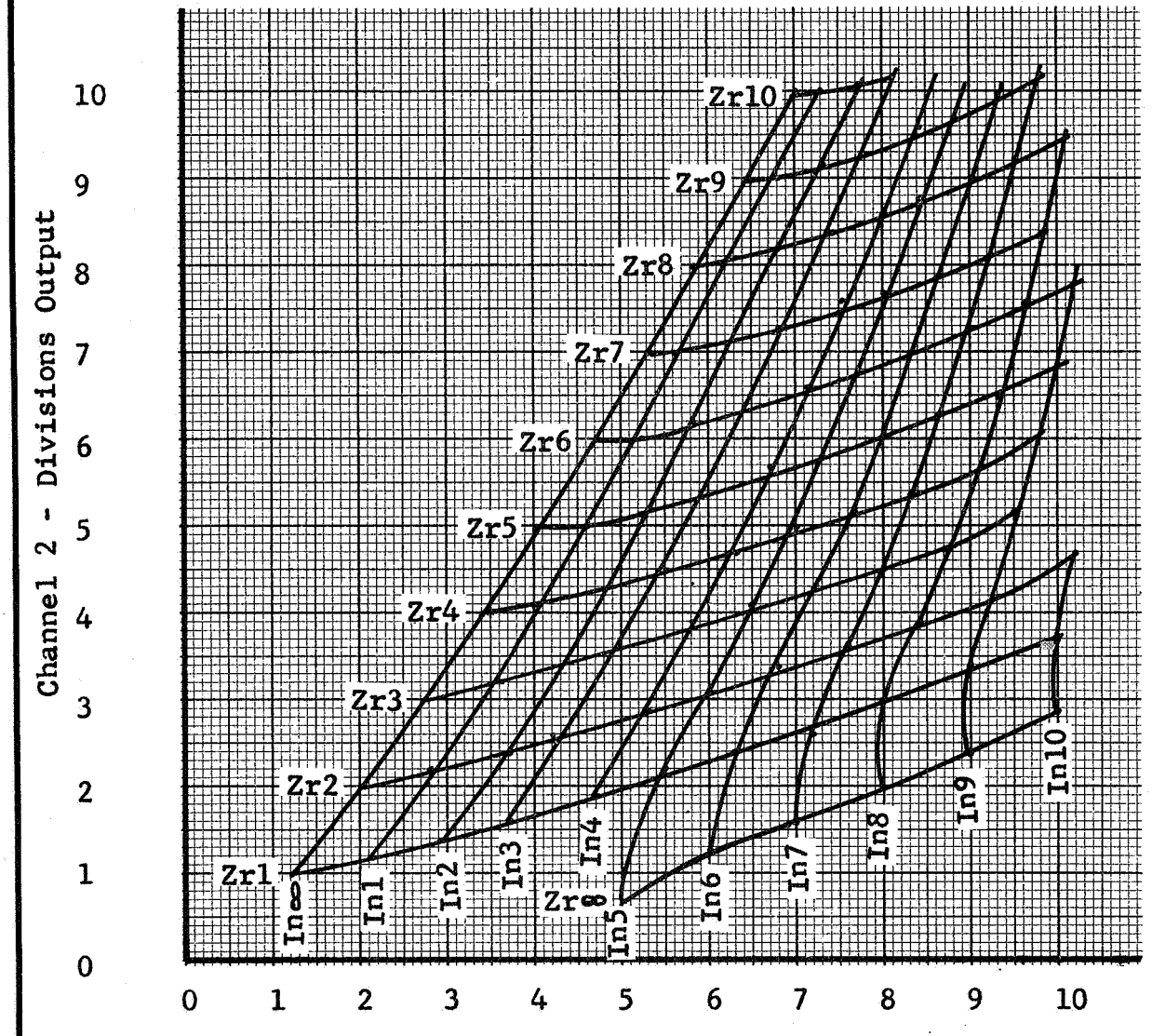

Figure 48
Functional Tests - System #2 - 12/1/67

Dual Ablation Measuring System #2
System CH1 T/C4 Fine 5 Coarse 2
Switches CH2 T/C4 Fine 5 Coarse 2
Output 5 VDC - 10 Divisions

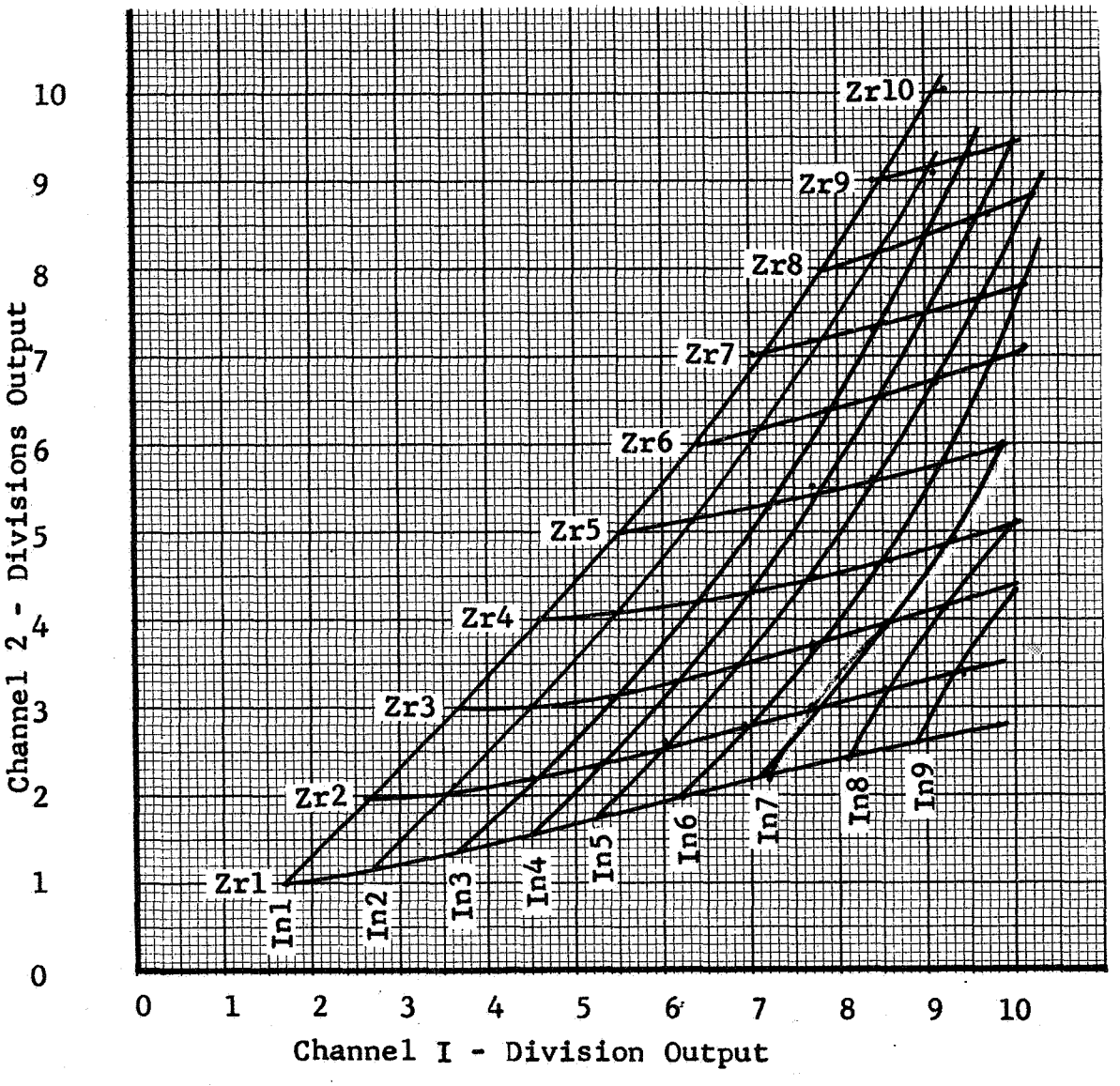

Figure 49
Functional Tests - System #2 - 11/27/67

Dual Ablation Measuring System Breadboard
System CH1 T/C4 Fine 5 Coarse 2
Switches CH2 T/C4 Fine 5 Coarse 2
Output 5 VDC = 10 Divisions

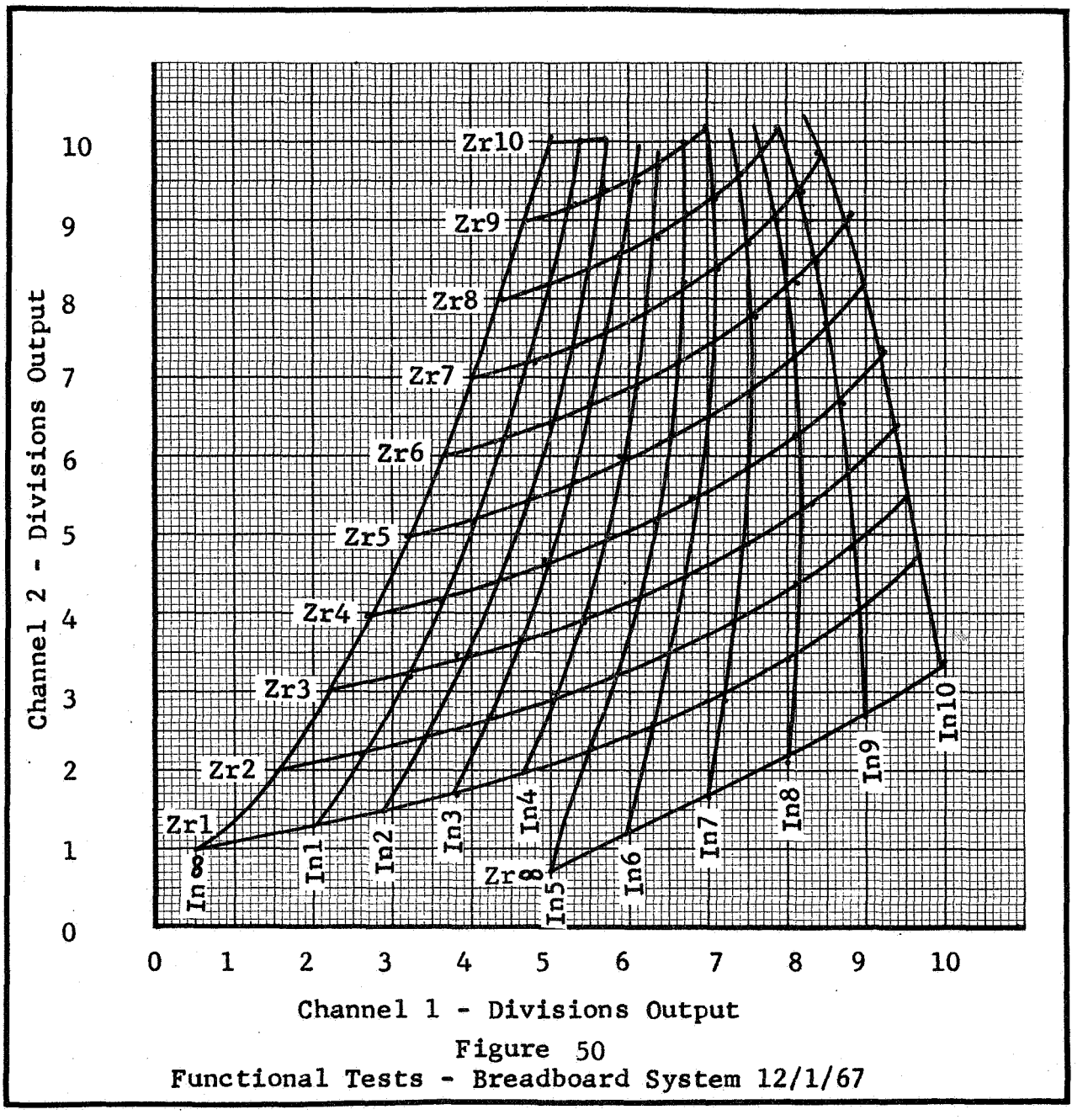

Figure 50
Functional Tests - Breadboard System 12/1/67

Dual Ablation Measuring System #2
System CH1 T/C 4 Fine 5 Coarse 2
Switches CH2 T/C 4 Fine 5 Coarse 2
Output 5 VDC = 10 Divisions 11/29/67

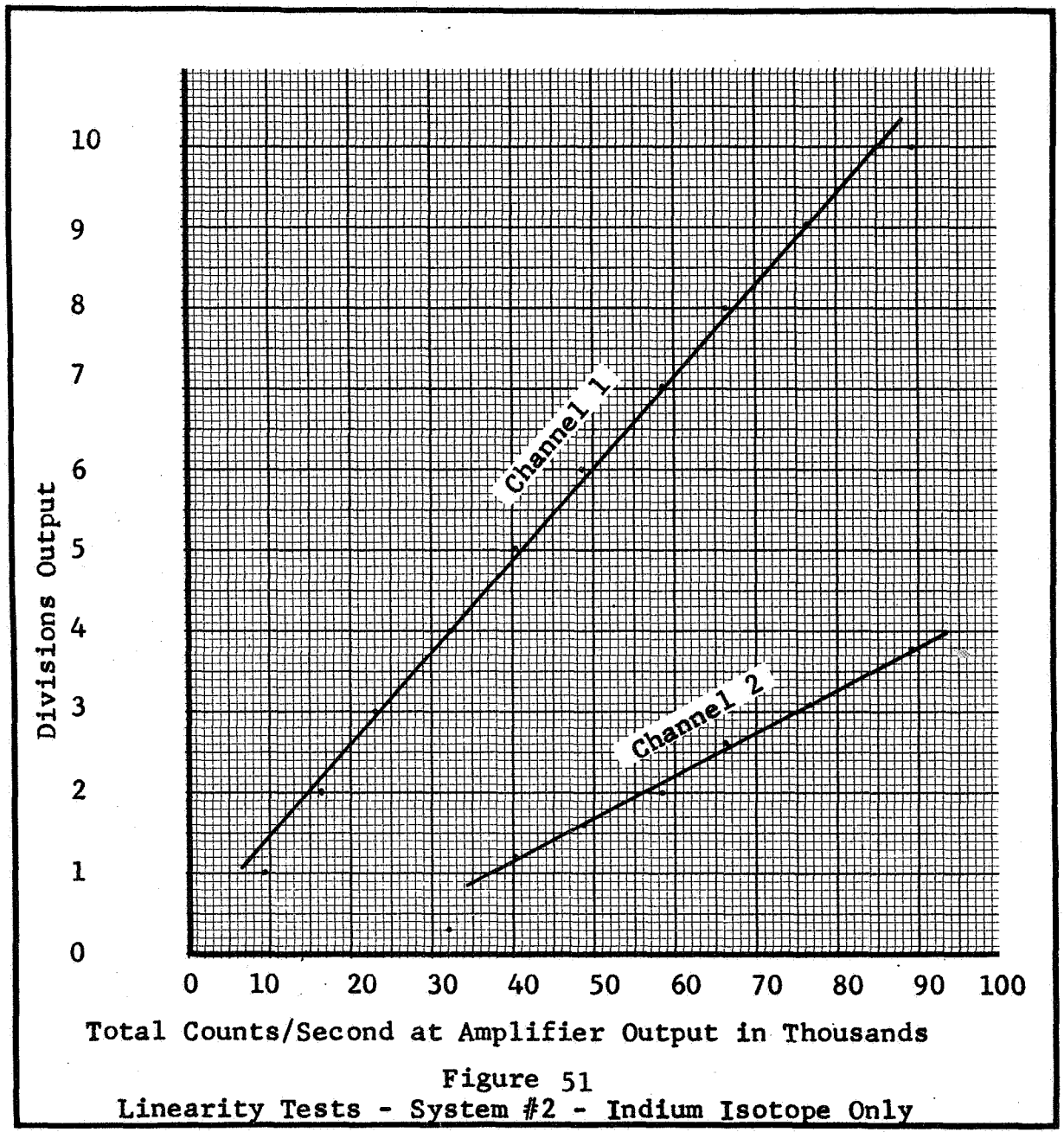

Figure 51
Linearity Tests - System #2 - Indium Isotope Only

Dual Ablation Measuring System #2
System CH1 T/C 4 Fine 5 Coarse 2
Switches CH2 T/C 4 Fine 5 Coarse 2
Output 5 VDC = 10 Divisions 11/29/67

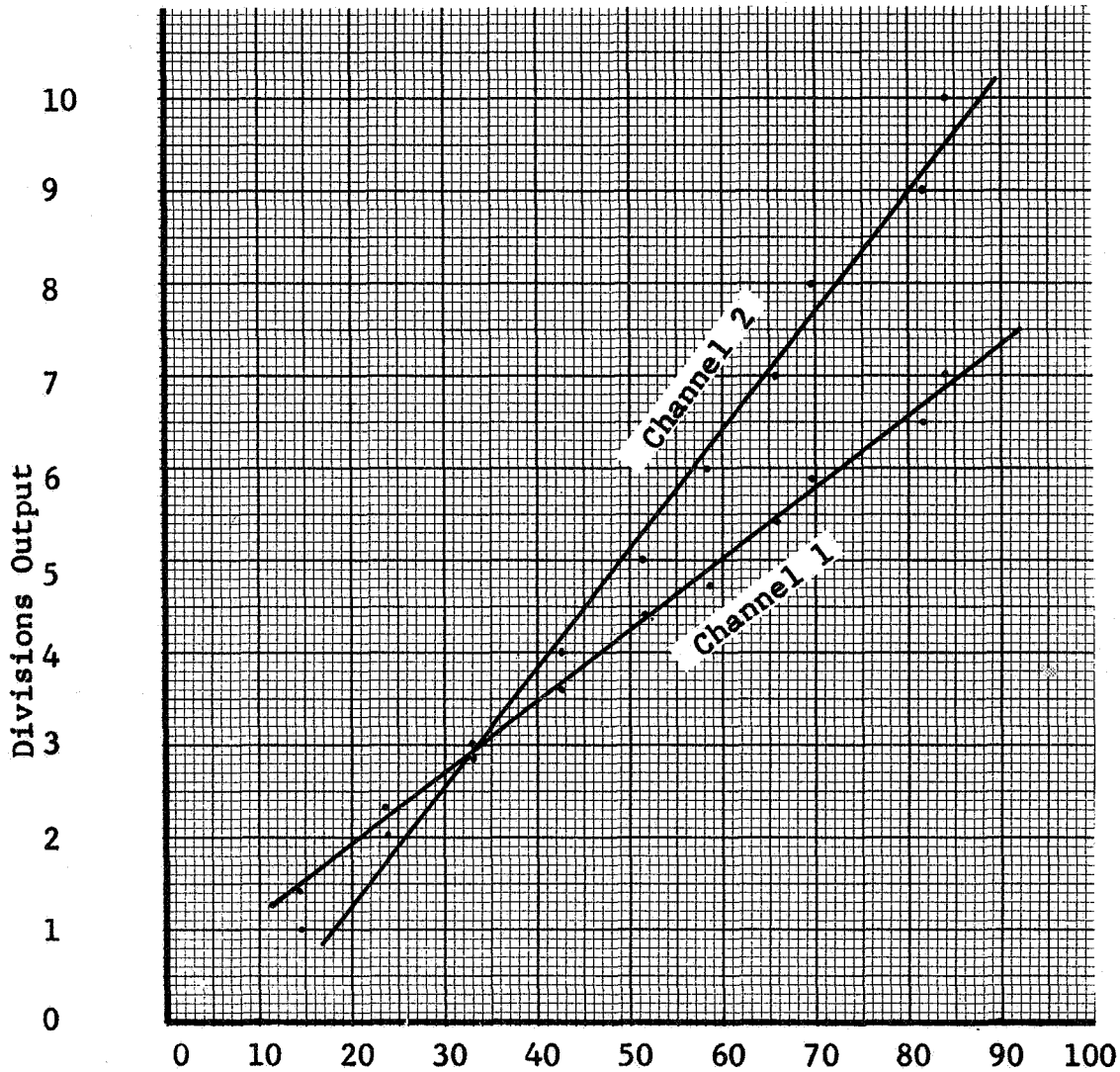

Figure 52
Linearity Tests - System #2 - Zirconium Isotope Only

Dual Ablation Measuring System Breadboard
System CH1 T/C 4 Fine 5 Coarse 2
Switches CH2 T/C 4 Fine 5 Coarse 2
Output 5 VDC = 10 Divisions 11/29/67

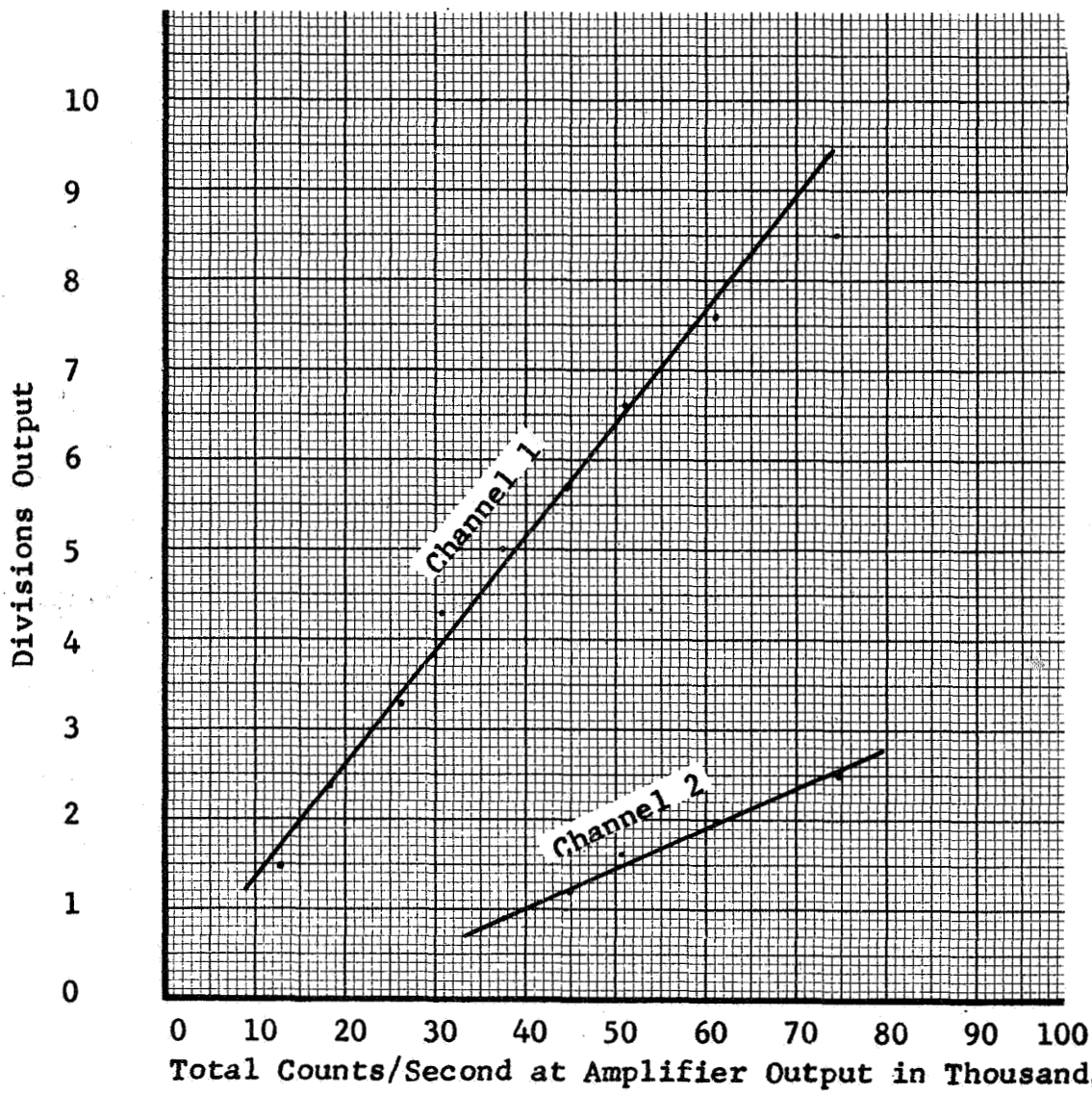

Figure 53
Linearity Tests - Breadboard System - Indium Isotope Only

Dual Ablation Measuring System Breadboard
System CH1 T/C 4 Fine 5 Coarse 2
Switches CH2 T/C 4 Fine 5 Coarse 2
Output 5 VDC = 10 Divisions 11/29/67

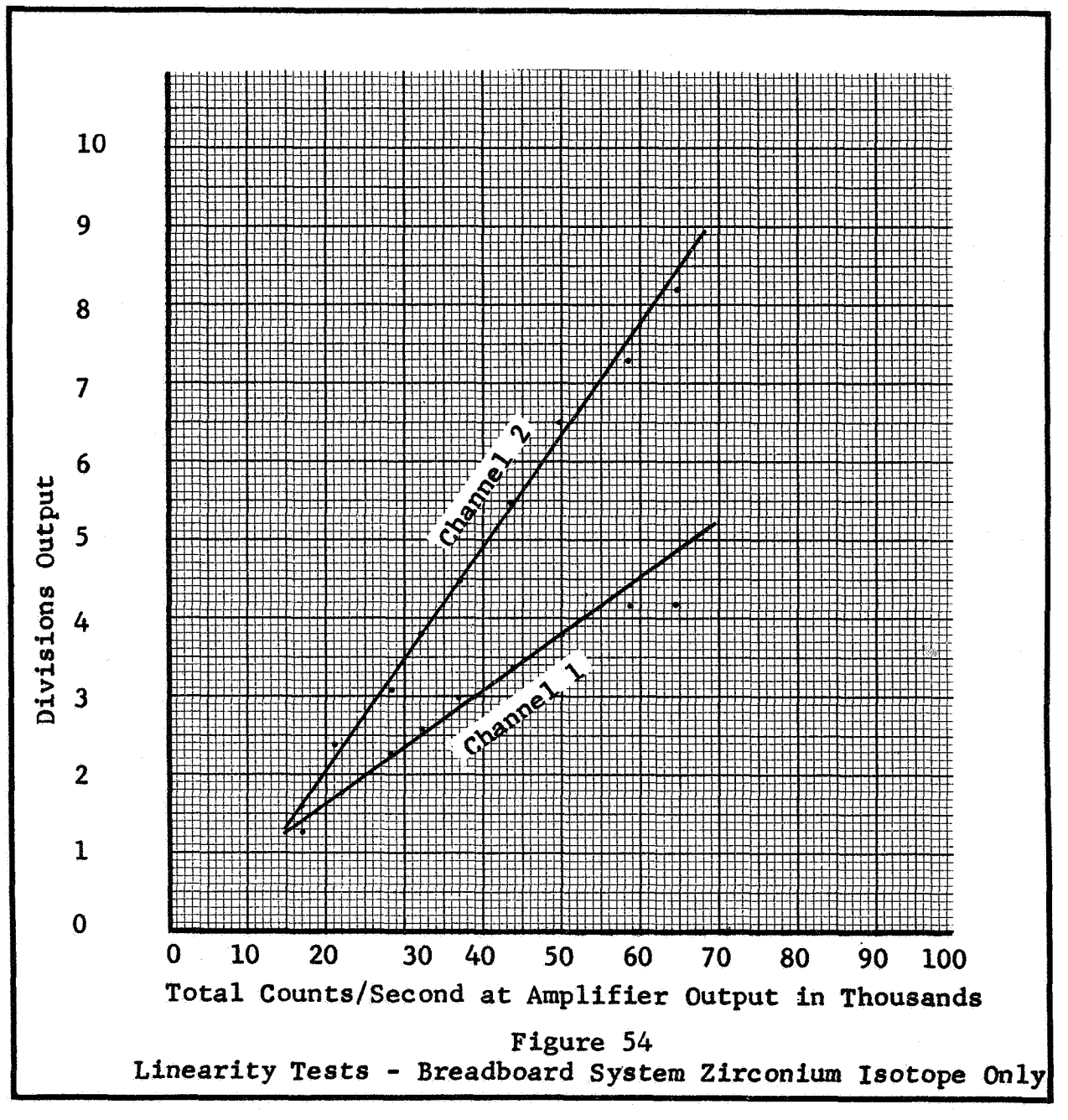

Figure 54
Linearity Tests - Breadboard System Zirconium Isotope Only

The gain of the Breadboard is lower than the Prototype System #2 for the same system switch settings. Counting rates of 120,000 counts per second provided full scale output at Channel 1 (5 VDC or 10 Divisions) and 93,000 counts per second for full scale output at Channel 2.

4.4.3 Linearity. The static linearity of the system may be estimated in a gross manner by plotting the Channel outputs versus input counting rates for each isotope. These plots are shown in Figures 51 through 54. The method of testing and the uncertainty in repeating isotope position is apparent in the Zirconium input graphs.

Another method of checking the linearity is to plot the channel output versus the isotope distance from the Radiation Detector. There is an uncertainty as to the exact amount of additional distance to be added to each measurement because of the geometry of the Radiation Detector. Figures 55 and 56 present this data plotted on log-log paper with no correction for the Radiation Detector geometry.

4.4.4 Detector Dead Time. The dead time for the Radiation Detector assemblies was determined using the method described in Appendix T. The Prototype System dead time is computed to be 3.6 microseconds which is the same order of magnitude as the pulse width of the signal from the Radiation Detector pre-amplifier. The calculated value of the Breadboard system in the overloaded region is an unrealistic 7.4 microseconds. Using data within the linear region the time is between 3.3 and 4.5 microseconds, which is comparable to the prototype system and characteristic of this detector configuration.

4.4.5 Time Constant. The time constant settings of each channel were varied and the channel output observed for fixed radiation level inputs. The average reading remained constant but the amplitude of the random deviations about the average value increased as the integration time decreased.

Dual Ablation Measuring System #2
System CH1 T/C 4 Fine 5 Coarse 2
Switches CH2 T/C 4 Fine 5 Coarse 2
Output 5 VDC = 10 Divisions 12/1/67

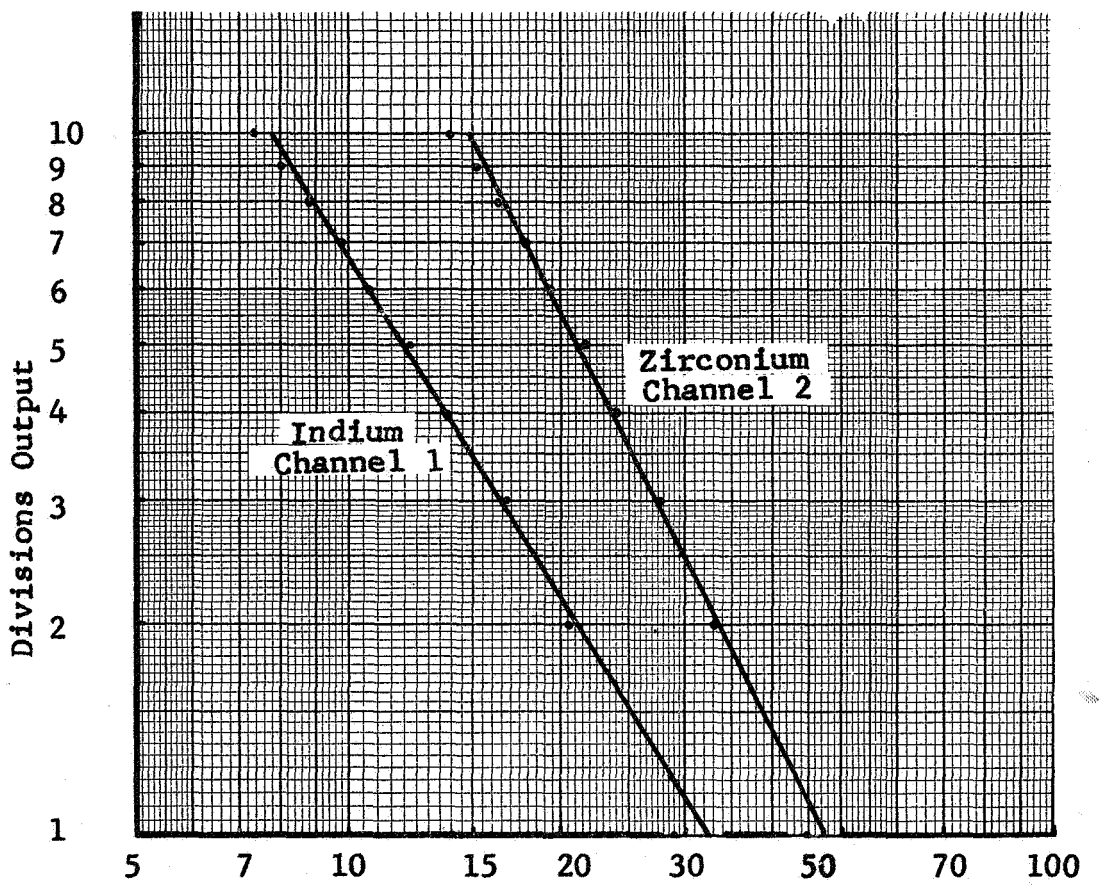

Figure 55
Output vs. Source Distance - System #2

Dual Ablation Measuring System Breadboard
System CH1 T/C 4 Fine 5 Coarse 2
Switches CH2 T/C 4 Fine 5 Coarse 2
Output 5 VDC = 10 Divisions 12/1/67

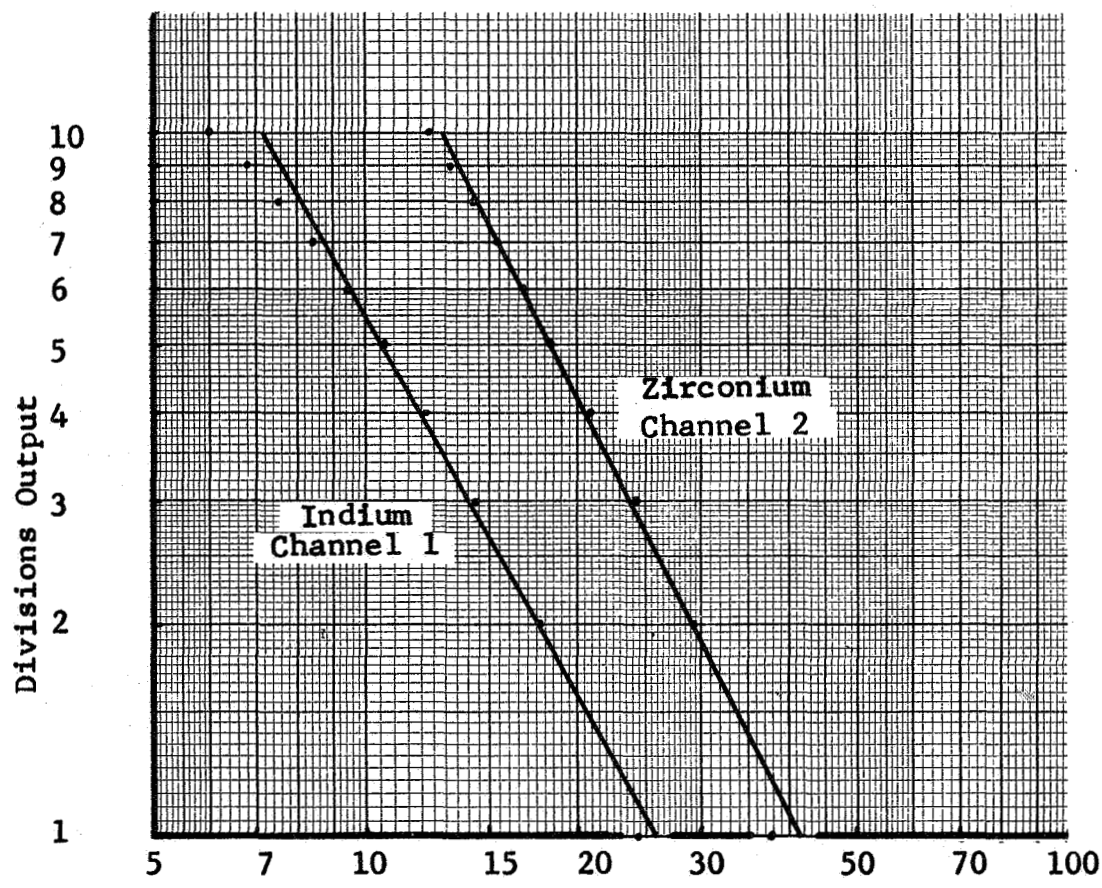

Figure 56
Output vs. Source Distance - Breadboard

5.0 CONCLUSIONS AND RECOMMENDATIONS

5.1 Conclusions.

The feasibility of simultaneous and continuous measurement of heat shield total and virgin material thickness by a nucleonic technique has been investigated. Gamma emitting radioisotopes were selected compatible with two heat shield materials phenolic nylon and phenolic graphite. The Isotope Accuracy test series demonstrated that these isotopes would leave the heat shield at proper times and in such proportions to allow measurements of heat shield thicknesses to be made from the observed intensities of radiations remaining in the heat shield material. Techniques for uniformly incorporating the isotopes into Ablation Sensor Plugs were developed. A Radiation Detector was designed and fabricated that could discriminate between the energy levels of the radiations from the two chosen isotopes. Environmental tests, conducted by the NASA, indicated that the Radiation Detector would withstand the severe environment associated with small solid propellant research rockets. A prototype flight system was designed, fabricated, and tested. System Operational Ablation tests indicated proper functioning of the system. Thermal environmental tests performed on the system indicated that it was not properly thermally compensated.

The results of ablation tests showed that the average sensor output at the end of a test agreed well with physical measurements of test specimen thickness remaining. However, the instantaneous sensor indication fluctuated widely during the tests. These fluctuations were due primarily to uncertainties in the low count rate which resulted from the limited amounts of activity which could be placed in the laboratory test specimens. Thus, it was impossible to accurately determine the precision with which the dual radioactive technique could continuously measure both surface recession and char layer interface recession.

The important achievement of this contract was the demonstration of a technique of measurement that does not perceptibly change the aerothermodynamic behavior of ablative materials while providing continuous and simultaneous measurements of their total and virgin material thicknesses, at the same vehicle location.

The techniques developed may easily be applied to other current heat shield materials whether they be electrical conductors in the virgin state or not.

5.2 Recommendations.

It is recommended that further ablation tests be performed with Emerson's Dual Ablation Measuring System. Further tests are necessary to demonstrate its usefulness at higher ablation rates, typical of advanced research vehicles. These tests should be conducted using the millicurie levels of activity which would be employed in a flight application of this technique. They should then demonstrate that higher levels will smooth out the data fluctuations that occurred during laboratory testing under this contract, and allow a precise determination of measurement accuracy.